Experimental and Computational Analysis of Epidermal Growth Factor Receptor Pathway Phosphorylation Dynamics

By

Laura B. Kleiman

B.A. Biomathematics
B.A. Mathematics
Rutgers University, 2004

Submitted to the Computational and Systems Biology Program in partial fulfillment of the requirements for the degree of

Doctor of Philosophy in Computational and Systems Biology
at the
Massachusetts Institute of Technology

June 2010

Signature of Author:_____
Computational and Systems Biology Program
May 21, 2010

Certified by:_____
Peter K. Sorger
Professor of Systems Biology (Harvard Medical School)
Professor of Biological Engineering (Massachusetts Institute of Technology)
Thesis Supervisor

Certified by:_____
Douglas A. Lauffenburger
Ford Professor of Biological Engineering, Chemical Engineering, and Biology
Thesis Supervisor

Accepted by:_____
Christopher Burge
Associate Professor of Biology
Director, Computational and Systems Biology Graduate Program

Experimental and Computational Analysis of Epidermal Growth Factor Receptor Pathway Phosphorylation Dynamics

By
Laura B. Kleiman

Submitted to the Computational and Systems Biology Program on May 21, 2010, in partial fulfillment of the requirements for the degree of Doctor of Philosophy in Computational and Systems Biology

Abstract

The epidermal growth factor receptor (EGFR, also known as ErbB1) is a prototypical receptor tyrosine kinase (RTK) that activates multi-kinase phosphorylation cascades to regulate diverse cellular processes, including proliferation, migration and differentiation. ErbB1 hetero-oligomerizes with three close homologues: ErbB2, ErbB3 and ErbB4. ErbB1-3 receptors are frequently mutated, overexpressed or activated by autocrine or paracrine ligand production in solid tumors and have been the target of extensive drug discovery efforts. Multiple small molecule kinase inhibitors and therapeutic antibodies against ErbB receptors are in clinical use or development. Despite their importance as RTKs, oncogenes and drug targets, regulation of ErbB receptors by the interplay of conformational change, phosphorylation, phosphatases and receptor trafficking remains poorly understood, and the impact of these dynamics on physiological activity and cellular responses to anti-ErbB drugs is largely unknown.

This thesis investigates the dynamic opposition of kinases and phosphatases within the ErbB pathway. By standard biochemical analysis, ErbB receptors and downstream proteins appear to become phosphorylated and then dephosphorylated in approximately 30 minutes. However, pulse-chase experiments where cells are exposed to ligand and then to small molecule kinase inhibitors reveal that individual proteins must in fact cycle rapidly between being phosphorylated and dephosphorylated in seconds. We construct a succession of differential equation-based models of varying biochemical resolution, each model appropriate for analyzing a different aspect of ErbB regulation, to help interpret the data and gain quantitative insight into receptor and drug biology.

Rapid phosphorylation and dephosphorylation of receptors has important implications for the assembly dynamics of signalosomes. We find that signals are rapidly propagated through some downstream pathways but slowly through others, resulting in prolonged activation in the absence of upstream signal. We show that fast phosphorylation/dephosphorylation may provide cells with the flexibility necessary to rapidly detect and respond to changes in their extracellular environment. These fast dynamics also play a crucial role in determining the response to ErbB1-targeting cancer therapies, which we find to vary significantly between drugs with different mechanisms of action. We show that treatment with one class of these drugs results in sustained signaling, instead of inhibition, and thus may actually promote tumor proliferation or invasion. Our work may help explain why certain drugs have been more effective in patients than others and suggests new approaches for evaluating biochemical signaling networks and targeted therapeutics.

Thesis Supervisor: Peter K. Sorger, Ph.D.
Title: Professor of Systems Biology, Harvard Medical School and Professor of Biological Engineering, Massachusetts Institute of Technology

Thesis Supervisor: Douglas A. Lauffenburger, Ph.D.
Title: Ford Professor of Biological Engineering, Chemical Engineering, and Biology, Massachusetts Institute of Technology

Thesis Committee

Forest M. White
Associate Professor of Biological Engineering (Massachusetts Institute of Technology)
Thesis Committee Chair

Peter K. Sorger
Professor of Biological Engineering (Massachusetts Institute of Technology)
Professor of Systems Biology (Harvard Medical School)
Thesis Supervisor

Douglas A. Lauffenburger
Ford Professor of Biological Engineering, Chemical Engineering, and Biology (Massachusetts Institute of Technology)
Thesis Supervisor

Tyler Jacks
David H. Koch Professor of Biology (Massachusetts Institute of Technology)
Thesis Committee Member

Dennis Vitkup
Assistant Professor of Biomedical Informatics (Columbia University)
Thesis Committee Member

Table of Contents

Figures and Tables

Acknowledgements

Many people have contributed to making this thesis possible, and I am unable to recognize everyone individually. Nevertheless, there are several people who played a particularly important role in my graduate career and I would like to take this opportunity to acknowledge their contributions.

I must begin by thanking my primary advisor, Peter Sorger. Peter gave me the time and freedom to explore projects and learn how to become an independent scientist. He encouraged me to form effective collaborations, and provided valuable guidance throughout my thesis project. His enthusiasm for science is infectious and working in his lab has been an enjoyable experience.

Nor would this thesis have been possible without the constant support, encouragement and guidance provided by my co-advisor, Doug Lauffenburger. The rest of my thesis committee, Forest White, Tyler Jacks and Dennis Vitkup, also played a key role in developing this thesis.

I feel very privileged to have been in the first class of students in the Computational and Systems Biology Ph.D. program at MIT. I will be forever thankful to all of those at MIT who made it possible for me to have this amazing opportunity. I hope that I am able to honor the faith they placed in me throughout my scientific career.

In 2006, Peter's lab moved to the Department of Systems Biology at Harvard Medical School (HMS), and I was fortunate to become a member of that community, as well. The HMS Systems Biology Department provides a wonderful, jovial learning and research environment that stimulates cross-disciplinary collaborations through which I cultivated special friendships.

I could not have made it through graduate school without my friends in Peter's lab and at HMS, all of whom were bottomless wells of friendship, support and lively scientific conversations. In particular, I would like to thank Julio Saez-Rodriguez, Thomas Maiwald, Floris Foijer, Debbie Flusberg, Will Chen, Holger Conzelmann, Yangqing Xu, Sudhakaran Prabakaran, Jenny Gallop, Leo Alexopoulos and Carlos Lopez. Sabrina Spencer, my "partner-in-crime" throughout graduate school, deserves special recognition. Sabrina and I serendipitously met before we even applied to MIT and we wound up experiencing almost every aspect of our graduate careers at MIT and HMS together – it would not have been the same without her.

I would also like to thank John Albeck, Suzanne Gaudet and Keara Lane for taking me under their wings when I was just a first-year graduate student rotating through their labs, and for helping me ease into experimental biology. Their guidance and encouragement helped me persevere through a sometimes overwhelming first year.

The work detailed in this thesis would not have been possible without my collaborators. Holger Conzelmann and Thomas Maiwald each made invaluable contributions to this project and, just as importantly, they taught me how effective collaborations can make science so much more fun and rewarding. Will Chen originally encouraged me to work on this project and was always there to brainstorm ideas, talk me through setbacks and celebrate exciting results.

Words cannot adequately express my gratitude for the love and unwavering support of my family. I have been very lucky to have much of my family nearby for the last several years. While I moved up to Boston alone in 2004, my brother, husband, parents and then sister-in-law were soon to follow!

Dad, thank you for introducing me to the field of systems biology before most people even knew that it existed. I am extremely grateful to have inherited your passion for science, learning and critical thinking.

Mom, thank you for your love and support through the years and for still doing “mom things” for me, even though I am sure I am too old for that.

To my brother, David, and my sister-in-law, Violeta, your friendship and support means so much to me; it has been fantastic having you both with me here at MIT.

To my in-laws, Michael and Frayda, thank you for welcoming me into your family from the start, for encouraging me to be strong in the face of challenges, and for reminding me to always focus on the important things in life.

And, most importantly, to Matt, my husband and my best friend, who has patiently listened to endless stories of the highs and lows of graduate school, who has celebrated my successes and comforted me when I have been down, you are my rock and I would not have made it through this journey without you. Thank you for always reminding me that there is more to life than science.

CHAPTER 1: Introduction

Protein phosphorylation regulates signal transduction and physiological processes

Cellular signal transduction is regulated by various forms of post-translational modification, and phosphorylation of cellular proteins is arguably the most common and important type of reversible post-translational modification. Protein phosphorylation networks in cells are an integral part of almost all physiologic processes, including the immune response, cardiovascular system and endocrine action (Tarrant and Cole, 2009). The first direct evidence for the enzymatic phosphorylation of a protein substrate was obtained by Eugene Kennedy in 1954 (Burnett and Kennedy, 1954). In 1955, Fischer *et al.* showed that the metabolic enzyme phosphorylase, which is responsible for the conversion of glycogen to glucose-1-phosphate, can be converted from an inactive to active state by a protein kinase that catalyzes the attachment of a phosphate group to phosphorylase (Fischer and Krebs, 1955). It is now thought that approximately 30% of all proteins are phosphorylated at any given time (Cohen, 2000). Phosphorylation of an enzyme can be activating (e.g. by energizing an enzyme to participate in subsequent reactions) or inhibitory (e.g. through a conformational change that masks its kinase domain), and can alter protein-protein interactions. Some proteins have multiple phosphorylation sites, with phosphorylation of certain sites being activating and others inhibitory. This thesis focuses on activating phosphorylation events.

Net phosphorylation levels are determined by kinases and phosphatases

Protein phosphorylation levels are determined by the balanced action of protein kinases and phosphatases (Fig. 1.1). Kinases catalyze the incorporation of covalently bound phosphate groups to their substrates, usually on serine, threonine or tyrosine residues, by using ATP. Five hundred different protein kinases have been identified in mammals (approximately 2% of all human genes (Manning et al., 2002)). Protein kinases are highly regulated by their

phosphorylation, binding of activating or inhibitory proteins or small molecules, and their subcellular localization with respect to substrates. Phosphatases act in opposition to kinases to catalyze the removal of phosphate groups from their substrates by hydrolysis. Much less is known about the factors and cellular components that regulate protein dephosphorylation than phosphorylation.

Receptor tyrosine kinases (RTKs) sense the extracellular environment and initiate phosphorylation cascades

Tyrosine-specific protein kinases play an important role in signal transduction by acting as growth factor receptors and as cytoplasmic proteins that regulate downstream signaling from growth factors. There are 90 protein tyrosine kinases (PTKs) in humans (Manning et al., 2002), of which more than 50 are receptor tyrosine kinases (RTKs) (Robinson et al., 2000) such as the epidermal growth factor receptor (ErbB1), platelet-derived growth factor receptor (PDGFR) and insulin receptor (IR). RTKs are composed of an extracellular N-terminal domain that serves as the ligand-binding part of the molecule, a transmembrane-spanning domain, and a cytoplasmic C-terminal domain that includes the catalytic subunit responsible for their kinase activity. RTKs and other cell surface receptors help cells sense and respond to their surroundings by binding ligands in the extracellular environment. Once an RTK is activated by ligand, it can bind to and phosphorylate specific target proteins via its intracellular domain and trigger a cascade of protein phosphorylation events that relay the extracellular signal to downstream pathways that modulate phenotypic responses to the environmental stimulus.

General goals of this work

Signal transduction by kinases is thought to depend on the extent and duration of substrate phosphorylation. Since phosphorylation plays an essential role in complex signaling

networks, it is crucial to understand how phosphorylation events are regulated and how they influence signal propagation in order to understand how cellular fate decisions are controlled. This thesis investigates the dynamic interplay between kinases and phosphatases. The following general questions are addressed: (1) how frequently individual proteins are phosphorylated and dephosphorylated and (2) what the consequences are of these time scales. Since ErbB1 is well studied and relevant in disease processes, this thesis focuses on analyzing the phosphorylation dynamics of the ErbB receptor family and its downstream pathways following activation by growth factors. Nevertheless, the results may be generalizable to other RTKs and signaling pathways.

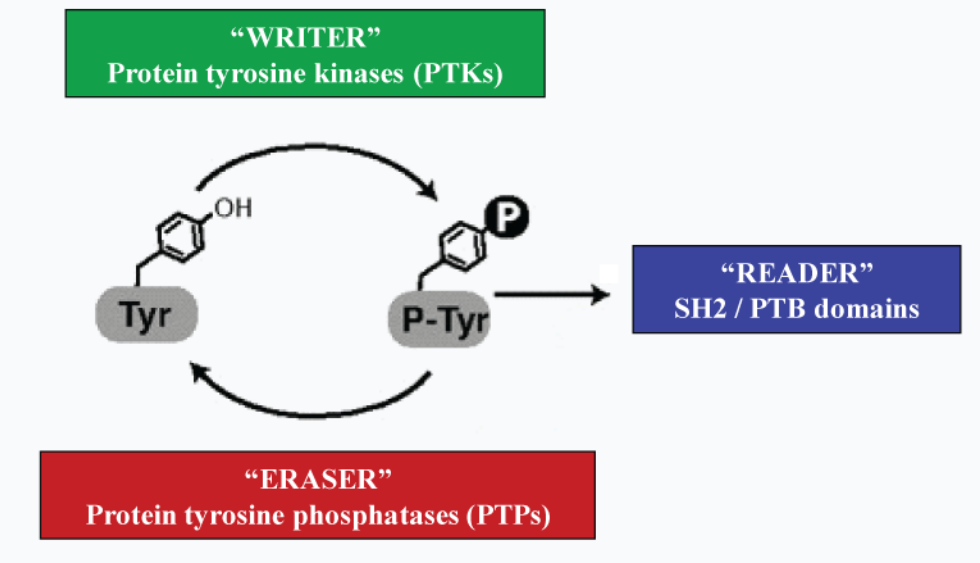

Figure 1.1 - Protein phosphorylation on tyrosine residues is regulated by the dynamic opposition of PTKs and PTPs.

Tyrosine phosphorylation leads to activation of downstream signaling pathways through binding of SH2- or PTB-domain containing proteins. SH2 = Src homology 2; PTB = phosphotyrosine binding. Figure adapted from Pincus, D., Letunic, I., Bork, P., and Lim, W.A. (2008). "Evolution of the phospho-tyrosine signaling machinery in premetazoan lineages." *Proc Natl Acad Sci* U S A 105, 9680-9684.

The ErbB receptor family

ErbB1 is a prototypical RTK that activates multi-kinase phosphorylation cascades to regulate diverse cellular processes including proliferation, migration and differentiation (Citri and Yarden, 2006; Fry et al., 2009; Yarden and Sliwkowski, 2001). ErbB1 (also known as EGFR or Her1) hetero-oligomerizes with three close homologues: ErbB2 (Her2 or Neu2), ErbB3 (Her3 or Neu3) and ErbB4 (Her4). Deficiencies in ErbB signaling are associated with the development of neurodegenerative diseases in humans, and the importance of these receptors during development and in normal adult physiology has become apparent from analyses of genetically modified mice (Bublil and Yarden, 2007; Hynes and Lane, 2005). Excessive ErbB signaling, on the other hand, is associated with many types of cancers (Holbro and Hynes, 2004; Hynes and Lane, 2005).

Mechanisms regulating activation of the ErbB receptors and downstream signaling pathways

The 11 known extracellular ligands for the ErbB receptors exhibit differential binding to ErbB1, ErbB3 and ErbB4 (Linggi and Carpenter, 2006). For example, EGF and TGFα bind to only ErbB1 and neuregulins bind to ErbB3 and ErbB4. ErbB2 has no known high-affinity ligand and instead functions by associating with other ErbB receptors (Klapper et al., 1999) or, in tumors that overexpress ErbB2, by forming active ErbB2 homodimers independent of ligand (Yarden and Sliwkowski, 2001). Ligand-independent activation is possible because ErbB2 constitutively exists in a quasi-active conformation that resembles the ligand-bound state of ErbB1, ErbB3 and ErbB4 (Garrett et al., 2003).

Ligand binding promotes homo- and heterodimerization of ErbB receptors, as well as higher-order oligomers (Clayton et al., 2008), and a conformational change that positions the cytoplasmic C-terminal tail of one receptor near the activation loop of the other, thereby

facilitating receptor phosphorylation *in trans* (Fig. 1.2). Phosphorylation of RTKs within their activation loop normally stabilizes activity (Huse and Kuriyan, 2002); however, this form of regulation has not been found for ErbB1. Receptor homo- and heterodimers may also form in the absence of ligand, but under most circumstances these receptors are inactive, switching to an active conformation only upon ligand binding (Tao and Maruyama, 2008).

Activated ErbB receptors phosphorylate each other *in trans* on 4-12 tyrosine residues that serve as docking sites for the recruitment of diverse Src homology 2 (SH2) and phosphotyrosine binding (PTB) domain containing intracellular adaptor proteins (Jones et al., 2006; Kaushansky et al., 2008; Schulze et al., 2005). These adaptor proteins, and the proteins that bind to them, are often themselves targets for phosphorylation by ErbB receptors or by cytoplasmic kinases. ErbB3 lacks key residues present in other ErbB kinase domains and is therefore catalytically inactive, but ErbB3 is biologically active as part of heterodimers containing ErbB1, ErbB2 or ErbB4 (Jura et al., 2009). Receptor phosphorylation and binding of multiple SH2/PTB proteins leads to assembly of large multi-protein "signalosomes" that transmit signals to downstream targets that include Ras, the mitogen activated protein kinase/extracellular signal-regulated kinase (MAPK/ERK) and phosphoinositide 3-kinase (PI3K)-Akt cascades (Yarden and Sliwkowski, 2001) and the Cdc42-regulated actin cytoskeleton (Hirsch et al., 2006).

Mechanisms leading to downregulation of ErbB signaling

A fundamental question in the study of ErbB signaling is what determines the magnitude and duration of receptor activation. In cells exposed to a pulse of exogenous ligand, particularly following serum starvation, receptors and adaptor proteins become phosphorylated in a response that peaks ~10 minutes later and then declines to the pre-stimulus level within ~1-2 hours (the immediate-early response; (Chen et al., 2009)). Activated ErbB1 receptors are endocytosed and then either degraded in the lysosome or recycled to the plasma membrane

where they are once again able to bind ligand (Sorkin and Goh, 2009). Internalized receptors are also capable of signaling to some, but not all, downstream pathways.

In cells stimulated with low concentrations of EGF, ErbB1 is internalized through clathrin coated pits and is not ubiquitinated (Sigismund et al., 2005). In contrast, at higher EGF concentrations, ErbB1 becomes ubiquitinated and endocytosed through caveolae via a clathrin-independent pathway. Ubiquitin is required for early endosomal cargoes to be sent to the lysosome for degradation. The E3 ubiquitin ligase Cbl is recruited to ErbB1 after ligand stimulation (Levkowitz et al., 1998), binds directly to ErbB1 on phosphorylated tyrosine 1045 (pY1045) or indirectly through Grb2 (Waterman et al., 2002), and mediates ubiquitination and degradation of the receptor. During the period between receptor uptake and subsequent recycling to the membrane, but before receptor resynthesis, ErbB1-mediated responses are significantly downregulated. The mechanisms responsible for downregulation of other ErbB receptors are less well understood, but internalization is not thought to play a major role (Baulida et al., 1996).

ErbB1 degradation is a potential mechanism to terminate receptor signaling following ligand stimulation. In addition, negative feedback regulators of ErbB1 such as MIG6 and Sprouty2 have been found to be activated after ~1-2 hours (Amit et al., 2007; Wong et al., 2001; Zhang et al., 2007). It is unclear whether these proteins play a role in downregulation of activated ErbB1 or only prevent subsequent ligand-induced activation. Furthermore, ERK-dependent phosphorylation of ErbB1 on a threonine residue in the receptor juxtamembrane cytoplasmic domain has been shown to contribute to ErbB1 downregulation (Li et al., 2008), possibly by inducing an inactivating conformational change in the receptor (Yang et al., 2009). Extensive evidence also points to an important role for phosphatases in ErbB1 dephosphorylation.

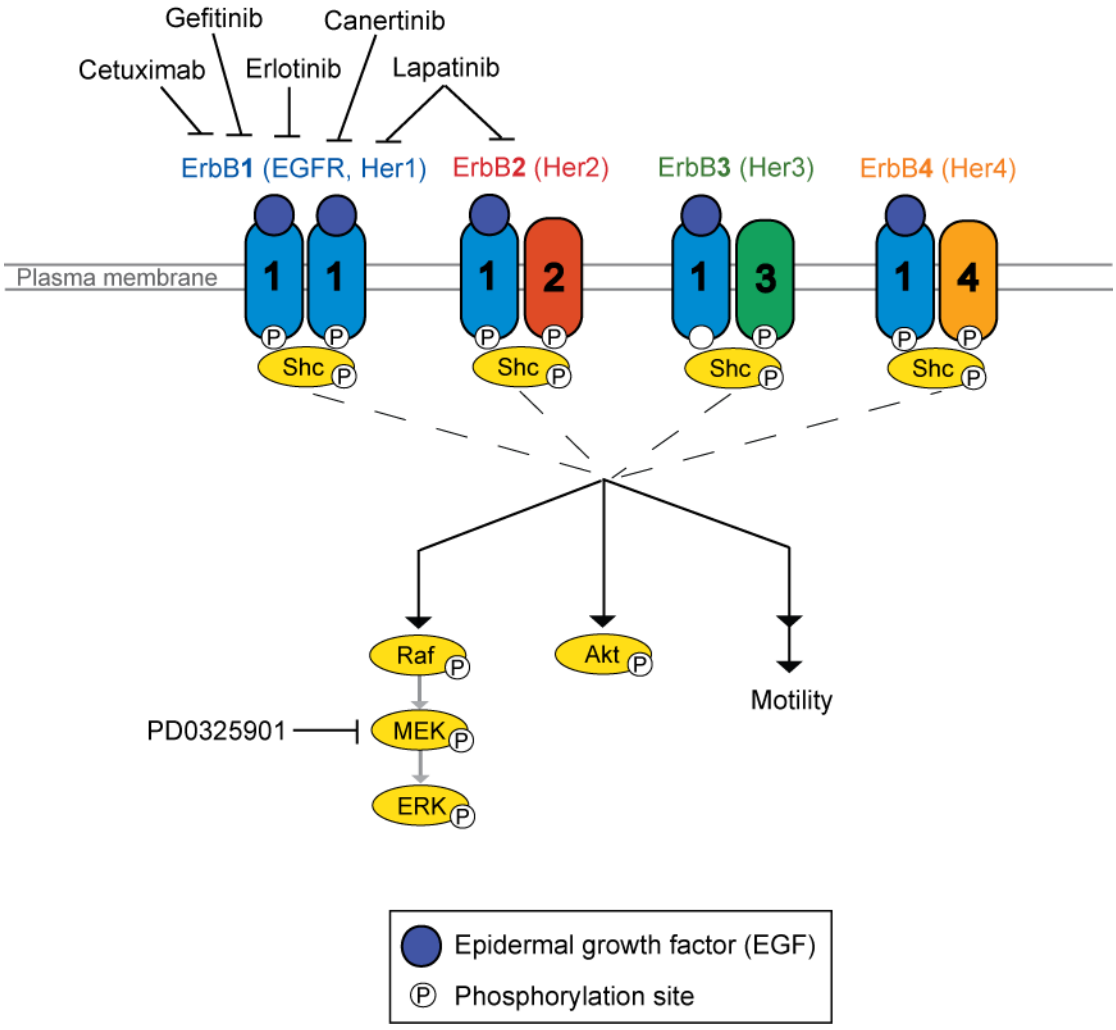

Figure 1.2 - Simplified illustration of immediate-early ErbB pathway activation initiated by binding of EGF to ErbB1.

EGF binds to ErbB1 directly and induces formation and phosphorylation of ErbB1-containing homo- and heterodimers. ErbB3 lacks catalytic activity so ErbB1 is not phosphorylated in an ErbB1-ErbB3 dimer. Binding of adaptor proteins such as Shc to the receptors leads to activation of many downstream proteins, including the canonical MAPK (Raf-MEK-ERK) and Akt kinase pathways. Targets of several inhibitors of the pathway are indicated.

Protein tyrosine phosphatases (PTPs)

Phosphatases can be divided into the following groups based on their substrate specificity: tyrosine-specific phosphatases, serine/threonine-specific phosphatases, dual specificity phosphatases (tyrosine as well as serine/threonine-specific), histidine phosphatases

and lipid phosphatases. Since activated ErbB1 becomes phosphorylated primarily on tyrosine residues following ligand stimulation (Olsen et al., 2006), phosphorylated ErbB1 is thought to be a target of various protein tyrosine phosphatases (PTPs). PTPs are characterized by the active site signature motif H**C**$(X)_5$**R** in the conserved catalytic domain. The cysteine residue in this motif acts as a nucleophile to attack the phosphorus atom of the phosphotyrosine residue of the PTP substrate, whereas the arginine residue interacts with the phosphate moiety of the phosphotyrosine. An invariant aspartic acid residue outside of the signature motif is also essential for catalytic activity and serves as the catalytic acid that protonates the phenolic oxygen of the tyrosyl leaving group (Zhang, 2002).

Interestingly, there are roughly the same number of tyrosine-specific phosphatases as kinases (Alonso et al., 2004; Manning et al., 2002). Approximately 100 members of the PTP family have been identified and can be divided into four classes based on the primary structure of their catalytic domains (Alonso et al., 2004). Class I PTPs is the largest group and is divided into classical PTPs, defined by cysteine-based phosphotyrosine specificity, and VH-1-like or dual specificity phosphatases (DSPs), which includes the MAPK phosphatases (MPKs) and PTEN. The classical PTPs can be further subdivided into transmembrane receptor PTPs (RPTPs) or non-transmembrane cytoplasmic PTPs (Fig. 1.3). Through their extracellular domains, RPTPs can bind soluble ligands and mediate cell-cell and cell-matrix interactions. Substrate specificity of non-transmembrane PTPs is conferred by their noncatalytic regulatory domains, which can regulate their activity, subcellular localization and interaction with other proteins. DSPs are non-transmembrane PTPs with a shallower catalytic pocket conformation (compared to PTPs that can only act on phosphotyrosines) that allows them to also interact with phosphoserines and phosphothreonines (Yuvaniyama et al., 1996). The other three classes of PTPs are very small: class II contains the low-molecular-weight phosphotyrosine phosphatase (LMPTP), class III contains CDC25A, B and C, and class IV contains Eya1-4. Most cells express 30-60% of all PTPs, however, hematopoietic and neuronal cells express a higher

number of PTPs in comparison to other cell types (Alonso et al., 2004). PTP signaling specificity is determined by their expression pattern, subcellular localization, post-translational modifications such as phosphorylation and oxidation that regulate PTP activity, and intrinsic structural differences within the PTP domain and noncatalytic domains.

Identification and characterization of PTPs and their substrates

PTPs have traditionally been identified and characterized using purified proteins, isolated membranes and permeabilized cells (Butler et al., 1989; Swarup et al., 1982). PTP function has typically been studied using *para*nitrophenyl phosphate or synthetic phosphopeptides as substrates *in vitro*. These reactions critically neglect what are now known to be important subcellular localization effects. A more accurate view of PTP regulation requires *in vivo* measurements. Various techniques have been used to identify physiological PTP substrates, such as dephosphorylation assays for substrates *in vitro*, modulating substrate tyrosine phosphorylation in cells (e.g. by increasing or decreasing expression of the PTP) and measuring the interaction of substrates with PTP substrate-trapping mutants. Mutagenesis of the invariant catalytic aspartate residue to alanine converts an active PTP enzyme into a "substrate trap" (Flint et al., 1997). These catalytically inactive PTPs form stable, phosphotyrosine-dependent associations with their substrates both *in vitro* and in cells.

Evidence for ErbB1 PTPs

The full spectrum of phosphatases acting on ErbB1 and their means of regulation are unknown, but many PTPs have been shown to interact with or have some specificity for ErbB1 (Tiganis, 2002). Much less is known about PTPs that act on the other ErbB receptors. The best characterized ErbB1 PTPs are PTP1B, Shp-1 and Shp-2. This section will describe in detail what is known about the regulation of ErbB1 by PTP1B, Shp-1 and Shp-2, and will then briefly discuss other potential ErbB1 PTPs.

PTP1B

Although PTP1B$^{-/-}$ mice show no obvious evidence of increased ErbB1 signaling, primary and immortalized PTP1B$^{-/-}$ fibroblasts exhibit increased and sustained ErbB1 phosphorylation following ligand stimulation (Frangioni et al., 1992). Similarly, in HeLa cells knockdown of PTP1B prolongs ErbB1 phosphorylation after EGF stimulation (Eden et al., 2010). Substrate-trapping mutants of PTP1B form a stable, phosphotyrosine-dependent complex with ErbB1 (Flint et al., 1997) and PTP1B displays specificity for ErbB1 Y992 and Y1148 (Milarski et al., 1993). The COOH-terminal extension of PTP1B contains a small hydrophobic stretch that is necessary and sufficient for targeting the enzyme to the cytoplasmic side of the endoplasmic reticulum (ER), where it resides (Frangioni et al., 1992). PTP1B-mediated dephosphorylation of ErbB1 thus requires receptor endocytosis (Reynolds et al., 2003), and the two proteins interact through direct membrane contacts between the perimeter membrane of multivesicular bodies and the ER (Eden et al., 2010). Following EGF stimulation and binding to ErbB1, PTP1B has been found to be tyrosine phosphorylated, and this phosphorylation correlates with a 3-fold increase in PTP catalytic activity (Liu and Chernoff, 1997).

Shp-1 and Shp-2

Shp-1 and Shp-2 contain two SH2 domains that face away from the active phosphatase domain and interact with phosphotyrosine containing peptides, and a C-terminal tail that can be phosphorylated by receptor-mediated kinase activity at two tyrosine sites. These phosphorylated sites can bind the SH2 domains, relieving basal autoinhibition and activating the PTP catalytic domain (Hof et al., 1998; Lu et al., 2001; Zhang et al., 2003). Phosphorylation of Shp-1 may also promote interactions with adaptor proteins such as Grb2 (Zhang et al., 2003), sequestering the PTP near its substrates (Neel et al., 2003). In this way, PTPs may use receptor-associated phosphorylation to modulate their own phosphatase catalytic activities.

Shp-1 negatively regulates signaling primarily in hematopoietic cells by dephosphorylating signaling molecules that promote signaling (Zhang et al., 2000). Shp-1 has been shown to bind ErbB1 at Y1173 through an SH2 domain (Keilhack et al., 1998), and both SH2 domains of Shp-1 appear to be important for binding to ErbB1 and receptor dephosphorylation.

Shp-2 positively regulates growth factor-induced signaling pathways in a wide variety of cell types (Feng, 1999). Shp-2 substrate-trapping mutants identified ErbB1 as an interactor and substrate (Agazie and Hayman, 2003a). Autophosphorylation sites on ErbB1 were mutated such that they could not become phosphorylated, and only the Y992F mutant did not now bind to the substrate trapping mutant of Shp-2 (Agazie and Hayman, 2003b). Furthermore, a dominant negative Shp-2 construct mutated in its phosphatase active site led to an increase in basal phosphorylation of ErbB1 Y992, and overexpression of wild-type Shp-2 decreased phosphorylation of this site (Sturla et al., 2005). GTPase-activating proteins (GAPs) can stimulate the low intrinsic GTPase activity of Ras, thus accelerating Ras deactivation. Dephosphorylation of ErbB1 Y992 has been shown to prevent p120RasGAP from being recruited to a complex to inactivate Ras (Agazie and Hayman, 2003b), and Shp-2 can also directly dephosphorylate RasGAP (Kontaridis et al., 2004). Thus, Shp-2 positively stimulates the Ras-MAPK pathway (Neel et al., 2003).

Other potential ErbB1 PTPs

A number of potential ErbB1 PTPs exist in addition to PTP1B, Shp-1 and Shp-2. To identify PTPs specific for ErbB1, an siRNA screen was performed where expression of each PTP was knocked down and the effect on basal and ligand-stimulated ErbB1 phosphorylation was measured. Knocking down DEP-1, a PTP that resides on the cell surface and does not internalize along with ErbB1, significantly increased basal ErbB1 phosphorylation (Tarcic et al.,

2009). EGF stimulation resulted in more ErbB1 receptors bound by substrate-trapping mutants of DEP-1, but no significant increase in receptors bound by wild-type DEP-1, suggesting that their interaction is transient.

Co-expression of ErbB1 and various RPTPs in cells lacking ErbB1 receptors enabled identification of RPTPκ as an enzyme capable of reducing ErbB1 phosphorylation (Xu et al., 2005). ErbB1 phosphorylation was also reduced upon inducible expression of RPTPσ (Suarez Pestana et al., 1999). Similarly, decreasing expression of the phosphatase LAR increased EGF-induced but not basal ErbB1 phosphorylation (Kulas et al., 1996). TCPTP was identified as an ErbB1 phosphatase (Tiganis et al., 1998) and is activated at the plasma membrane by a collagen-binding integrin to negatively regulate ErbB1 (Mattila et al., 2005). Although normally located in the nucleus, a substrate-trapping mutant of TC45 (a 45 kDa variant of TCPTP) co-localized with phosphotyrosine ErbB1 at the cell periphery within minutes of EGF stimulation (Tiganis et al., 1999).

The effects of modulating relative PTP/RTK expression levels were studied by transient co-overexpression of ErbB1 along with TCPTP, PTP1B or CD45 (Lammers et al., 1993). ErbB1 overexpression without PTPs led to a high level of basal ErbB1 phosphorylation with no significant increase after ligand stimulation. With expression of each of the three PTPs, the basal level of ErbB1 phosphorylation was almost completely suppressed and the receptor was able to respond to ligand. These experiments point to a high degree of redundancy in PTP regulation of ErbB1.

Dynamic regulation of ErbB1 PTPs after ligand stimulation

As described above, PTP activity can be dynamically regulated by various mechanisms following ligand-induced ErbB1 activation. Activating mechanisms include PTP phosphorylation, co-localization with ErbB1 and allosteric activation by binding directly to

activated ErbB1 via SH2 domains. Conversely, induction of hydrogen peroxide synthesis in EGF-treated cells transiently inhibits phosphatases such as PTP1B, thereby acting to increase net ErbB1 phosphorylation (Lee et al., 1998).

Deregulation of PTPs

While ErbB receptors are often overactive in cancer, potential ErbB1 phosphatases are also deregulated and play a role in promoting disease (reviewed in (Ostman et al., 2006)). DEP-1 is deleted or mutated in some cancers (Ruivenkamp et al., 2002) and decreased expression of DEP-1 leads to sustained ErbB1 signaling and hyperproliferation (Tarcic et al., 2009). Shp-1 is epigenetically silenced in leukemias and lymphomas (Oka et al., 2002). On the other hand, gain of function Shp-2 mutations have been identified in various malignancies such as hereditary and sporadic leukemias and Noonan syndrome (Fragale et al., 2004; Tartaglia et al., 2001; Tartaglia et al., 2003). PTP1B is upregulated in ErbB2-transformed cell lines (Zhai et al., 1993) and promotes tumorigenesis mediated by ErbB2. The majority of human breast tumors overexpress PTP1B (Wiener et al., 1994).

PTPs have been proposed to act as both tumor suppressors and oncogenes, and are being considered as drug targets. For example, PTP1B inhibitors are under development as anti-diabetic compounds (reviewed in (Johnson et al., 2002)). As discussed later in this thesis, developing selective phosphatase inhibitors is proving to be more challenging than targeting kinases.

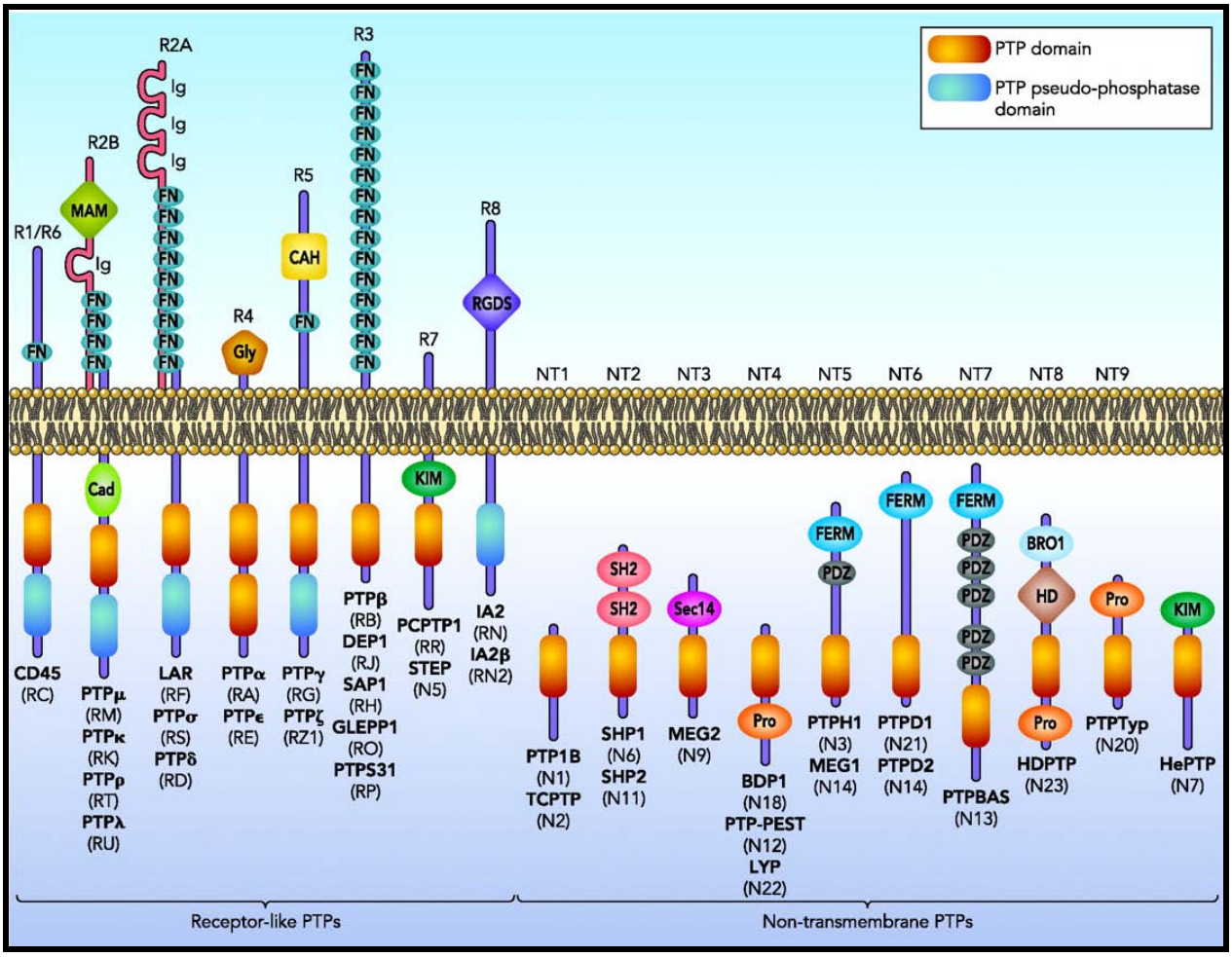

Figure 1.3 - The diverse family of classical protein tyrosine phosphatases (PTPs) includes both receptor-like and non-transmembrane PTPs.

BRO-1, BRO-1 homology; CAH, carbonic anhydrase-like; Cad, cadherin-like juxtamembrane sequence; FERM, FERM domain; FN, fibronectin type III-like domain; Gly, glycosylated; HD, histidine domain; Ig, immunoglobulin domain; KIM, kinase-interaction motif; MAM, mephrin/A5/μ domain; Pro, proline-rich; RGDS, RGDS-adhesion recognition motif; SEC14, SEC14/cellular retinaldehyde-binding protein-like; SH2, Src-homology 2. Figure reproduced from Soulsby, M., and Bennett, A.M. (2009). "Physiological signaling specificity by protein tyrosine phosphatases." *Physiology* 24, 281-289.

Hyperactivation of the ErbB pathway in cancer

ErbB1-3 receptors are frequently mutated, overexpressed or activated by autocrine or paracrine ligand production in solid tumors (Holbro and Hynes, 2004; Hynes and Lane, 2005; Sharma and Settleman, 2009) and have been the target of extensive drug discovery efforts (Sebastian et al., 2006). The ErbB pathway is further implicated in cancer through activating mutations in downstream signaling molecules (e.g. Cbl mutations in lung cancer (Tan et al., 2010) and B-Raf mutations in melanoma (Tuveson et al., 2003)) and inactivation of tumor suppressors (e.g. PTEN (Parsons, 2004)). Pharmaceutical companies are therefore aggressively targeting this pathway, and gaining a better understanding of how signals are propagated through this network and how alterations within the pathway deregulate signaling should help in this effort.

Drugs targeting the ErbB receptors

Multiple small molecule kinase inhibitors and therapeutic antibodies against ErbB receptors are in clinical use or development. The ErbB2-targeting antibody trastuzumab (Herceptin®) is a front-line therapeutic for ErbB2-overexpressing breast cancers (Nahta and Esteva, 2007). Cetuximab (Erbitux®; C225) is a chimeric monoclonal antibody that binds directly to the ligand-binding site on the extracellular domain of ErbB1 and is used to treat metastatic colorectal cancer and head and neck cancers (Gebbia et al., 2007; Maiello et al., 2007). Small molecule tyrosine kinase inhibitors compete with ATP for binding to the ErbB1 intracellular tyrosine kinase domain and inhibit receptor catalytic activity.

<u>ErbB1-specific small molecule kinase inhibitors</u>

Various 4-anilinoquinazoline derivatives have been exploited as selective and effective

ErbB inhibitors (inhibitor structures and information relevant to this thesis are shown in Fig. 1.4 and Table 1.1) (Johnson, 2009). Gefitinib (Iressa®; ZD1839) and erlotinib (Tarceva®; OSI-774) are selective tyrosine kinase inhibitors that bind reversibly to ErbB1 with high affinity and likely bind to ErbB1 when in an active or inactive conformation (Jecklin et al., 2009). Both drugs are used to treat non-small cell lung carcinoma and erlotinib is also approved to treat pancreatic cancer (Eck and Yun, 2009; Stamos et al., 2002; Yun et al., 2007). These drugs have been found to be particularly effective in tumors expressing mutated forms of ErbB1 (Eck and Yun, 2009).

An alternative approach has been to target ErbB1 using kinase inhibitors with non-canonical mechanisms of action, such as drugs that bind irreversibly or with a preference for the inactive conformation of the kinase (Liu and Gray, 2006). Canertinib (CI-1033) acts through covalent modification of a conserved cysteine residue present in the ErbB1 ATP binding pocket and thus binds to the receptor irreversibly (Fry et al., 1998). ErbB2 and ErbB4 contain the same active site cysteine and therefore are also inhibited by canertinib. Lapatinib (Tykerb®; GW572016) is a selective and reversible ATP-competitive dual ErbB1/ErbB2 inhibitor approved to treat patients with advanced or metastatic breast cancer whose tumors overexpress ErbB2. While the ATP binding cleft of ErbB1 complexed with erlotinib or gefitinib is more open (active), lapatinib-bound ErbB1 is in a relatively closed (inactive) conformation (Wood et al., 2004; Yun et al., 2007). A bulky aniline substituent off the quinazoline ring of lapatinib may make the compound unable to complex with the small back pocket found in the active-like conformation of ErbB1 (Wood et al., 2004).

Lapatinib also differs dramatically from gefitinib and erlotinib in that it binds to ErbB1 with slow kinetics. A very slow off rate for lapatinib dissociation from ErbB1 results in a long half life of ~220 minutes as opposed to a gefitinib half life of ~10 minutes (Gilmer et al., 2008; Wood et al., 2004). ErbB1 is no longer inhibited 24 hours after washing away erlotinib, but 72 hours after washing away gefitinib, receptors are still 40% inhibited (Wood et al., 2004). However, 96 hours

after washing away lapatinib, ErbB1 receptors are still 85% inhibited. Since these three drugs have similar dissociation constants for ErbB1, lapatinib also binds with a much slower on rate. Slower kinetics may be explained by the considerable structural differences between active and inactive ErbB1 kinase conformations and the notion that to bind and/or release lapatinib may require a conformational change in the receptor. Indeed, lapatinib is thought to stabilize the inactive-like ErbB1 conformation (Wood et al., 2004).

Use of inhibitors as tools to study signaling pathways

Deregulation of kinase activity is a common cause of various cancers, and kinases have thus been attractive drug targets. Imatinib (Gleevec®), an inhibitor of the Abl tyrosine kinase, has been extremely successful in patients with chronic myelogenous leukemia (Capdeville et al., 2002). Unfortunately, the search for other kinase inhibitors as successful as imatinib has proved to be very challenging and may be partially due to our still primitive understanding of the function and regulation of protein kinases, phosphatases, and their substrates and effectors. Beyond their use as therapeutics, kinase and phosphatase inhibitors are useful tools to probe signaling states and can potentially reveal rapid (short-term) kinetics, as opposed to genetic and conventional biochemical approaches such as RNAi that typically only elucidate the effects on steady state behavior. In this thesis, we use potent kinase and phosphatase inhibitors to study the ErbB signaling network in cells and examine the time scales of phosphorylation events.

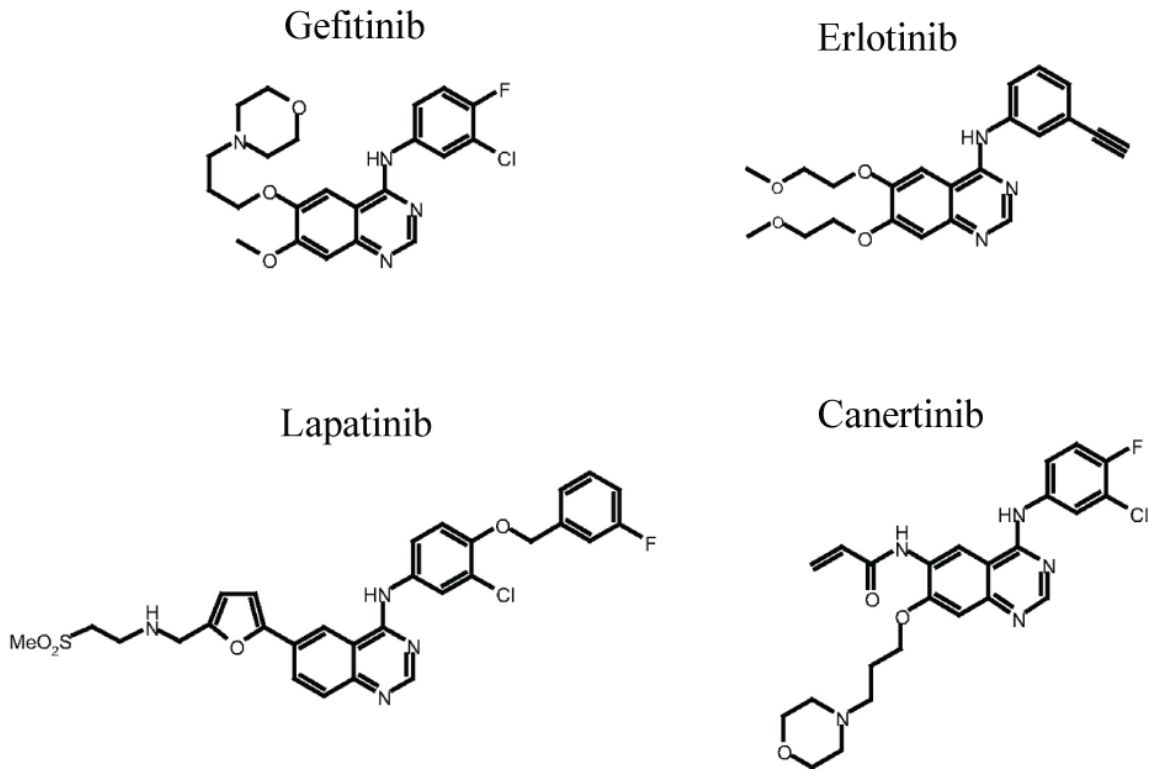

Figure 1.4 – Structures of ATP-competitive small molecule kinase inhibitors targeting the ErbB receptors.

Figure adapted from Wood, E.R., Shewchuk, L.M., Ellis, B., Brignola, P., Brashear, R.L., Caferro, T.R., Dickerson, S.H., Dickson, H.D., Donaldson, K.H., Gaul, M., et al. (2008). "6-Ethynylthieno[3,2-d]- and 6-ethynylthieno[2,3-d]pyrimidin-4-anilines as tunable covalent modifiers of ErbB kinases." *Proc Natl Acad Sci* U S A 105, 2773-2778. © 2008 National Academy of Sciences, U.S.A.

Table 1.1 – Dissociation constants, mechanisms of action and FDA approval status of ErbB-targeting kinase inhibitors.

Lower binding results (K_d values) indicate higher affinity. Since ErbB3 lacks catalytic activity it is not inhibited by these drugs. K_d values were reproduced with permission from Macmillan Publishers Ltd: Karaman, M.W., Herrgard, S., Treiber, D.K., Gallant, P., Atteridge, C.E., Campbell, B.T., Chan, K.W., Ciceri, P., Davis, M.I., Edeen, P.T., et al. (2008). "A quantitative analysis of kinase inhibitor selectivity." *Nat Biotechnol* 26, 127-132. Erlotinib binding to ErbB2 was weak (K_d > 10μM) or not detected in a primary screen (10μM). Slightly different values are reported in other sources (Wood et al., 2004).

	ErbB1 (nM)	ErbB2 (nM)	ErbB4 (nM)	Mechanism of binding to ErbB1	US FDA-approved indication
Gefitinib	1	3,500	410	Fast binding to active conformation	Lung cancer
Erlotinib	0.67	>10,000	230	Fast binding to active conformation	Lung and pancreatic cancers
Lapatinib	2.4	7	54	Slow binding to inactive conformation	Breast cancer
Canertinib	0.19	87	29	Irreversible binding	Not approved

Inhibitors elucidate the dynamic opposition of phosphorylation and dephosphorylation

Despite their importance as prototypical RTKs, oncogenes and drug targets, regulation of ErbB receptors through the interplay of conformational change, phosphorylation, phosphatases and receptor trafficking remains poorly understood, and the impact of these dynamics on physiological activity and cellular responses to anti-ErbB drugs is largely unknown. The rapid rise in ErbB1 tyrosine phosphorylation within the first 10 minutes of ligand stimulation is thought to reflect kinase activation, and the gradual fall from approximately 10 to 90 minutes the time required to internalize and degrade active signaling complexes.

However, several experiments hint at a much more dynamic balance between activation and inactivation than assumed by the standard model. The potent pan-specific tyrosine phosphatase inhibitor pervanadate (the combination of vanadate and hydrogen peroxide) is commonly used to study PTP activity in cells due to a lack of good inhibitors of specific PTPs (Gordon, 1991; Huyer et al., 1997; Zhao et al., 1996). The activity of PTPs is tightly regulated *in vivo* by oxidation and reduction reactions involving the invariant cysteine in the PTP catalytic domain. Pervanadate irreversibly inhibits PTPs such as PTP1B by oxidizing their catalytic cysteine (Huyer et al., 1997). Treatment of cells with pervanadate causes an immediate and large increase in phosphorylation of ErbB1 (and many other proteins) in the absence of added ligand (e.g. (Reynolds et al., 2003)), implying auto-activation that is continuously opposed by phosphatases.

Similarly, sequential exposure of cells to ligand and small molecule kinase inhibitors causes phosphorylation to fall rapidly (Bohmer et al., 1995; Offterdinger et al., 2004; Yudushkin et al., 2007). These dynamics have primarily been measured by live-cell imaging techniques with the purpose of showing reversibility of probes for ErbB1 phosphorylation. In an elegant study, a sensor for ErbB1 tyrosine phosphorylation was constructed by fusing a YFP-tagged

PTB domain of the adaptor protein Shc to CFP-tagged ErbB1 (Fig. 1.5A) (Offterdinger et al., 2004). Intramolecular binding of the PTB domain to specific phosphotyrosine residues on ErbB1 provides a readout of the phosphorylation state of ErbB1 and was monitored by forester (fluorescence) resonance energy transfer (FRET) in cells expressing this construct. After two minutes of EGF stimulation, an ErbB1-specific tyrosine kinase inhibitor was added and led to reversion of the YFP/CFP fluorescence emission ratio changes (Fig. 1.5B & C). These experiments hint at rapid dephosphorylation of drug-bound ErbB1 even in the continued presence of ligand.

While useful for tracking real-time dynamics and subcellular localization within a single cell, live-cell imaging approaches have some limitations that may influence the interpretation of these measurements. Typically, artificial constructs are overexpressed in cells lacking the target protein, and overexpression may misrepresent the dynamics of endogenous kinases. Activation of substrates of the target protein is often measured in live-cell microscopy and these measurements are therefore indirect with a time delay between phosphorylation of the target protein and the readout. Furthermore, the activity of only one protein is normally monitored in live-cell microscopy, yet it is important to understand how that protein functions within a signaling network. Nonetheless, the ErbB1 dephosphorylation kinetics described above seem to have profound implications for the dynamic regulation of ErbB1 activity by PTPs and the time scale of ErbB1 phosphorylation cycling. A mechanistic study of these dynamics and their functional consequences is thus warranted.

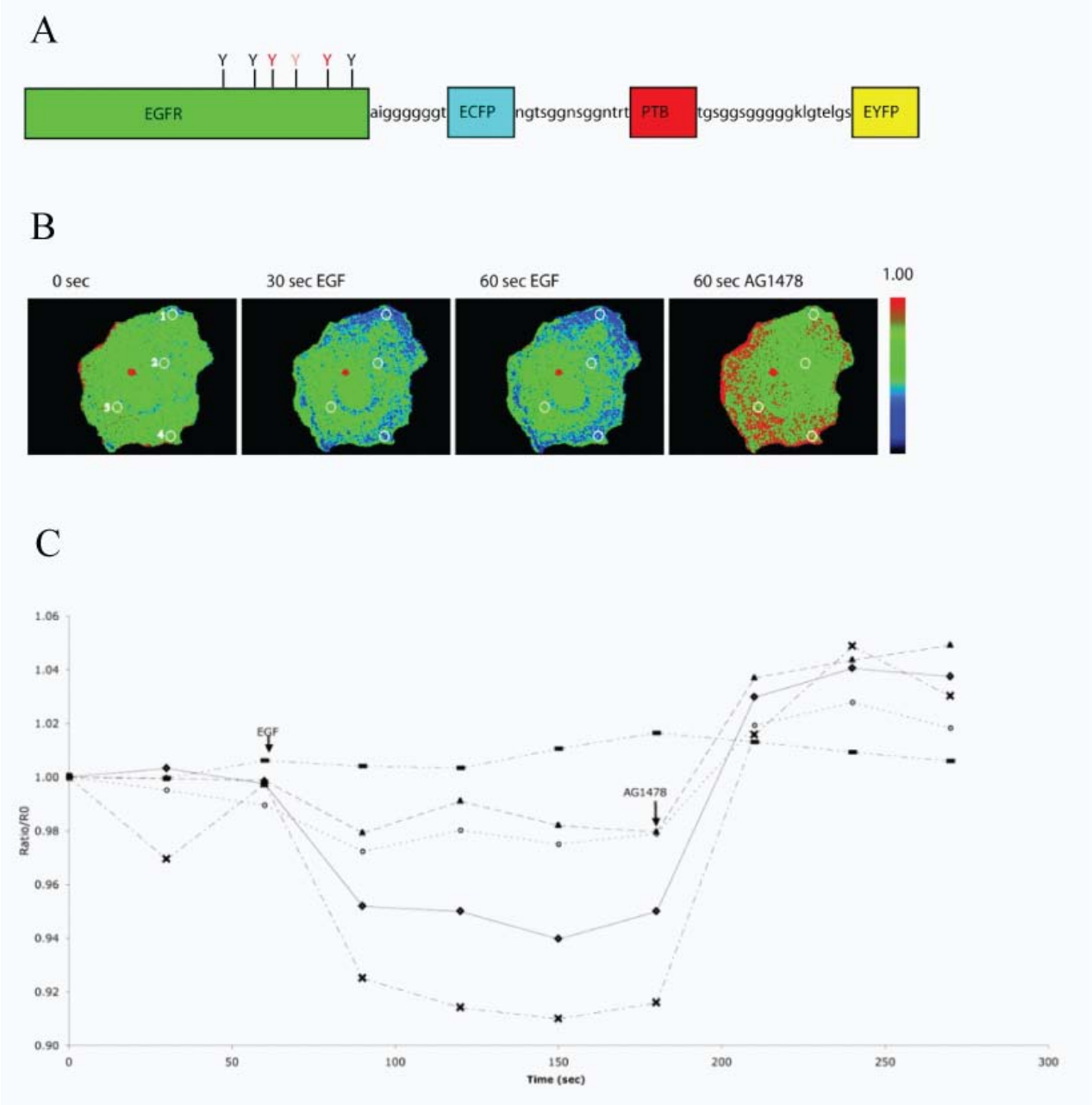

Figure 1.5 - Ratiometric imaging of COS7 cells after EGF stimulation and kinase inhibition.

(A) Fusion construct of ErbB1 (EGFR) and the PTB domain of Shc ("FLAME"). ECFP, enhanced cyan fluorescent protein; EYFP, enhanced yellow fluorescent protein; Y, tyrosine residues on ErbB1. Potential PTB domain binding sites are highlighted in red and light red. (B) COS7 cells expressing FLAME were stimulated with 100 ng/ml EGF. EYFP/ECFP ratios are presented. AG1478 (100 nM), an ErbB1-specific tyrosine kinase inhibitor, was added after 2 minutes of EGF stimulation. (C) Quantitation was performed in four regions of interest (white circles) or on the whole image for FLAME_F5 (a construct where all major autophosphorylation sites were knocked out by replacing tyrosine residues with phenylalanine residues). Region of interest 1, X; region of interest 2, ○; region of interest 3, △; region of interest 4, ⋄; cells expressing FLAME_F5, -. This research was originally published in Journal of Biological

Specific goals of this thesis and key findings

This thesis examines ErbB receptor phosphorylation dynamics following stimulation of cells with exogenous ligand. The experiments involve the exposure of cells to EGF or other ligands followed by a kinase or phosphatase inhibitor (“pulse-chase” experiments) and biochemical assays that measure receptor modification. Relative to earlier studies, our experiments benefit from potent and selective kinase inhibitors, many of which are therapeutic drugs, and phospho-specific antibodies. More importantly, we analyze pulse-chase data using a series of computational models of receptor enzymology that help us interpret the experimental data and make it possible to derive quantitative information on receptor dynamics. Although multiple models of ErbB signaling have previously been developed, we find it necessary to build new models to accurately describe regulation of ErbB1 phosphorylation, and no one model was sufficient to address all aspects of ErbB regulation by phosphatases and drugs.

We arrive at lower bounds for the rate of phospho-ErbB1 turnover showing receptors to cycle rapidly between being phosphorylated and dephosphorylated on the time scale of seconds, in stark contrast to the 30 minutes or so suggested by standard biochemical analysis. Rapid phosphorylation and dephosphorylation of receptors has important implications for the assembly dynamics of signalosomes and results in strikingly different dose-response behaviors for different ErbB1-targeting drugs. Our revised view of receptor dynamics may also help explain why some anti-ErbB1 drugs are more effective in the clinic than others.

CHAPTER 2: Results

The material in this thesis is an extended version of a manuscript to be submitted for publication:

Coupled fast and slow dynamics regulate ErbB1 signaling
Laura B. Kleiman, Holger Conzelmann, Thomas Maiwald, Douglas A. Lauffenburger and Peter K. Sorger

(All experiments were performed by Laura Kleiman. Mathematical modeling was done by Laura Kleiman in collaboration with Holger Conzelmann and Thomas Maiwald.)

The dynamics of ErbB receptor activation and inactivation were analyzed in the well-characterized H1666 human non-small cell lung carcinoma (NSCLC) cell line that expresses only wild-type ErbB1 receptors (Paez et al., 2004). Receptor expression levels are lower and presumably more physiological in H1666 cells (~10^5 molecules per cell, see Chapter 4) than in lines such as A431 commonly used to study ErbB1 (~10^6 molecules per cell (Kwok and Sutherland, 1991)). Moreover, NSCLC is an important target of anti-ErbB1 therapy and the H1666 line is often considered to be representative of NSCLC lines lacking drug-sensitizing ErbB1 mutations (e.g. (Mukohara et al., 2005)). Following serum starvation to lower the level of basal phosphorylation, H1666 cells were treated with epidermal growth factor (EGF), an ErbB1 ligand, at 100ng/ml (t=0) and levels of total ErbB1 and phosphorylated ErbB1 on tyrosine 1173 (pY1173) were measured using a variety of methods, including immunofluorescence, ELISA assays and Western blotting. Y1173 is a physiologically important site on the ErbB1 tail to which the adaptor protein Shc binds. Levels of pY1173 increased after EGF addition, peaking at ~4.5-fold over unstimulated levels at t=10 min, declining slowly thereafter and returning to pre-stimulus levels by t~2 hours; over this period total receptor levels also declined (Fig. 2.1A). If we assume simple exponential decay from peak total or phosphorylated receptor levels (see Chapter 4), the estimated half lives ($t_{1/2}$) of total and phosphorylated receptor are ~30 minutes.

Next we performed a pulse-chase experiment by treating cells with 100ng/ml EGF (the pulse) and subsequently with the ATP-competitive ErbB1 kinase inhibitor gefitinib (the chase) at 10μM. Gefitinib (Iressa®) is a potent ErbB1 inhibitor approved for the treatment of NSCLC (Eck and Yun, 2009) whose selectivity has been established using a variety of kinome profiling methods (Karaman et al., 2008). Measurable pY1173-ErbB1 levels fell rapidly ($t_{1/2}$ ~6 sec; see Chapter 4 for details) in the presence of gefitinib (Fig. 2.1B; ~4-fold decrease in signal within the first minute). Western blotting revealed no detectable decrease in total ErbB1 levels over the short time period (30 seconds) during which gefitinib promoted loss of the pY1173-ErbB1 signal

(Fig. 2.1C). Thus, ErbB1 appeared to be dephosphorylated rather than degraded following gefitinib addition. Similarly rapid ErbB1 dephosphorylation was observed by ELISA assays at six other tyrosine phosphorylation sites for which selective antibodies are available (Fig. 2.1D) and for ErbB1 agonists other than EGF (e.g. amphiregulin; not shown). Rapid dephosphorylation of pY1173-ErbB1 was also observed in gefitinib-treated non-transformed MCF-10A mammary epithelial cells (Fig. 2.1E) and in several other tumor cell lines (A549, H3255 and PC9 cells; not shown). Thus, addition of gefitinib after an EGF pulse causes rapid receptor dephosphorylation, resulting in a half life for active receptor of ~6 seconds in contrast to ~30 minutes in cells treated with EGF alone. In the former case receptors must cycle rapidly between phosphorylated and unphosphorylated states in a kinase-dependent manner, a point we examine in much greater detail below.

The best characterized protein tyrosine phosphatase (PTP) for ErbB1, PTP1B, resides in the endoplasmic reticulum (ER) (Frangioni et al., 1992; Reynolds et al., 2003) and we therefore wondered whether these proteins have to be co-localized for ErbB1 dephosphorylation. PTP1B is thought to interact with ErbB1 in perinuclear regions of the cell ~30 minutes after EGF stimulation (Haj et al., 2002). Immunofluorescence of ErbB1 in EGF-stimulated cells showed receptor to be present largely on the plasma membrane at t=2 min but by t=10 min receptor was substantially internalized and in early endosomes, and by t=30 min presumably in late endosomes (Fig. 2.2A; (Oksvold et al., 2000)). However, when gefitinib was added at t=10 min and receptor localization then examined one minute later (at which point pErbB1 levels had fallen to background levels) no change in receptor localization was observed (Fig. 2.2A). Moreover, when gefitinib was added at different times after exposure of cells to EGF (t=2 to 30 min), pY1173-ErbB1 had a similarly short half life despite the fact that the bulk of the receptor was transiting from the cell surface to internal compartments (Fig. 2.2B). We therefore conclude that ErbB1 is rapidly dephosphorylated regardless of its localization in the cell, implying that the receptor is continuously accessible to PTPs.

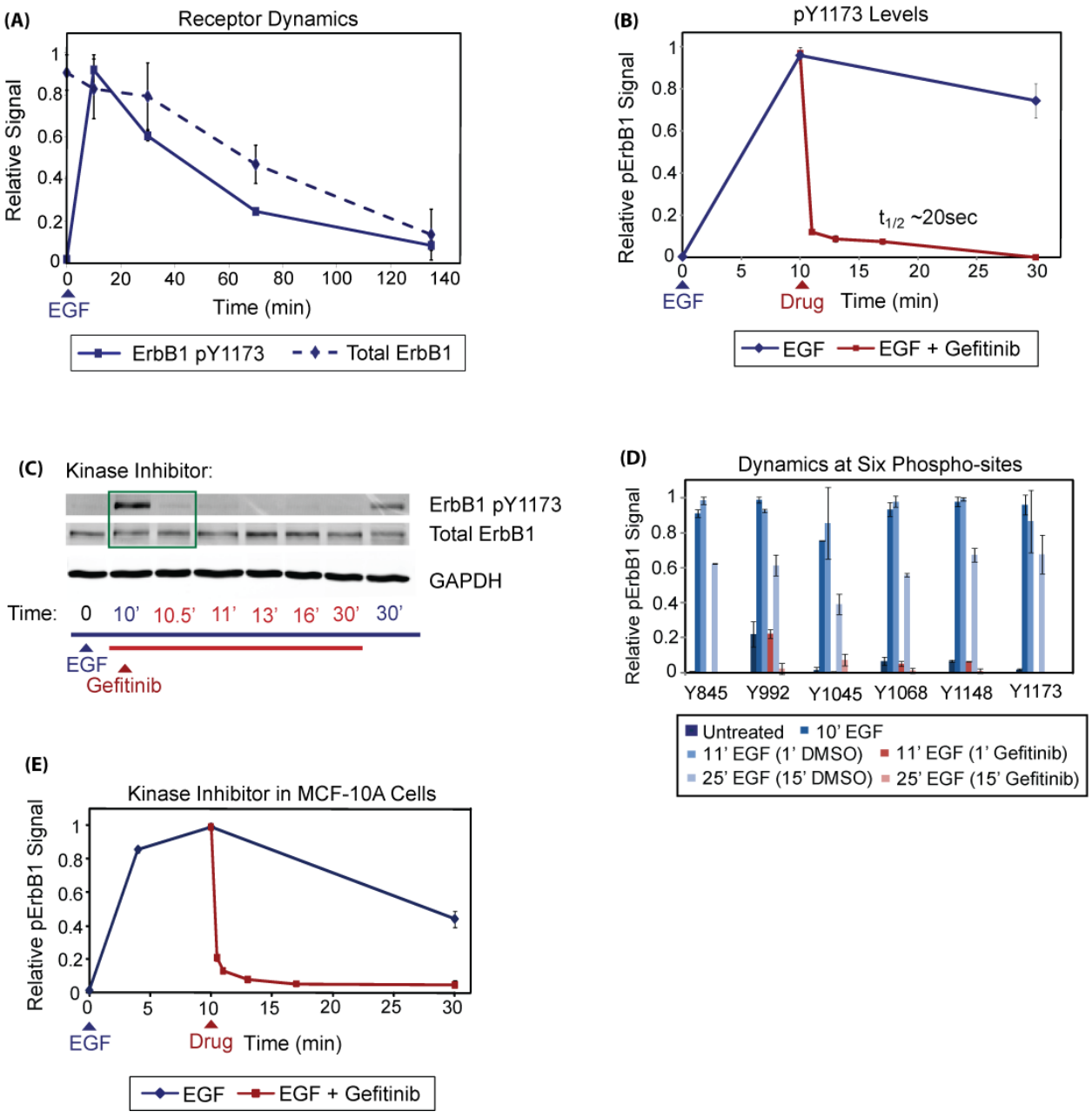

Figure 2.1 – ErbB1 is rapidly dephosphorylated in the presence of 10μM gefitinib.

High-throughput fluorescence microscopy (HTM) measurements of total (cell surface and internal) or phosphorylated (Y1173) ErbB1 dynamics after stimulation of H1666 cells with 100ng/ml EGF followed by addition of 10μM gefitinib after 10 minutes (unless otherwise noted). The average and standard deviation of triplicate measurements is plotted. (A) Receptor dynamics for EGF stimulation only. The two time courses were normalized separately and the intensity values are not comparable. (B) ErbB1 dephosphorylation dynamics in the presence of gefitinib. (C) ErbB1 dephosphorylation with gefitinib as measured by Western blotting. (D) Dephosphorylation of ErbB1 on six different phospho-sites by ELISA. These data are from the non-targeting (NT) siRNA controls in Fig. 2.8D. (E) Effects of gefitinib in MCF-10A non-transformed mammary epithelial cells.

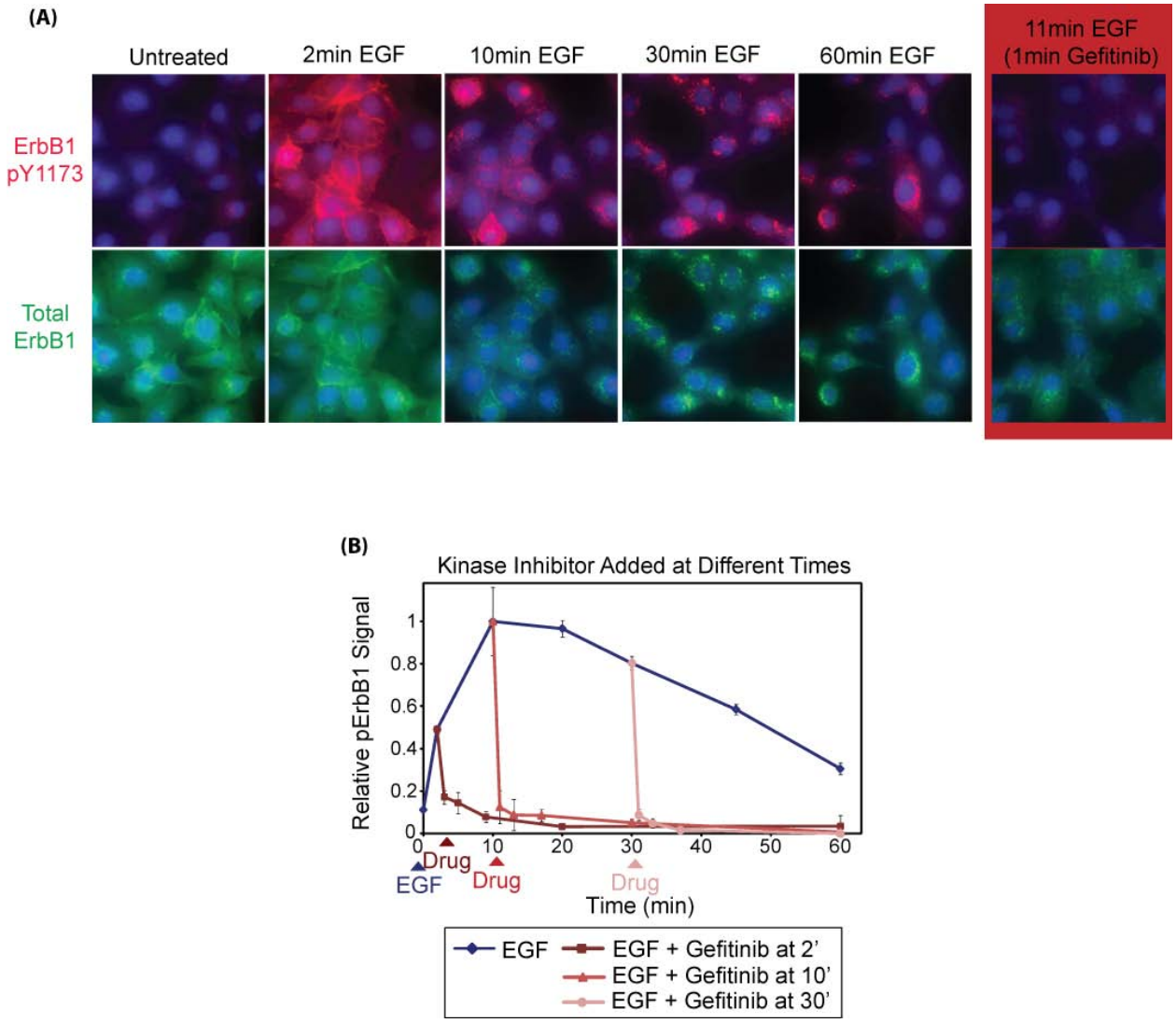

Figure 2.2 – Rapid ErbB1 dephosphorylation regardless of intracellular localization.

High-throughput fluorescence microscopy (HTM) measurements of total (cell surface and internal) or phosphorylated (Y1173) ErbB1 dynamics after stimulation of H1666 cells with 100ng/ml EGF followed by addition of 10μM gefitinib. (A) H1666 cells treated with 100ng/ml EGF. In the indicated well gefitinib was added after 10 minutes of EGF. Green = total ErbB1, Red = ErbB1 pY1173, Blue = Hoechst and protein dye. (B) Gefitinib addition after 2, 10 or 30 minutes of EGF and ErbB1 phosphorylation was measured.

ErbB1 receptors rapidly dephosphorylated were actively signaling

Is the pool of pErbB1 receptors that is rapidly dephosphorylated following gefitinib treatment the pool that is active in signaling to downstream pathways? To answer this question we assayed activating phosphorylation levels on several direct and indirect ErbB1 targets including co-receptors, adaptor proteins, and components of the ERK and Akt kinase cascades. We reasoned that by showing these downstream proteins to be phosphorylated and dephosphorylated with similar kinetics to ErbB1 following EGF pulse/gefitinib chase we could establish functional consequences for rapid pErbB1 turnover. ErbB2 and ErbB3 are known to be phosphorylated following EGF stimulation of cells (Wolf-Yadlin et al., 2006), presumably by ErbB1 since EGF binds with high affinity only to ErbB1 (Linggi and Carpenter, 2006). In H1666 cells both ErbB2 Y1221/1222 (a Shc-binding site) and ErbB3 Y1289 (a PI3K-binding site) (Schulze et al., 2005) were rapidly phosphorylated following EGF addition and were then rapidly dephosphorylated upon subsequent addition of gefitinib at t=10 min ($t_{1/2}$ ~15 sec and 32 sec, respectively; Fig. 2.3A). The SH2- and PTB-containing adaptor protein Shc was also phosphorylated rapidly upon EGF addition, concomitant with binding to ErbB1, as assayed by co-immunoprecipitation (Fig. 2.3B). Upon subsequent addition of gefitinib, pShc was rapidly dephosphorylated ($t_{1/2}$ ~26 sec) and it then dissociated from receptor complexes (Fig. 2.3A & B). SH2 and PTB domains are thought to protect phosphotyrosine residues from the action of phosphatases (Brunati et al., 1998; Lammers et al., 1993; Rotin et al., 1992) but our data suggest that the Shc-pErbB1 interaction is too transient to significantly protect modified receptors. This is consistent with fast association and dissociation rates reported for interactions of various SH2 and PTB domains with tyrosine phosphorylated proteins (Felder et al., 1993; Zhou et al., 1995).

The PI3K-Akt and MAPK (Raf-MEK-ERK) kinase cascades are two of the canonical signaling pathways downstream of ErbB1 and both are activated in H1666 and MCF-10A cells

following growth factor stimulation. Upon EGF addition, levels of active pS473-Akt increased in both cell lines and then fell rapidly upon subsequent exposure to gefitinib at t=10 min ($t_{1/2}$ ~80 sec; Fig. 2.4). The same was true of pT202/Y204-ERK1/2 in MCF-10A cells, although ERK was dephosphorylated slightly slower than Akt ($t_{1/2}$ ~211 sec; Fig. 2.4). In H1666 cells however, the rate of ERK dephosphorylation was significantly slower ($t_{1/2}$ >10 min), implying either that ERK phosphatases are not as active as in MCF-10A cells or that the activating signal is longer lived. Treatment of EGF-stimulated H1666 cells with the small molecule MEK kinase inhibitor PD0325901 at t=10 min resulted in rapid ERK dephosphorylation ($t_{1/2}$ ~43 sec; Fig. 2.4) however, arguing against the former hypothesis. We speculate that the mutant Raf found in H1666 cells (Pratilas et al., 2008) may be involved in extending the duration of signaling. For the current discussion the important point is that EGF-induced Akt phosphorylation in H1666 and MCF-10A cells and ERK phosphorylation in MCF-10A cells are subject to negative regulation following gefitinib addition with similar fast kinetics as pErbB1. We therefore conclude that the pool of ErbB1 receptors subject to rapid dephosphorylation represents the pool of receptors active in signal transduction. We turn to a kinetic analysis of receptor biochemistry to further interpret these dynamics.

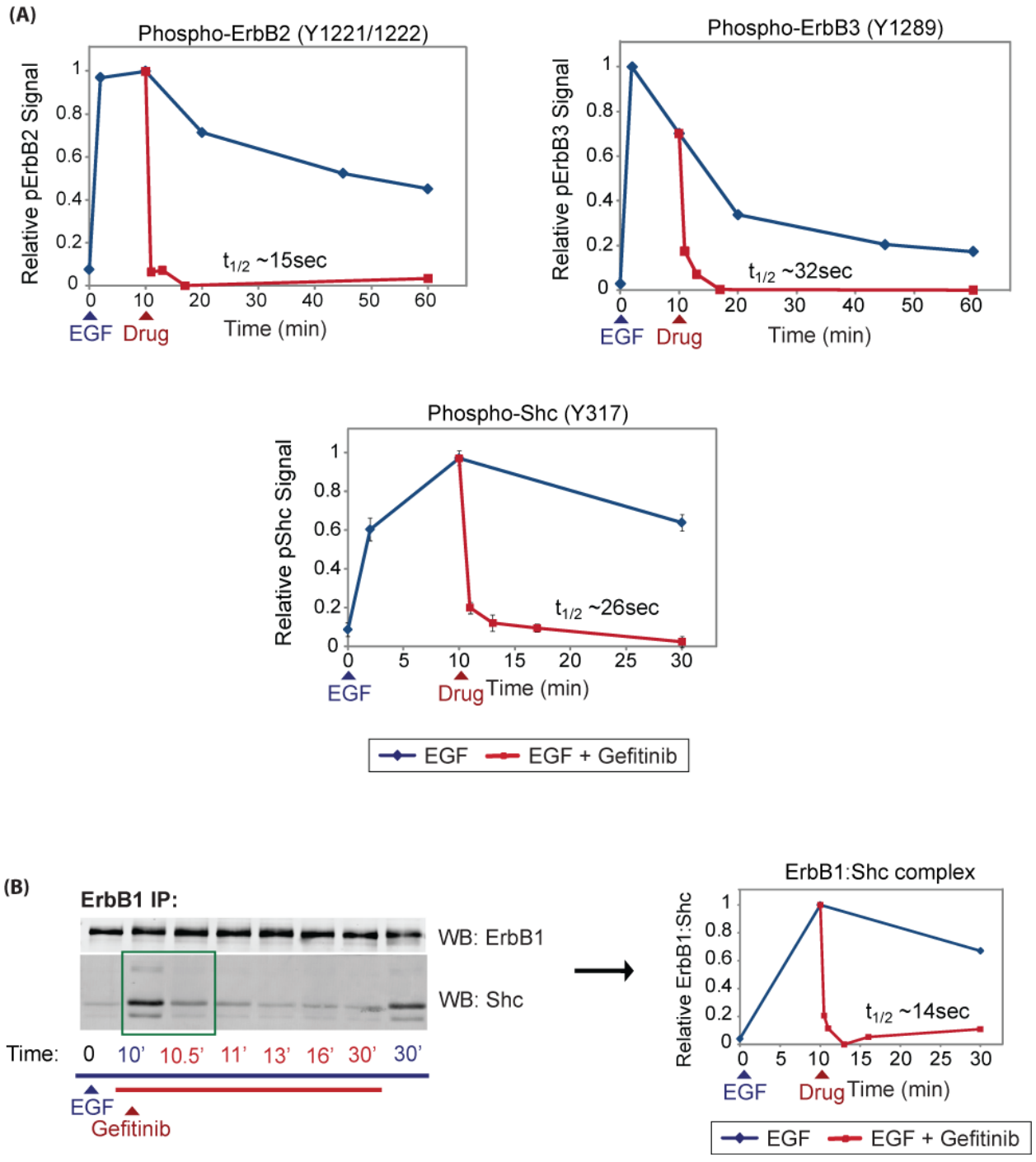

Figure 2.3 – Rapid dephosphorylation of ErbB2, ErbB3 and Shc after ErbB1 inhibition.

Stimulation of H1666 cells with 100ng/ml EGF followed by addition of 10µM gefitinib after 10 minutes. (A) Rapid dephosphorylation of ErbB2, ErbB3 and Shc. Phosphorylation of ErbB2 and ErbB3 were measured by ELISA and Shc phosphorylation was measured by HTM. (B) Co-immunoprecipitation of ErbB1 and Shc (left). Quantification (right) was done by background correction and normalizing to the total amount of ErbB1 immunoprecipitated for each sample. The three Shc bands are different Shc isoforms.

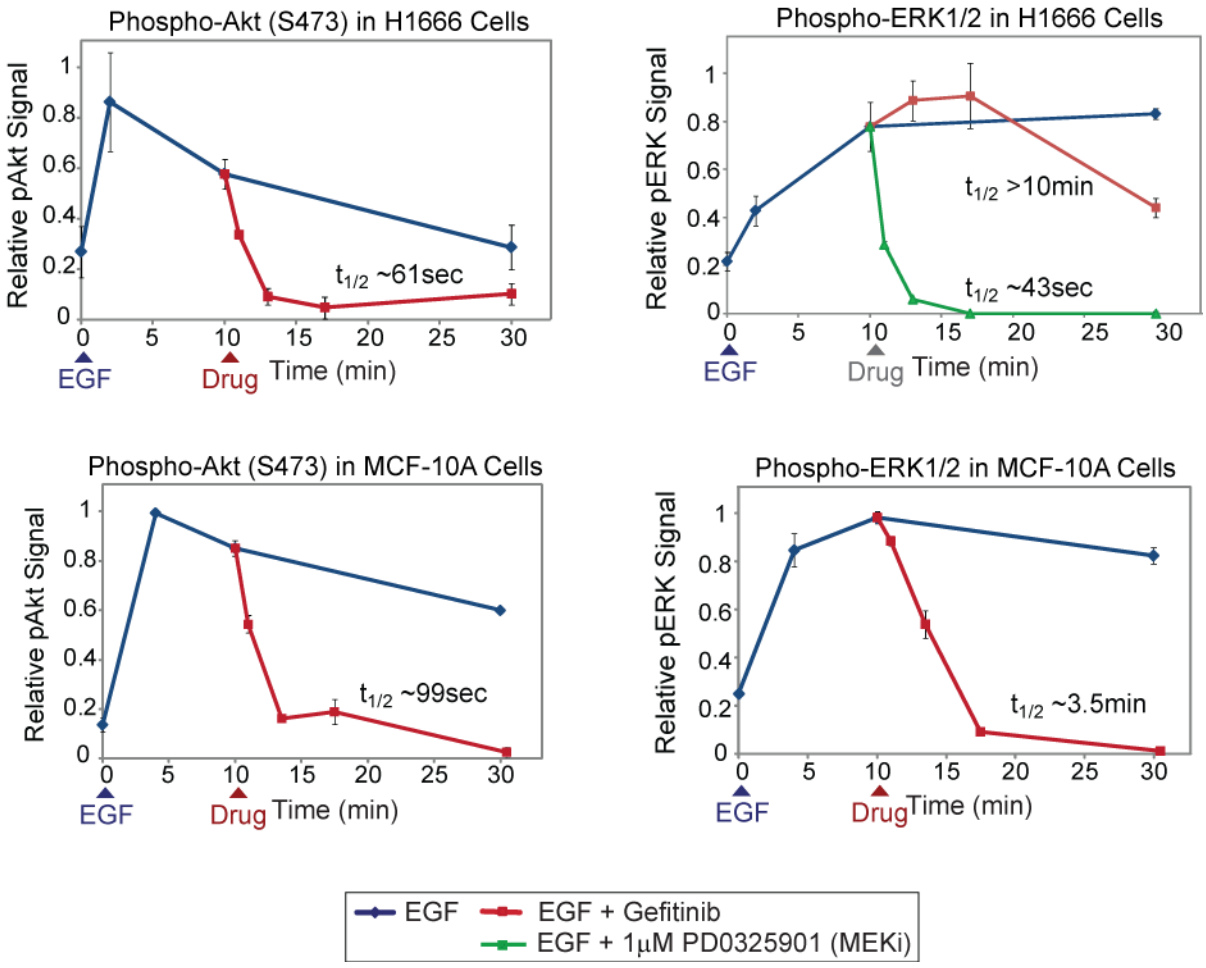

Figure 2.4 – Dephosphorylation dynamics of the Akt and ERK pathways.

Measurements of Akt (left) or ERK (right) phosphorylation by high-throughput fluorescence microscopy (HTM) after stimulation of H1666 or MCF-10A cells with 100ng/ml EGF followed by addition of 10μM gefitinib or 1μM PD0325901 (an allosteric MEK inhibitor) added after 10 minutes.

Estimating rates of phospho-ErbB1 turnover using a kinetic model

Mass-action models based on sets of coupled differential equations represent the simplest means to encapsulate different kinetic schemes of receptor regulation. By incorporating data from previous studies and by calibrating models against time course data collected from EGF and drug-treated cells, we can estimate the values of rate constants that appear in the models as free parameters. In formulating models we have a choice: with the

simplest models, available data can uniquely specify parameter values (that is, uncertainty arises only from experimental error), but the models are not particularly realistic. Complex models incorporate more of the known or suspected biochemistry of ErbB regulation, but parameter values cannot be fully constrained (the models are non-identifiable given the data). For some parameters, calibration is expected to yield a narrow range of estimated values, but for other parameters values can assume a much wider range without altering model output. In an attempt to balance competing demands of biological realism and model identifiability, we constructed a series of models of increasing complexity. In each case, we performed additional experiments to improve parameter estimation or to test specific model predictions. Both simple and complex models are most consistent with the view that ErbB phosphorylation is antagonized by potent phosphatases. However, many results can only be explained using relatively complex models, thereby justifying the complexity and adding additional insight to our analysis.

We estimate rate constants for both ErbB1 dephosphorylation and degradation in the presence of EGF only to be ~0.02/min by fitting a simple exponential decay ODE model to the experimental data. However, in the presence of gefitinib we estimate an ErbB1 dephosphorylation rate constant of ~7/min. If we assume that 40% of receptors are phosphorylated after 10 minutes of EGF stimulation (40,000 molecules per cell; see Chapter 4), these rate constants correspond to ~5,000 receptors per cell dephosphorylated within the first second after drug addition, compared to ~10 receptors in the presence of EGF only. This suggests that individual receptors are constantly undergoing cycles of phosphorylation and dephosphorylation and that these cycles are masked in measurements of population-level phosphorylation dynamics after treatment with ligand alone.

The exponential decay model is the simplest model to describe ErbB1 dephosphorylation dynamics and does not allow for any mechanistic insight or for estimates of the receptor phosphorylation rate. To deduce the frequency with which individual receptors

cycle between being phosphorylated and dephosphorylated, we developed a slightly more detailed biochemical scheme that describes how the concentration of phosphorylated receptors changes over time in the presence and absence of gefitinib (Fig. 2.5A). From this scheme we built a simple computational model and then attempted to infer the rate constants. To calibrate the model and constrain it as much as possible, we measured the effects of 1, 10 and 20μM gefitinib, added at t =10 min after EGF stimulation, on pY1173-ErbB1 dephosphorylation with dense temporal sampling (including 10, 20 and 30 seconds after drug addition) (Fig. 2.5B). Surprisingly, 1μM gefitinib resulted in very rapid dephosphorylation with no further decrease after the initial ~50% drop. We aimed to characterize this fast dephosphorylation of ErbB1 immediately following gefitinib addition, and therefore, in this scheme we only considered reactions we believed to be important from t=10-20 min after EGF stimulation of H1666 cells.

During this time, maximum ErbB1 phosphorylation has been reached and the average level of phosphorylation stays approximately constant; slow processes such as ligand binding, dimerization and degradation are likely not changing significantly so we do not describe these processes. Moreover, we consider only ErbB1 receptors in this model since H1666 cells express considerably more of these receptors than other ErbB receptors (see Chapter 4), and thus, after cells are stimulated with EGF we expect ErbB1 homodimers to be the predominant oligomer. ErbB1 species in the model describe individual receptors that are in a homodimeric state. Because the six ErbB1 phosphotyrosine sites we examined have similar dynamics (Fig. 2.1D) we use easily measured pY1173-ErbB1 dynamics as a proxy for all sites. We assume that all receptors are phosphatase-bound and that adaptor proteins do not bind to phosphotyrosine sites to protect them from dephosphorylation (Brunati et al., 1998; Lammers et al., 1993; Rotin et al., 1992), which is reasonable due to the observed fast dynamics.

To extract kinetic data from this scheme, we assume that the ErbB1 phosphorylation rate effectively decreases with increasing concentrations of gefitinib, and that gefitinib binding and phosphorylation are independent. We are able to estimate a phosphorylation rate constant

that is independent of the gefitinib concentration by calculating the fraction of receptors bound by gefitinib and therefore unable to become phosphorylated (f_G), assuming that gefitinib binding is in pseudo-equilibrium, a reasonable assumption since gefitinib binding is likely diffusion limited (Northrup and Erickson, 1992). We can calculate f_G because we have experimental measurements for the effects of modulating the gefitinib concentration. In this scheme, ATP is implicitly bound to ErbB1 due to high cellular ATP concentrations (Lehninger et al., 2000), but gefitinib is allowed to bind and once bound the receptor is immediately catalytically inactive (i.e. gefitinib displaces ATP). We define the ordinary differential equation (ODE) describing the change in the fraction of phosphorylated receptors (x_p) with respect to time as:

$$\dot{x}_p = k_1(1 - f_G)(1 - x_p) - k_{-1}x_p \qquad \textbf{(1)}$$

where k_1 = phosphorylation rate constant, k_{-1} = dephosphorylation rate constant, the term $1 - x_p$ represents the fraction of all ErbB1 receptors that are unphosphorylated, and $1 - f_G$ represents the fraction of receptors that are not gefitinib-bound. At steady state, the association constant for gefitinib binding to ErbB1 (K_{eqG}) is:

$$K_{eqG} = \frac{f_G}{(1 - f_G)G} \qquad \textbf{(2)}$$

where G = gefitinib concentration. By solving for f_G and substituting it into (1), it follows that:

$$\dot{x}_p = \frac{k_1}{1 + K_{eqG}G}(1 - x_p) - k_{-1}x_p \qquad \textbf{(3)}$$

We assume that 40% of the receptors are phosphorylated at steady state (corresponding to 10 minutes after EGF addition) and 0.5% after 20μM gefitinib treatment (see Chapter 4).

We performed Monte Carlo simulations to obtain probabilistic estimates of the three parameters (k_1, k_{-1} and K_{eqG}) from the variance in the experimental data. To do this, we generated 1,000 artificial time courses by choosing random values from a log-normal distribution with the same mean and standard deviation as the experimental measurements in Figure 2.5B for each time point and concentration of gefitinib. For each artificial time course the parameters were fitted (see Chapter 4 for details) and we obtained good fits to the experimental data (Fig. 2.5B). We simulated the gefitinib dose-response behavior based on fitting to only the experiments of 1 and 10μM gefitinib and asked how well the model could predict the response of cells to additional concentrations of drug; we found that the model could indeed predict new experimental results (Fig. 2.5C).

We estimated parameter values of k_1 ~4.5/min, k_{-1} ~8/min and K_{eqG} ~1.3/μM (Fig. 2.5D). The ErbB1 phosphorylation and dephosphorylation rate constants (k_1 and k_{-1}, respectively) are consistent with those used in previously published models of ErbB signaling. These values fall within a large range and if estimated from fitting to experimental data they are usually obtained from fitting to data of cells treated with EGF only (Blinov et al., 2006; Chen et al., 2009; Kholodenko et al., 1999). *In vitro* kinase measurements of wild-type ErbB1 estimate k_{cat} ~1.5/min (Yun et al., 2008). We provide reasonable estimates for ErbB1 phosphorylation and dephosphorylation rate constants based on experimental data of dense temporal sampling following inhibitor perturbations. The estimated value for K_{eqG} (equivalent to a dissociation constant of ~1μM) seems high but reflects competition with ATP, which we do not describe explicitly in the model and is therefore incorporated into the estimated value. The underlying microscopic dissociation constant for gefitinib can be calculated using the Cheng-Prusoff equation based on our data showing an IC_{50} of 1μM: using an ATP concentration of 2mM (Lehninger et al., 2000) and a K_m for ATP of 5μM (Yun et al., 2008) we calculate a drug affinity

of 2.5nM, which is similar to measured values (Karaman et al., 2008).

The solution to the ODE in **(3)** can be calculated analytically, and we can prove that by measuring the level of receptor phosphorylation all parameters are identifiable (i.e. exact values of the parameters could be obtained if the measurements were exact; see Chapter 4 for details). Therefore, the distributions of parameter values obtained from fitting experiments using the experimental data comprise biological variation and error in the data, and not any non-identifiabilities. These distributions represent confidence intervals for the parameters; in other words, we can conclude that with a certain level of confidence the real parameter values fall in a given interval, assuming an accurate model and that all replicate experiments fall within the standard deviation measured and used here.

In this scheme receptors are phosphorylated and dephosphorylated based only on the catalytic phosphorylation and dephosphorylation rates and whether gefitinib is bound, assuming that gefitinib binding is in pseudo-equilibrium. In reality, ATP and gefitinib compete for binding to a single site on each ErbB1 molecule to regulate receptor catalytic activity, and whether a receptor can become dephosphorylated depends on whether a phosphatase and adaptor protein are bound at that time. Thus, only a fraction of the receptors that we consider can actually become phosphorylated or dephosphorylated, with this fraction changing over time. Calculating this fraction and fitting the model to the experimental data (as we did above) would lead to higher estimates for the phosphorylation and dephosphorylation rate constants. The estimates we obtained therefore represent lower bounds for the true rates. To obtain more accurate estimates we need to take into account the dynamics of other relevant binding processes that regulate the level of ErbB1 phosphorylation (see extended model below). However, these more realistic schemes are difficult to analyze computationally, and even a slightly extended model with 5 ODEs and 6 parameters where we describe the dynamics of gefitinib and adaptor protein binding is no longer identifiable given our measurements.

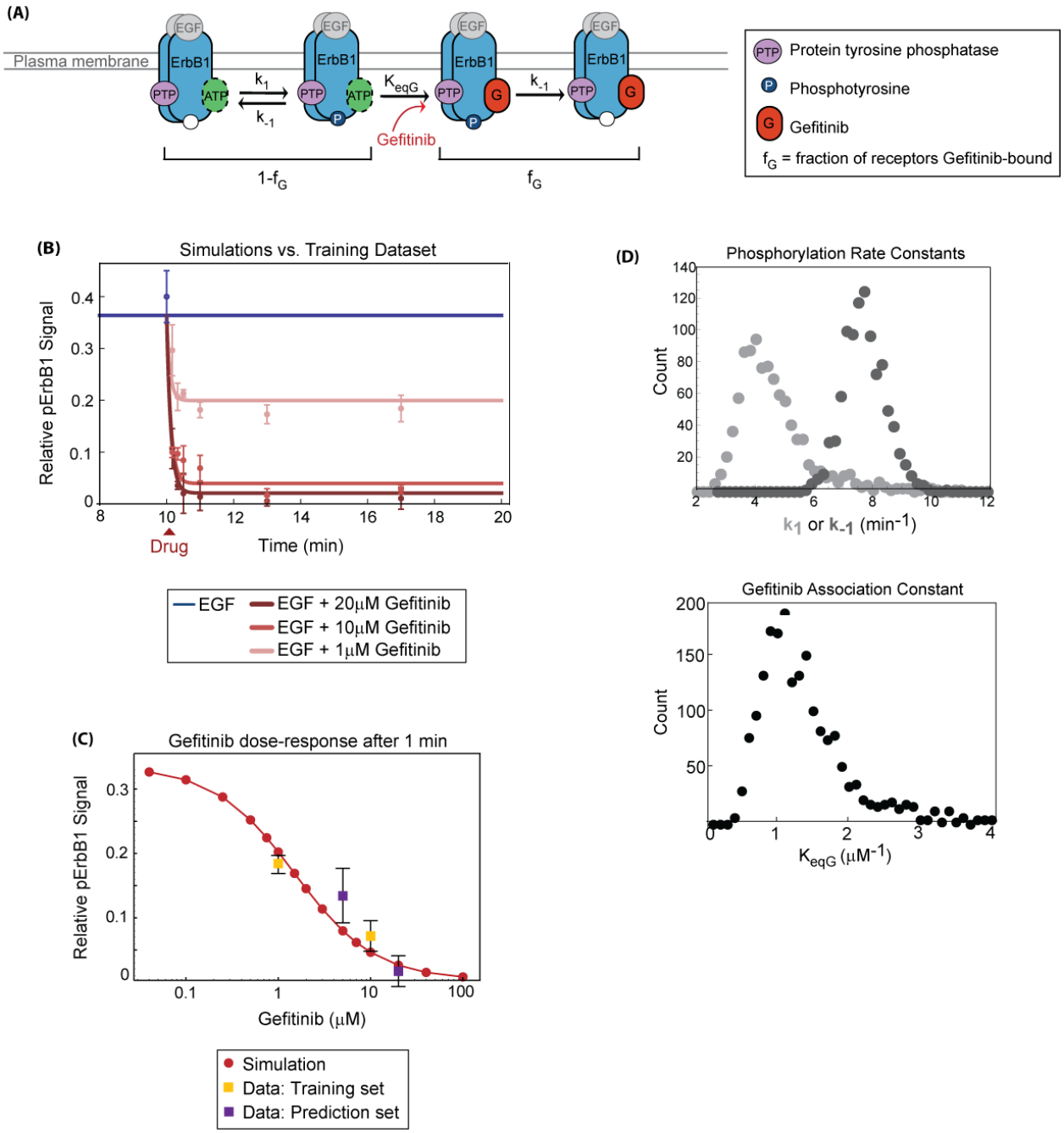

Figure 2.5 – Simple biochemical scheme describing ErbB1 phosphorylation dynamics and estimation of kinetic rate constants.

(A) Illustration of simple scheme describing ErbB1 phosphorylation. (B) Effects of various gefitinib concentrations on ErbB1 Y1173 phosphorylation in H1666 cells by HTM with 100ng/ml EGF stimulation followed by dense temporal sampling immediately after drug addition (including after 10, 20 and 30 seconds). Mean and standard deviations of experimental data points are shown along with simulation

results using the median parameter values obtained. (C) Simulation of predicted gefitinib dose-response behavior based on fitting to only the 1 and 10μM gefitinib experimental data shown in (B) (red). Also shown are some of the data points used for model training (orange) and experiments with additional concentrations of drug (purple). (D) Histograms of estimates for parameters based on fitting to all data in (B).

ErbB1 dephosphorylation dynamics in response to different drugs

To establish that rapid ErbB1 dephosphorylation is not a peculiarity of gefitinib inhibitor treatment, we performed the straightforward experiment of treating cells with EGF and then washing it away (replacing the media) after 10 minutes. This treatment resulted in ErbB1 Y1173 dephosphorylation with faster kinetics than in the presence of continued exposure to ligand (data not shown). Furthermore, we obtained similar results by stimulating cells with EGF and then adding saturating concentrations of the anti-ErbB1 monoclonal antibody 225 after 10 minutes, which competes with EGF for binding to ErbB1 ($t_{1/2}$ ~7 min; Fig. 2.6A). The ErbB1 dephosphorylation rate in these experiments likely reflects the rate at which EGF dissociates from ErbB1. Measuring the effects of blocking receptor catalytic activity directly eliminates these potentially slower time scales from the analysis and allows us to better constrain the rates of ErbB1 phosphorylation and dephosphorylation.

We asked whether ErbB1 is also rapidly dephosphorylated after treatment with ErbB-targeted kinase inhibitors other than gefitinib. Gefitinib and erlotinib (Tarceva®) bind with fast kinetics to ErbB1 when the receptor is in an active conformation (Stamos et al., 2002; Yun et al., 2007), whereas lapatinib (Tykerb®) binds with slow kinetics to ErbB1 when in an inactive conformation (Wood et al., 2004). Canertinib (CI-1033) covalently binds ErbB1 to act as an irreversible inhibitor (Fry et al., 1998). Cells were stimulated with 100ng/ml EGF and these inhibitors were subsequently added (t=10 min) at 10μM. Erlotinib (not shown) and canertinib result in rapid ErbB1 dephosphorylation, whereas lapatinib causes slow dephosphorylation ($t_{1/2}$ ~8 min) in both H1666 (Fig. 2.6B) and MCF-10A cells (Fig. 2.6C). We turned to a more detailed

computational model to better understand the different dephosphorylation dynamics induced by the various drugs.

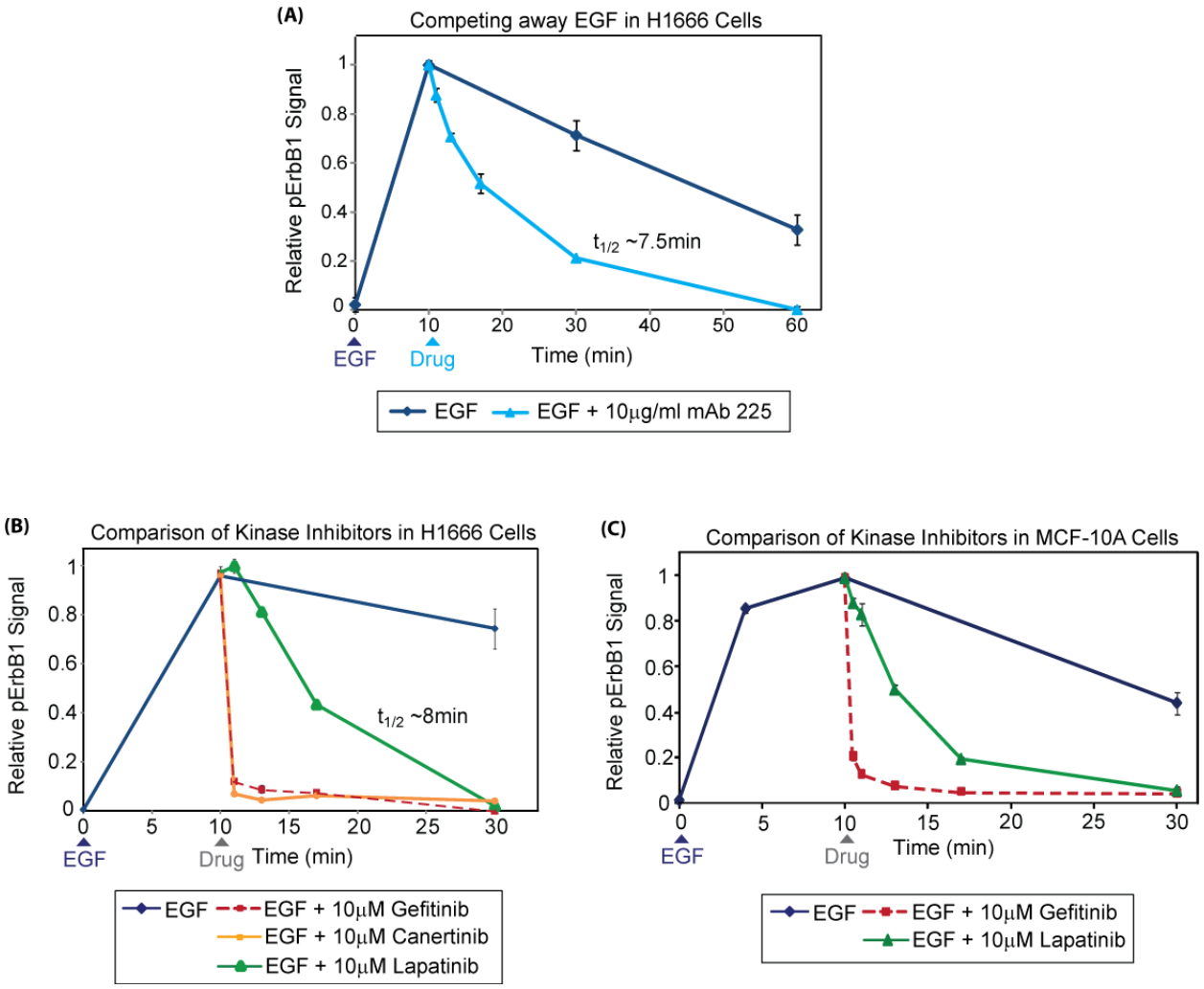

Figure 2.6 – ErbB1 dephosphorylation dynamics after competing away ligand or addition of ErbB1 small molecule kinase inhibitors with different mechanisms of action.

High-throughput fluorescence microscopy (HTM) measurements of ErbB1 Y1173 phosphorylation dynamics after stimulation of H1666 cells with 100ng/ml EGF followed by addition of drugs after 10 minutes (unless otherwise noted). (A) Effects of competing away EGF with 10μg/ml anti-ErbB1 monoclonal antibody 225 in H1666 cells. (B) ErbB1 dephosphorylation dynamics after treatment with 10μM gefitinib (as shown in Fig. 2.1B), canertinib or lapatinib. (C) Effects of 10μM gefitinib (as shown in Fig. 2.1D) or lapatinib in MCF-10A cells.

Development of a more detailed computational scheme to understand different inhibitor effects

We aimed to understand properties of ErbB1 receptors and drugs that give rise to the striking differences in ErbB1 dephosphorylation dynamics, specifically between gefitinib and lapatinib. The utility of the previously discussed model is clearly limited because it does not account for the dynamics of many important events regulating receptor phosphorylation. We therefore constructed an extended model consisting of 46 ODEs and 24 parameters (see Chapter 4 for model details). While the parameters in this larger model are not identifiable, the model nevertheless allows us to perform qualitative analyses. It describes the binding of ATP or drug (and competition between the two), phosphatases and adaptor proteins, and includes similar assumptions as for the previously described model, e.g. ErbB1 species are individual receptors in a homodimeric state and the model steady state is representative of EGF treatment only (Fig. 2.7A). We model Shc binding to the receptor since we measure phosphorylation of tyrosine 1173 on ErbB1, which is a high affinity binding site for Shc; however, this could also be interpreted as the family of adaptor proteins that bind to this site. We assume that phosphatases directly bind ErbB1 before catalyzing receptor dephosphorylation and consider one pool of phosphatases with an average binding constant and activity.

Although they have similar dissociation constants for ErbB1, gefitinib preferentially binds to ErbB1 when the receptor is in an active conformation, while lapatinib binds with slower on and off rates to an inactive receptor conformation (Johnson, 2009; Wood et al., 2004). We incorporated this conformational distinction into the model and assume that in the presence of EGF the active ErbB1 conformation is dominant. We assume that ATP and gefitinib bind much better to ErbB1 when in the active conformation but that they can still bind although with much lower affinity to the inactive conformation. On the other hand, lapatinib is only allowed to bind to ErbB1 when it is in the inactive conformation, and once bound the receptor cannot switch

conformations. However, when lapatinib dissociates ErbB1 is again allowed to switch conformations.

We performed model fitting and parameter estimation in the MATLAB toolbox PottersWheel (Maiwald and Timmer, 2008), where we simultaneously fit the model to a large dataset consisting of ErbB1 phosphorylation dynamics following treatment with 100ng/ml EGF and then various gefitinib or lapatinib concentrations or the phosphatase inhibitor pervanadate. We used a trust-region optimization approach, minimizing χ^2, the sum of weighted and squared residuals between the model trajectories and our measurements. Since the model is non-identifiable given our measurements, we consider a family of good fits of the model to data, and plot the fits along with a subset of the experimental training dataset (Fig. 2.7B). The model includes binding events that can slow down receptor dephosphorylation (e.g. Shc binding), and therefore we obtain faster estimates for the intrinsic phosphorylation and dephosphorylation rate constants (Fig. 2.7C; both ~ 50/min) compared to those estimated in Figure 2.5D. The model accurately predicts fast dissociation of Shc from ErbB1 following inhibition of receptor catalytic activity, and the Shc dissociation rate was estimated to be similar to the rates of receptor phosphorylation and dephosphorylation (not shown).

We find that the dose-response behavior of gefitinib and lapatinib look very different: only high gefitinib doses completely block receptor phosphorylation and lower doses result in a very fast equilibrium of partial inhibition, whereas even low dosing with lapatinib results in complete receptor inhibition, although at a slower rate (Fig. 2.7B). Gefitinib and lapatinib have similar K_d's for ErbB1, but in the model a preference for the inactive receptor conformation gives rise to more effective inhibition by lapatinib because lapatinib encounters less competition with ATP than gefitinib and leads to an increase in the number of inactive receptors.

We decreased the rates of ErbB1 phosphorylation and dephosphorylation in the best fit model to reveal the dependency of the different trends of ErbB1 dephosphorylation by 10μM gefitinib or lapatinib on these rates (Fig. 2.7D). We find that the different dynamics rely on the

fast kinetics; if the rates were slower we would not see a difference between treatments with the two drugs. ErbB1 dephosphorylation in the presence of these drugs is therefore determined by the velocity and mechanism of drug binding, and is dependent on fast ErbB1 phosphorylation and dephosphorylation cycling.

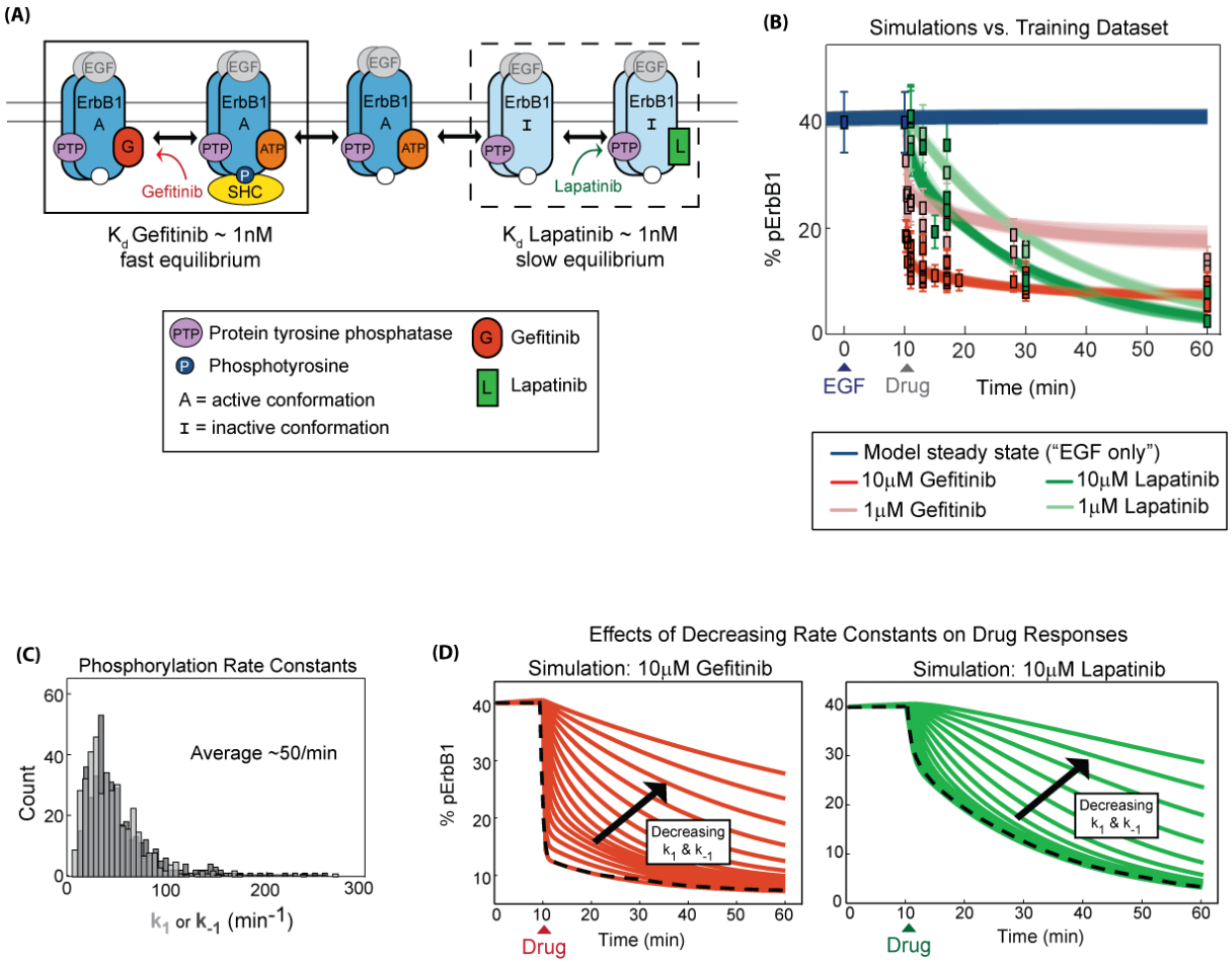

Figure 2.7 – More detailed model describing gefitinib and lapatinib binding to ErbB1.

High-throughput fluorescence microscopy (HTM) measurements of ErbB1 Y1173 phosphorylation dynamics after stimulation of H1666 cells with 100ng/ml EGF followed by addition of drugs after 10 minutes (unless otherwise noted). (A) Simplified illustration of a biochemical scheme describing ErbB1 phosphorylation dynamics as determined by the dynamics of binding of ATP, lapatinib ("L") or gefitinib ("G"), protein tyrosine phosphatase ("PTP") and the adaptor protein Shc. The ErbB1 species is a monomer that exists in a stable ErbB1 homodimer. The model also distinguishes between active and inactive conformations of ErbB1, and the dashed arrow denotes the change in conformation (not a change in binding state). Gefitinib preferentially binds to ErbB1 when it is in the active conformation, while lapatinib binds with slower on and off rates to the inactive receptor conformation (similar K_d's). EGF binding and receptor dimerization are not explicitly modeled here. (B) The best 100 model fits out of 2000 are shown along with a portion of the training dataset. Each data point is an average of replicate measurements made on the same day, and the error bars were calculated from an error model. The t=0 data point is artificial and was used to force pre-equilibration of the model (t<10min). (C) Histograms of phosphorylation and dephosphorylation rate constant estimates from ~400 separate fits. (D) Effects of decreasing the rates of phosphorylation (from 209/min to 0.3/min) and dephosphorylation (from 38/min to 0.06/min) in the best fit model (black dotted curves) on ErbB1 inhibition by 10μM gefitinib or lapatinib. Each curve is a decrease in the rates by a factor of ~1.5 where the ratio of the two rates is held constant. The curves were first normalized to 40% at t<10min to be able to compare the trends.

Investigating the role of ErbB1 phosphatases

Thus far we have assumed that phosphatases are responsible for the fast gefitinib-induced dephosphorylation. We wanted direct evidence of this and turned to phosphatase inhibitors, but unfortunately, the tools to study phosphatases are blunt and we are lacking good chemical inhibitors of specific phosphatases. Therefore, we first evaluated the effects of the non-specific tyrosine phosphatase inhibitor pervanadate, which results in the irreversible oxidation of the catalytic cysteine of PTPs such as PTP1B (Huyer et al., 1997).

As reported in other studies, inhibiting tyrosine phosphatases with pervanadate leads to significantly higher ErbB1 phosphorylation than saturating EGF (Fig. 2.8A), suggesting that phosphatases are constantly acting to suppress maximal receptor activation. Addition of pervanadate after EGF stimulation still leads to a large increase in receptor phosphorylation (Fig. 2.8B), suggesting that only ~50% of ErbB1 receptors are phosphorylated after ligand stimulation. This may be explained by pervanadate activating receptors located in all subcellular compartments (Offterdinger et al., 2004), whereas EGF activates only cell surface receptors.

We turned to the computational model depicted in Figure 2.7A to better understand the counteracting dynamics of simultaneous inhibition of kinase and phosphatase activity. The model predicts that treatment with 10μM gefitinib and 100μM pervanadate together would block the fast gefitinib-induced ErbB1 dephosphorylation, and we experimentally verified this prediction (Fig. 2.8B). We find that gefitinib binds rapidly, but when it also unbinds rapidly it leads to an increase in phosphorylation due to inactive phosphatases. The correspondence of the model and our data argues in favor of an accurate understanding of the biochemistry, and these results verify that ErbB1 dephosphorylation is dependent on active phosphatases.

Next, we investigated whether PTP1B regulates the fast gefitinib-induced ErbB1 dephosphorylation. We knocked down PTP1B levels by 80% with siRNA (Fig. 2.8C). This knockdown had no effect on basal phosphorylation or gefitinib-induced dephosphorylation of six

different phosphorylation sites on ErbB1 when gefitinib was added 10 minutes after EGF (Fig. 2.8D). Commercially available chemical inhibitors also had no effect (not shown). These results are not very surprising since many factors could contribute to the difficulty in pinpointing the exact phosphatase(s) responsible for the fast phosphorylation cycling.

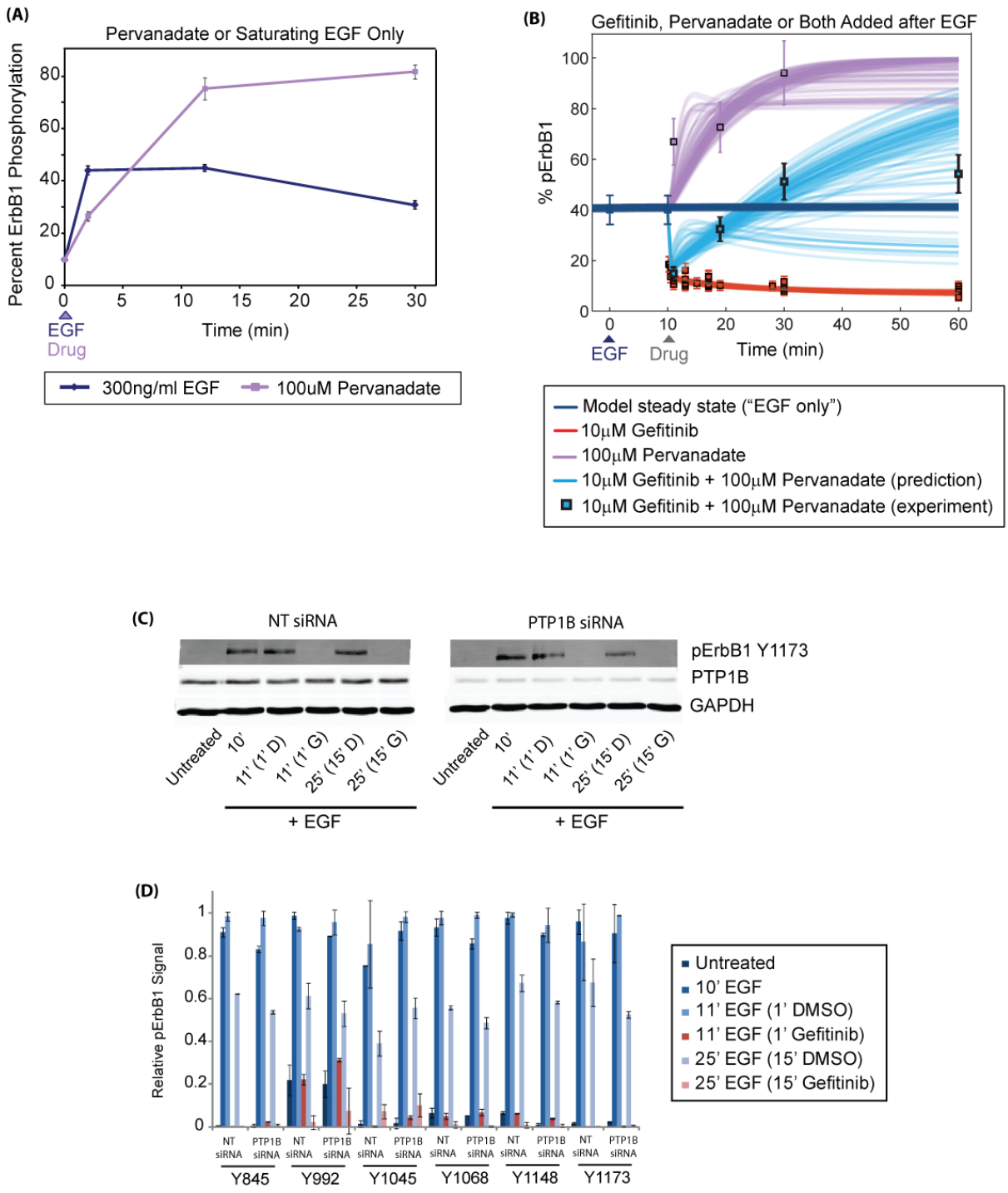

Figure 2.8 – Pervanadate treatment but not PTP1B knockdown blocks gefitinib-induced ErbB1 dephosphorylation.

(A) ErbB1 Y1173 phosphorylation as measured by high-throughput microscopy (HTM) after stimulation of H1666 cells with 300ng/ml EGF or pervanadate (the combination of sodium orthovanadate and hydrogen peroxide). (B) Model prediction (cyan curves) and experimental validation (dark black cyan-filled squares) of simultaneous treatment with gefitinib and pervanadate (best 100 fits out of 2000).

Pervanadate and/or gefitinib were added after 10 minutes of 100ng/ml EGF in H1666 cells and ErbB1 pY1173 was measured by HTM. Each data point (square) is an average of replicate measurements made on the same day, and the error bars were calculated from an error model (see Chapter 4). The t=0 data point is artificial and was used to force pre-equilibration of the model (t<10min). Long term treatments with 100μM pervanadate resulted in loss of cells from the plate, presumably due to effects on adhesion molecules, and for this reason it was not possible to obtain data for time points after ~30 min. Sodium orthovanadate and hydrogen peroxide alone each had no effect on ErbB1 phosphorylation when added after EGF in H1666 cells. (C)-(D) Effect of siRNA knockdown of PTP1B or a non-targeting control (NT) on ErbB1 Y1173 phosphorylation by Western blotting (C) or six different ErbB1 phosphotyrosine sites by ELISA (D) in H1666 cells. 10μM Gefitinib ("G") or a DMSO control ("D") was added after 10 minutes of 100ng/ml EGF stimulation.

Low dosing with gefitinib results in sustained ErbB1 phosphorylation

Whereas even low dosing with lapatinib eventually results in complete receptor inhibition (Fig. 2.9A), our modeling suggests that at some point low gefitinib dosing after EGF addition may result in more receptor activity than with EGF alone, which is eventually shut off. Indeed, we find that adding low concentrations of gefitinib (0.5 or 1μM) after a few minutes of EGF stimulation (t=1 or 2 min) results in a surprisingly stable level of receptor phosphorylation for many hours, crossing over the EGF only treatment curve (Fig. 2.9B for MCF-10A cells; H1666 cells not shown). Total ErbB1 levels (consisting of cell surface plus internal receptors) under these treatment conditions show that even low gefitinib concentrations prevent receptor degradation (Fig. 2.9B). Microscopy images illustrate altered ErbB1 trafficking in the presence of gefitinib such that only a fraction of receptors are located in endocytic compartments by 20 minutes, with no change in ErbB1 localization detected by 4 hours (Fig. 2.9C; 4 hour time point not shown).

It is unclear how frequently ErbB1 is exposed to growth factors, and therefore how active the receptor is, *in vivo*. We asked whether exposure of cells to low doses of gefitinib prior to ligand stimulation could turn a future transient response to ligand into a sustained signal. Cells were pretreated with various concentrations of gefitinib for one hour followed by stimulation with EGF for 4 hours. In control cells with no drug, the typical response to long-term ligand

stimulation was observed where ErbB1 phosphorylation returned to basal levels and receptors were degraded (Fig. 2.10). Pretreatment with gefitinib had a similar effect as addition after ligand stimulation: ErbB1 degradation was inhibited but receptor phosphorylation sustained in the presence of 0.5 and 1μM gefitinib (Fig. 2.10).

Only a fraction of receptors are gefitinib-bound at any given time, and while gefitinib is not bound the receptors can rapidly become phosphorylated again. This can result in rapid shuffling of individual receptors between being bound by drug and being phosphorylated and dephosphorylated, with a higher fraction of receptors not bound and therefore phosphorylated in the presence of low gefitinib concentrations. We propose that when low concentrations of gefitinib are added while ErbB1 is still at the cell surface, each ErbB1 molecule may not be phosphorylated long enough for activation and recruitment of a ubiquitin ligase complex (i.e. Cbl-Grb2), which may allow these receptors to evade internalization and degradation and lead to sustained signaling. Interestingly, according to pharmacokinetic data obtained in phase I clinical studies, the mean steady state plasma concentration of gefitinib at the FDA-approved dosing is approximately 1μM (Baselga et al., 2002), which is the “low” gefitinib concentration used here.

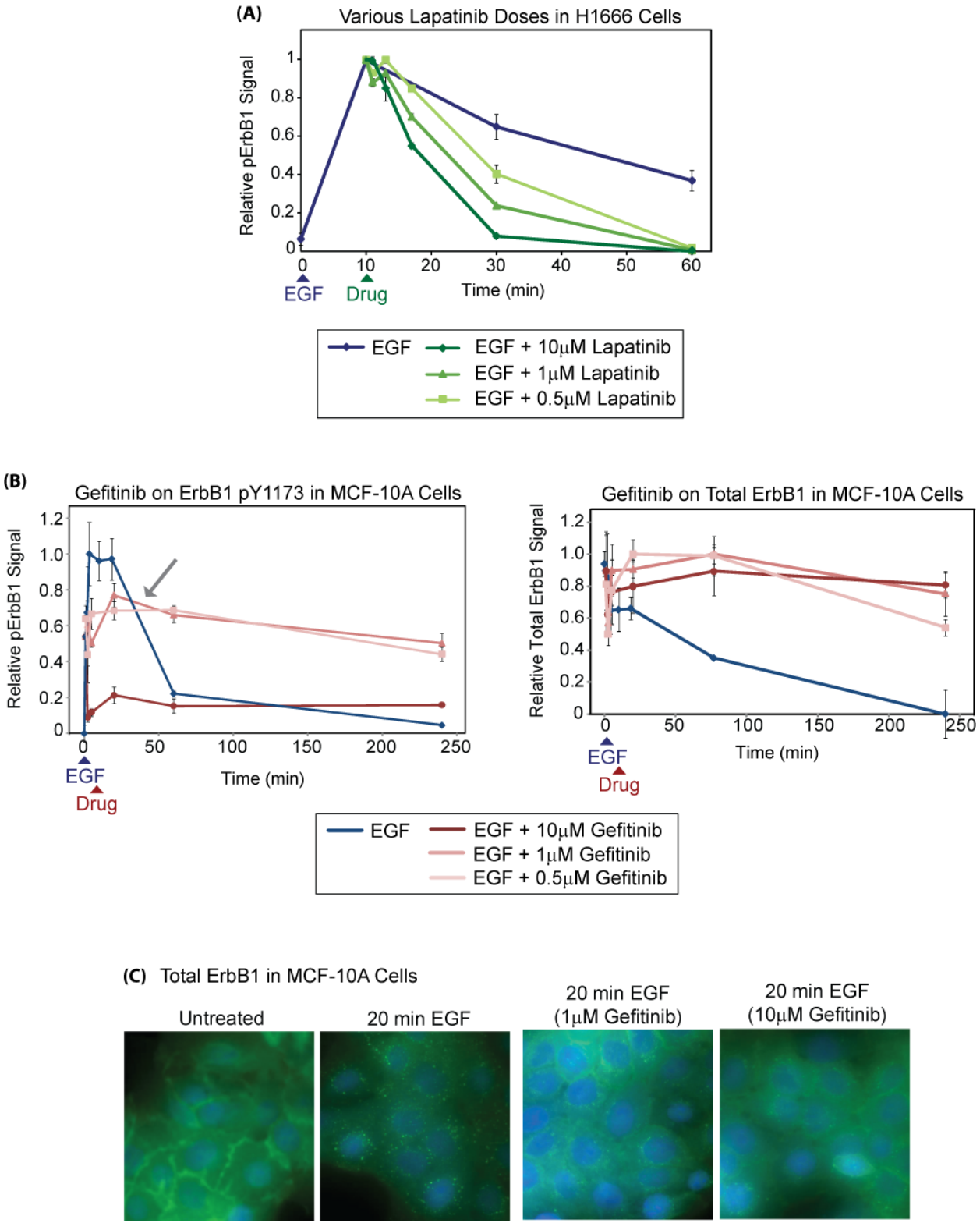

Figure 2.9 - Low gefitinib dosing converts a transient response to ligand into a sustained signal by altering receptor trafficking.

(A) Treatment of H1666 cells with various concentrations of lapatinib after 10 minutes of 100ng/ml EGF stimulation as measured by HTM. (B) Various gefitinib concentrations were added after one minute of EGF stimulation of MCF-10A cells, and ErbB1 pY1173 and total ErbB1were measured by HTM. (C) Higher magnification images of selected time points in (B). Blue = Hoechst and protein dye, Green = total ErbB1.

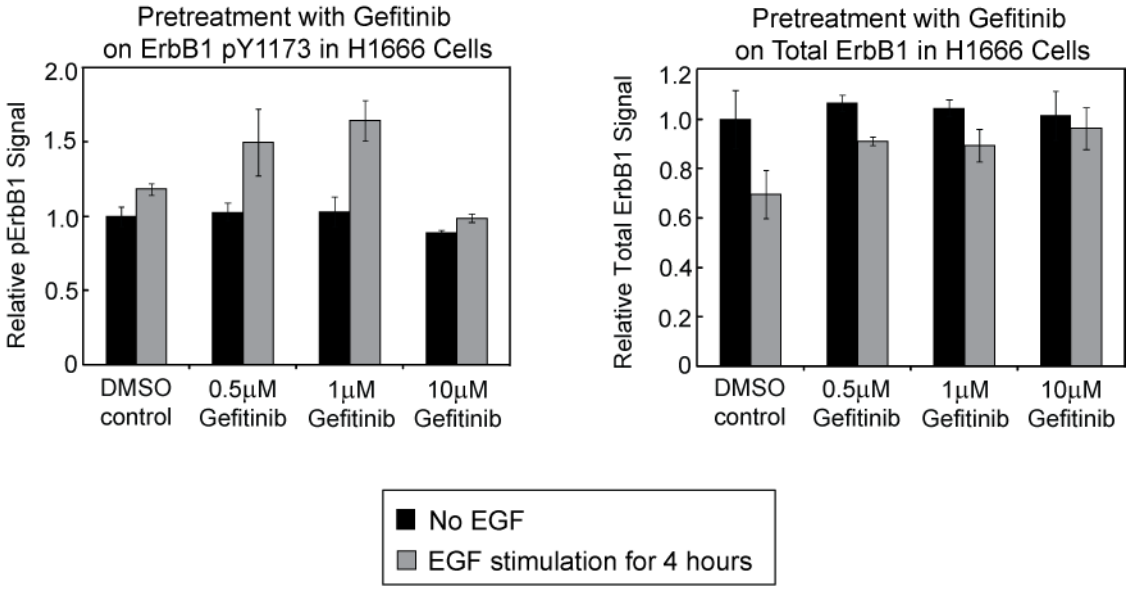

Figure 2.10 - Pretreatment with low concentrations of gefitinib also leads to sustained signaling.

H1666 cells were pretreated with various gefitinib concentrations or a DMSO control for one hour followed by stimulation of cells with 100ng/ml EGF for 4 hours, and ErbB1 pY1173 and total ErbB1 were measured by HTM.

Physiological consequences of fast phosphorylation cycling

We wondered whether there could be a functional consequence of rapid and continual protein phosphorylation, as opposed to becoming phosphorylated and staying phosphorylated for a longer duration. We hypothesized that these fast dynamics may allow cells to rapidly sense and respond to changes in their environment. EGF is a well-known initiator of cell migration (Jorissen et al., 2003) and protrusion of lamellipodia is a rapid and early event in the process of cell migration, beginning almost immediately after EGF stimulation of MCF-10A cells (Fig. 2.11A). Extension and retraction of these protrusions are normally complete after 20 minutes, although additional protrusions are common in the continued presence of ligand, but the timing is more variable between cells (not shown). We quantified protrusion dynamics using kymograph analysis (see Chapter 4).

Cells were treated with EGF and 10μM gefitinib was added 40 seconds later. ErbB1 receptors were dephosphorylated within 15 seconds (data not shown) and further lamellipodia extensions stopped in 40 seconds (Fig. 2.11B & C), followed by retraction of the lamellipodia with similar kinetics to EGF only (Fig. 2.11B). Similar retraction dynamics may be attributed to fixed dynamics of actin depolymerization. The difference between the time it takes for the receptor to be shut off and protrusions to halt is likely due to how long it takes for intermediates (e.g. ERK and Akt) to be inhibited under these conditions. Our results show that lamellipod extension is a reversible process that depends on continual receptor phosphorylation.

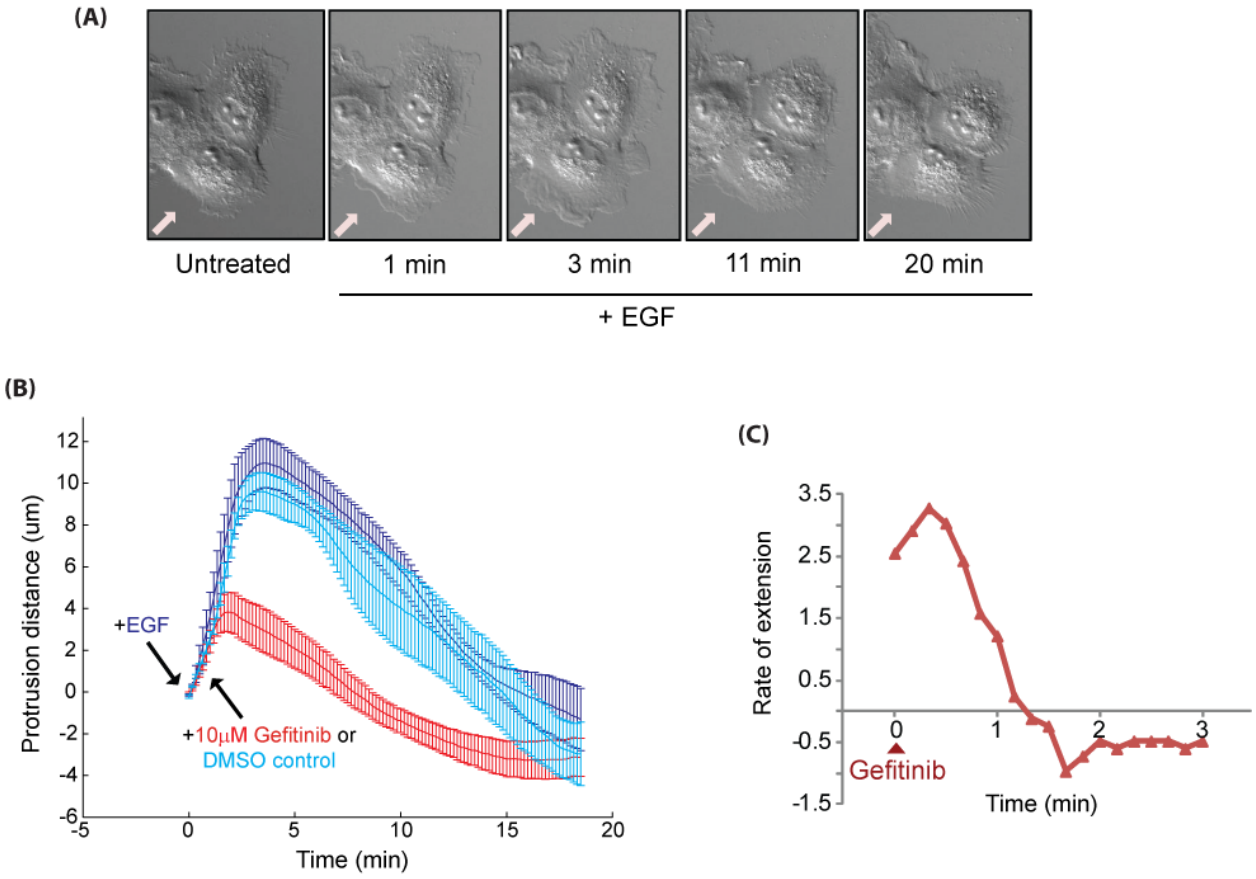

Figure 2.11 – Lamellipodia retract almost immediately after ErbB1 is dephosphorylated following gefitinib treatment.

(A) DIC images of MCF-10A cells stimulated with 300ng/ml EGF (pink arrows point to example membrane protrusions). (B) Results of kymograph analysis showing the effects of adding 10μM gefitinib or DMSO after 40 seconds of 100ng/ml EGF stimulation on protrusion dynamics in MCF-10A cells. For each treatment condition the average and standard error of the mean for 5-10 cells is plotted. (C) Derivatives of average data points in (B) immediately after addition of gefitinib.

Stochastic simulation illustrates switching times between phosphorylation states

To illustrate the cycling times of individual ErbB1 molecules between being phosphorylated and dephosphorylated in the presence or absence of gefitinib, we developed a stochastic simulation with a similar structure as the scheme depicted in Figure 2.5A. We used the parameters estimated for H1666 cells with that simple ODE model (Fig. 2.12A). The addition of gefitinib is mimicked by decreasing the phosphorylation rate after 10 minutes based on the equation $\frac{k_1}{1+K_{eqG}G}$ as derived in equations **(2)** and **(3)** above. Time courses of individual ErbB1 receptors before (t < 10min) and after (t > 10min) 10μM gefitinib treatment demonstrate the frequency of phosphorylation events (Fig. 2.12B).

While individual molecules are being phosphorylated and dephosphorylated at different times after EGF stimulation, the average level of phosphorylation stays constant at steady state. Shortly after gefitinib is added (i.e. the phosphorylation rate changes), a new average level of phosphorylation for the population is reached. We estimate that on average, receptors that are phosphorylated become dephosphorylated in ~8 seconds. In the presence of EGF only, unphosphorylated receptors become phosphorylated within ~14 seconds, and in the presence of 10μM gefitinib this increases to ~190 seconds. Therefore, ErbB1 can still become phosphorylated even in the presence of saturating gefitinib concentrations, but each receptor spends more time being unphosphorylated. This reasoning can help explain our results in Figure 2.8B where we added 10μM gefitinib and pervanadate simultaneously, and ErbB1 was rapidly dephosphorylated and then slowly re-phosphorylated. These infrequent re-phosphorylation events in the presence of 10μM gefitinib accumulate due to inactive phosphatases.

Overall, our results suggest that ErbB1 is regulated by processes that occur at both slow and fast time scales. Slow dynamics of ligand binding and dimerization result in increased receptor kinase activity and phosphorylation, and presumably slow degradation leads to signal attenuation. These slow time scales are coupled with constant fast cycling of individual receptors between being phosphorylated and dephosphorylated in the presence of ligand.

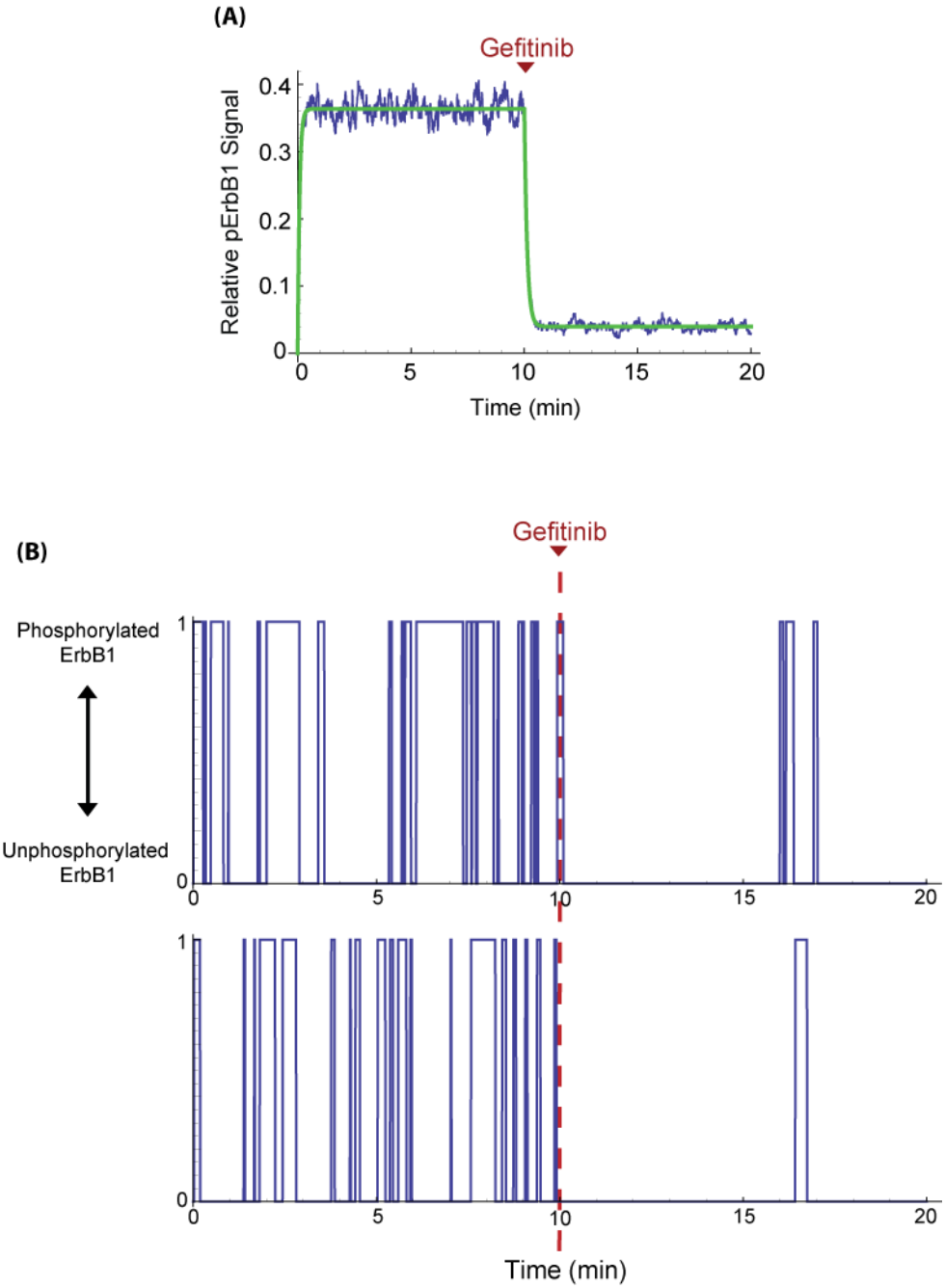

Figure 2.12 – Stochastic model illustrates fluctuations of individual ErbB1 receptors between being phosphorylated and unphosphorylated.

(A) The average ErbB1 phosphorylation over 1000 individual molecules from the stochastic simulation (blue) is overlaid with the ODE formalism (green). 10μM gefitinib is added after 10 minutes. (B) Time courses of two ErbB1 molecules before ($t < 10$ min) and after ($t > 10$ min) 10μM gefitinib addition.

Supplementary Data

Effects of gefitinib on levels of cell surface ErbB1

ErbB1 receptors in H1666 cells were internalized approximately 2 to 10 minutes after EGF addition, as detected by immunofluorescence using a total ErbB1 antibody that recognizes the extracellular domain of the receptor and by not permeabilizing the cell membrane (Fig. 2.13). This is also evident from the images shown in Figure 2.2A, where the cell membrane was permeabilized to allow for total (cell surface plus intracellular) ErbB1 staining. The addition of 10µM gefitinib after 2 minutes of EGF stimulation appears to have inhibited normal receptor internalization following EGF, whereas the addition of 10µM gefitinib after 10 minutes of EGF stimulation led to a slow rise in the number of cell surface receptors (Fig. 2.13). This increase in cell surface receptors could be due to inhibited internalization of newly synthesized receptors at the plasma membrane or recycling of drug-bound receptors already internalized.

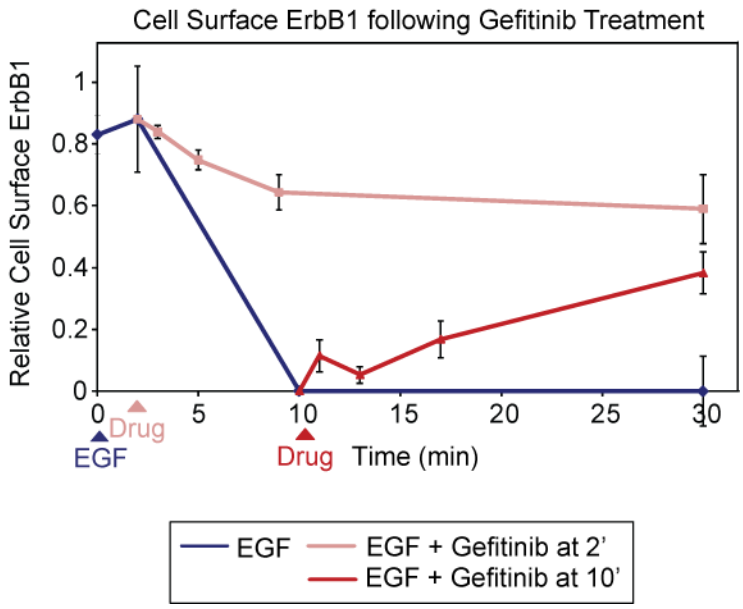

Figure 2.13 – Effects of gefitinib on levels of cell surface ErbB1.

H1666 cells were stimulated with 100ng/ml EGF and 10µM gefitinib was added to certain wells after 2 or 10 minutes, and cell surface ErbB1 receptors were measured by immunofluorescence. The cell membrane was not permeabilized and we used an antibody to total ErbB1 that recognizes the extracellular domain of the receptor.

Dose-response behavior of the irreversible ErbB1 inhibitor canertinib

The irreversible ErbB1 tyrosine kinase inhibitor canertinib has a dose-response behavior that looks different from gefitinib, erlotinib and lapatinib. In cells stimulated with EGF followed by high concentrations of canertinib after 10 minutes, ErbB1 is dephosphorylated very rapidly. However, at low concentrations of canertinib, ErbB1 dephosphorylation is slow but complete inhibition is reached (Fig. 2.14, *top*). Thus, canertinib seems to have a dose-response behavior that is intermediate between gefitinib/erlotinib and lapatinib, which could be explained by a fast on rate and a very slow off rate due to formation of a covalent bond with ErbB1 (Fry et al., 1998). The delay in ERK dephosphorylation that was measured following gefitinib treatment can also be seen after canertinib treatment (Fig. 2.14, *bottom*).

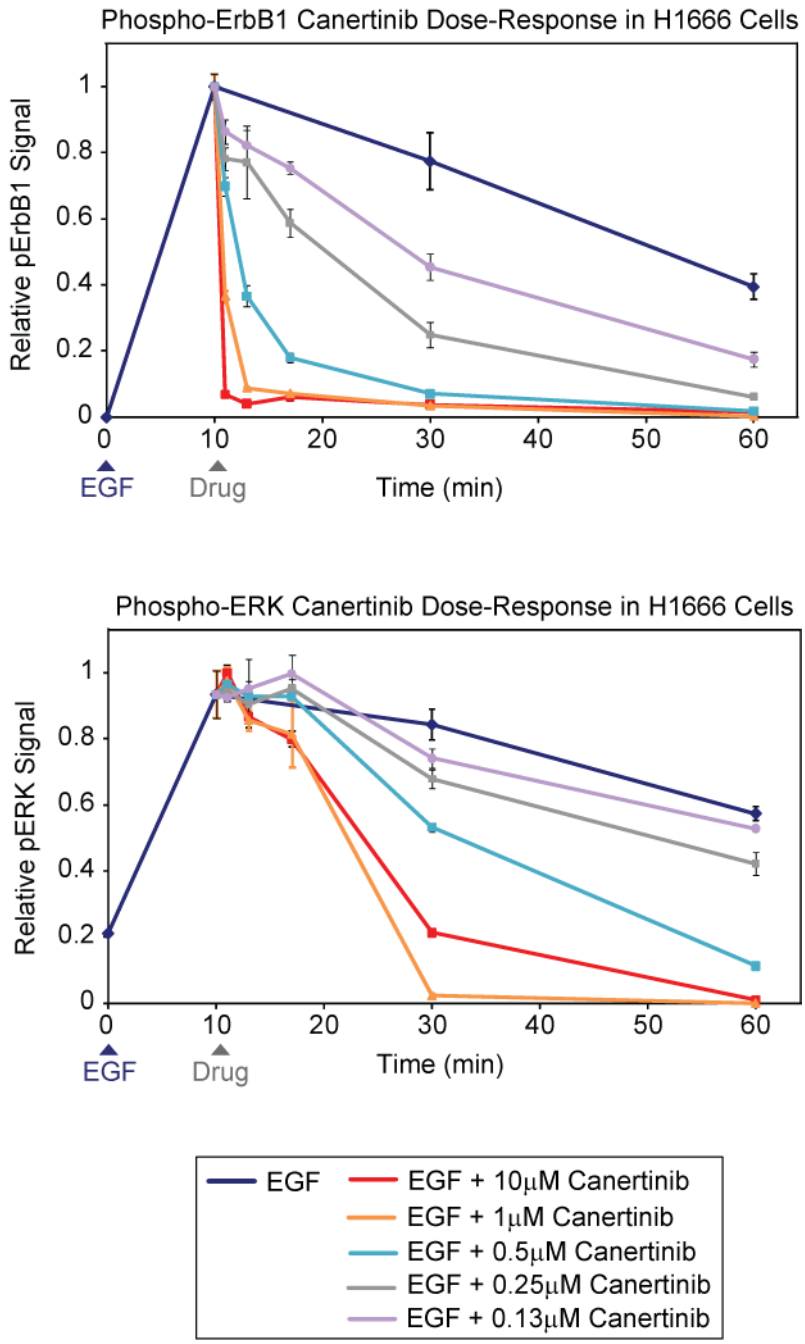

Figure 2.14 – Dose-response behavior of canertinib, an irreversible ErbB1 tyrosine kinase inhibitor.

H1666 cells were stimulated with 100ng/ml EGF followed by canertinib after 10 minutes, and phospho-ErbB1 Y1173 (top) or phospho-ERK1/2 (bottom) was measured using HTM.

ErbB3 is dephosphorylated slowly after heregulin stimulation

After EGF stimulation only, ErbB3 phosphorylation increased and decreased more rapidly than ErbB1 and ErbB2 (compare Fig. 2.1A and 2.3A). The phosphotyrosine site on ErbB3 that we measured is Y1289, a PI3K binding site (Schulze et al., 2005). ErbB3 is known to potently activate Akt via multiple binding sites for PI3K on its C-terminal tail (Schulze et al., 2005), and we found that Akt phosphorylation followed similar dynamics to ErbB3 after EGF stimulation (Fig. 2.4). When 10μM gefitinib was added after 10 minutes of exposure to EGF, both ErbB3 and Akt were quickly dephosphorylated (Fig. 2.3 and 2.4), again with very similar dynamics. These results imply potent downregulation mechanisms for ErbB3.

We wondered whether a ligand that binds directly to ErbB3 would induce similar transient dynamics. We therefore treated cells with 100ng/ml heregulin (HRG) and measured a time course of ErbB3 phosphorylation (Fig. 2.15). ErbB3 phosphorylation was sustained under these conditions, suggesting that ErbB3 may be downregulated by different mechanisms following exposure to the two different growth factors. Since ErbB3 was dephosphorylated rapidly after treatment with EGF and then gefitinib, we then tested the effects of gefitinib in the presence of HRG. After treating cells with 100ng/ml HRG followed by 10μM gefitinib, ErbB3 was dephosphorylated slowly. Possible explanations for the differences between ErbB3 regulation after EGF and HRG stimulation are discussed in detail in Chapter 3.

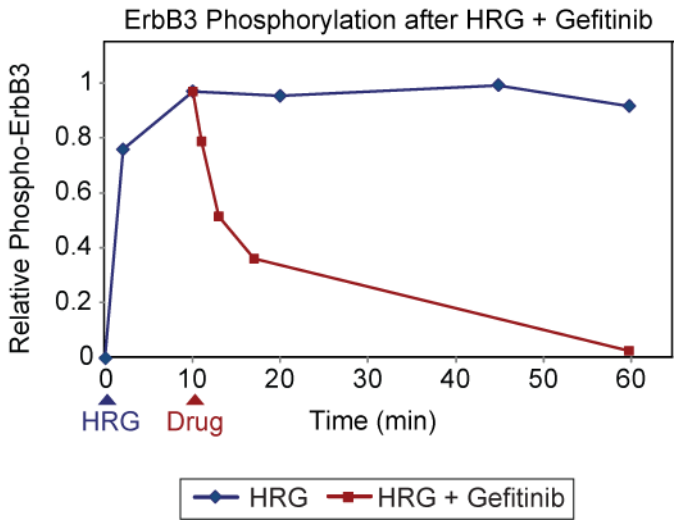

Figure 2.15 – ErbB3 is dephosphorylated slowly after HRG stimulation alone as well as after additional gefitinib treatment.

H1666 cells were stimulated with 100ng/ml HRG and after 10 minutes gefitinib was added at 10µM. ErbB3 phosphorylation at Y1289 was measured by ELISA.

Development of a more complete mathematical model that describes ErbB receptor trafficking

The computational models described so far have made the simplifying assumptions that EGF is bound and ErbB1 receptors are in stable homodimers, and since receptor downregulation was also not described in the models, they only allowed us to analyze receptor dynamics in a relatively short time frame from ~10-30 minutes after EGF stimulation. To study ErbB1 dephosphorylation dynamics in a larger context and the effects of gefitinib in the presence of normal receptor trafficking, we constructed a more complete mathematical model that describes the processes of ligand binding to the ErbB1-3 receptors (we considered EGF, HRG and amphiregulin), ErbB dimerization and phosphorylation, adaptor protein and phosphatase binding, and receptor ubiquitination, internalization and degradation. A complete mechanistic description of all the mentioned processes would result in a model composed of more than 100,000 ordinary differential equations (ODEs). Using the model reduction

techniques of Conzelmann et al. (Conzelmann et al., 2008) and Koschorreck et al. (Koschorreck et al., 2007), which had to be partly extended, we reduced the model to 648 ODEs. By focusing on the interplay of EGF and gefitinib, it was possible to further reduce the model to 203 ODEs. Development and reduction of this model was a substantial undertaking and both are described in detail in Chapter 4.

These two models (the 203 and 648 ODE versions) qualitatively produce remarkably similar receptor dynamics under various conditions compared to our experiments, even without systematic model calibration to estimate parameter values. For example, ErbB1-3 are rapidly dephosphorylated in the model following EGF stimulation and gefitinib inhibition (see Fig. 2.3A), while ErbB1 is slowly dephosphorylated under conditions of EGF stimulation and then addition of a competitor of EGF binding (see Fig.2.6A) (simulations not shown). Here we focus on a few of the biological insights we have gained from this model.

The role of degradation and phosphatases in regulating the lower steady state ErbB1 pY levels after EGF pulses of different durations followed by gefitinib

This thesis focuses on analyzing the rapid ErbB1 phosphorylation turnover that occurs throughout receptor trafficking and not on the mechanisms regulating the slow dephosphorylation of bulk ErbB1 following ligand stimulation, which we have assumed is from ErbB1 degradation or dephosphorylation of ErbB1 by PTPs immediately preceding degradation. Experiments using the protein synthesis inhibitor cycloheximide suggest that transcriptional upregulation of phosphatases or other negative regulators is likely not playing a role in the downregulation of ErbB1 phosphorylation following growth factor stimulation (Amit et al., 2007). However, as discussed in Chapter 1, other mechanisms can dynamically increase the activity of ErbB1 PTPs, such as phosphorylation of the PTP or co-localization of the PTP and ErbB1.

We tried to address whether ErbB1 phosphatase activity changes over time by monitoring ErbB1 dephosphorylation after EGF pulses of different durations followed by addition of subsaturating concentrations of gefitinib, which rapidly reduces ErbB1 phosphorylation levels by ~50% and results in a new steady state level. We hypothesized that the new steady state reached after gefitinib treatment would be representative of the ratio of kinases and phosphatases that can act on the receptors at that time. Following treatment of H1666 cells with 1μM gefitinib after different durations of EGF stimulation, we found that slightly lower steady state levels of ErbB1 Y1173 phosphorylation were reached when gefitinib was added at later times (Fig. 2.16A). Furthermore, the "steady state" level itself slowly decreased over time when gefitinib was added after ErbB1 internalization (~2-10 min after EGF addition; Fig. 2.13), perhaps due to some receptors already being on the path for degradation.

Without implementing a mechanism for PTP activity to increase after ligand stimulation in the 648 ODE model, we asked whether ErbB1 degradation alone could explain the different steady states reached. The model qualitatively captured the phosphorylation dynamics of ErbB1 Y1173 in H1666 cells even without systematic calibration of the model (Fig. 2.16B, *left*). We next asked whether these steady states are a result of ErbB1 degradation by normalizing the phosphorylation dynamics by total receptor levels, which then resulted in the same steady state (Fig. 2.16B, *right*). Therefore, the steady state differences when adding subsaturating concentrations of gefitinib after various durations of ligand stimulation can be attributed to receptor degradation alone and does not require an increase in phosphatase activity. These results suggest that there may not be a significant increase in overall phosphatase activity during a time course of ligand stimulation *in vivo*.

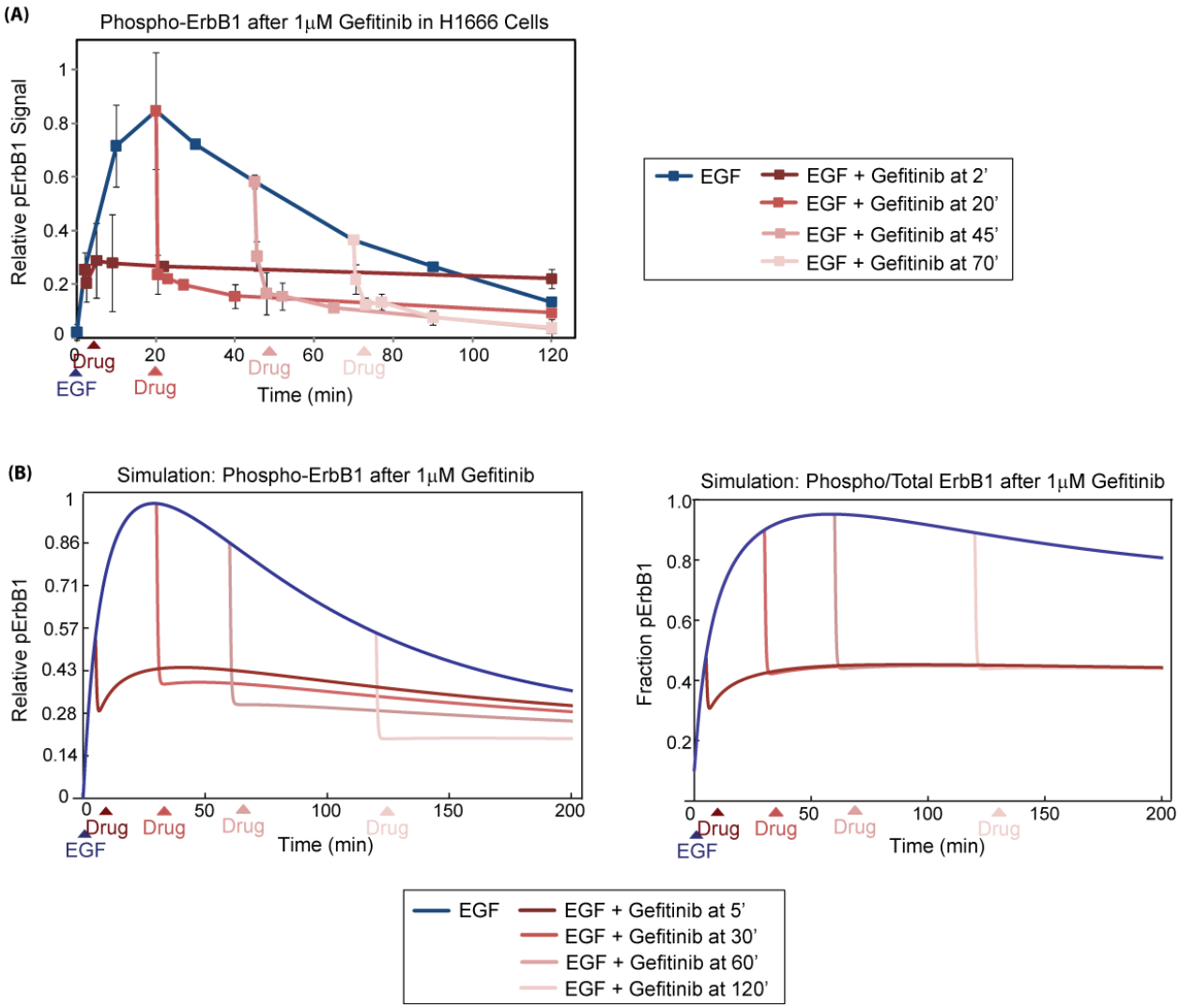

Figure 2.16 – ErbB1 phosphorylation after EGF pulses of different durations followed by addition of 1μM gefitinib.

(A) Treatment with 1μM gefitinib at different times after adding 100ng/ml EGF in H1666 cells where ErbB1 pY1173 was measured by high-throughput microscopy. (B) Model simulations of ErbB1 Y1173 phosphorylation (left) or ErbB1 Y1173 phosphorylation normalized by the total number of ErbB1 receptors (right) after addition of 1μM gefitinib at different times after adding 100ng/ml EGF. The values on the left are normalized between 0 and 1 to be able to easily compare the trends.

The ErbB1 dephosphorylation rate does not influence receptor dynamics after EGF alone but plays an important role in the presence of gefitinib

We performed systematic model calibration with the 203 ODE model to estimate and constrain the parameter values based on our experimental data shown in Fig. 2.9B, where MCF-10A cells were stimulated with EGF for one minute and then gefitinib was added at various concentrations, and ErbB1 Y1173 phosphorylation and total receptor levels were measured (see Chapter 4 for details of the fitting procedure). The data show that following treatment with low concentrations of gefitinib, ErbB1 Y1173 phosphorylation became sustained and the receptor was not degraded, suggesting that low concentrations of gefitinib can turn a transient ErbB1 response to ligand into a sustained receptor signal, a point we examined in more detail using this model.

To understand how the model parameters influence the transient-to-sustained ErbB1 behavior, we performed a sensitivity analysis to investigate relative changes of the derived system quantities as a result of relative changes in the parameter values (see Chapter 4 for details). We found that the only sensitive parameter with respect to the sustained phosphorylation of Y1173 after 20 and 240 minutes of 1μM gefitinib treatment was the parameter describing dephosphorylation of that ErbB1 phosphotyrosine site when phosphatase is bound to the receptor ("k2Poff"). Interestingly, this parameter was not sensitive with respect to the EGF only treatment curve. To illustrate this point, we plotted the fitted dynamics of ErbB1 Y1173 phosphorylation, as well as the predicted effects of modulating the rate (Fig. 2.17). Higher values for this dephosphorylation rate resulted in complete dephosphorylation of Y1173 following 1μM gefitinib treatment, while a lower rate surprisingly led to even higher levels of sustained phosphorylation, even after addition of saturating concentrations of gefitinib. There was basically no effect of changing this parameter on the EGF only treatment curve, suggesting that the rate of ErbB1 phosphorylation cycling does not control the overall levels of receptor

phosphorylation after exposure to growth factors and that this is instead regulated by the presumably slower processes of ligand binding, receptor dimerization and degradation. We are currently unable to modulate the receptor dephosphorylation rate experimentally, but these model simulations illustrate the importance of using perturbations to uncover underlying biochemistry and suggest that the rate of ErbB1 phosphorylation cycling is very important to determining the response to ErbB1-targeting drugs.

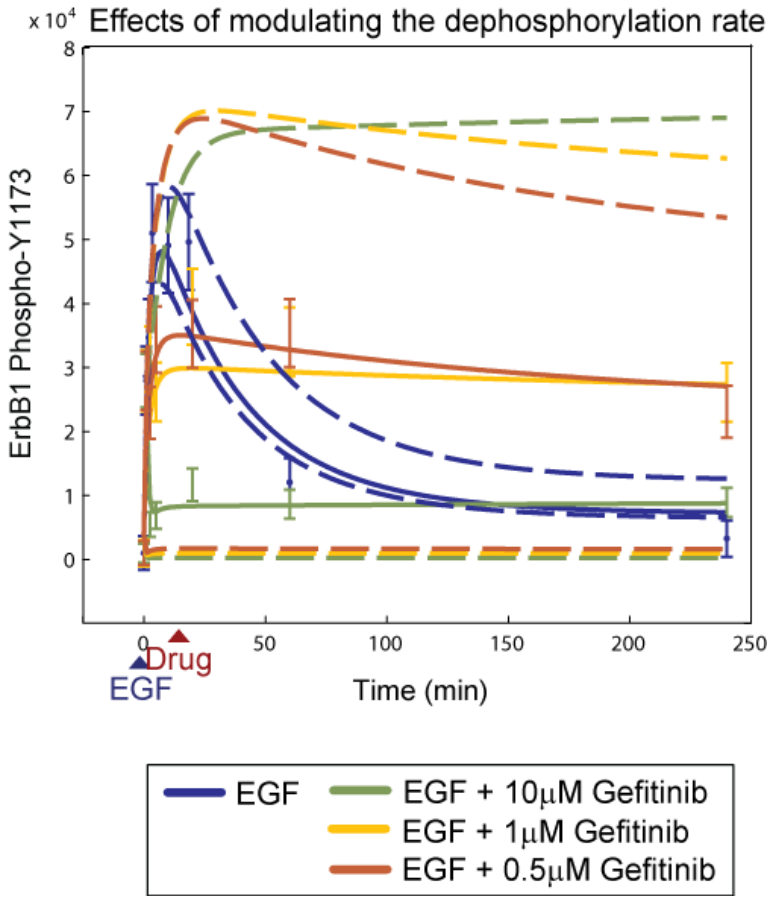

Figure 2.17 – Increasing or decreasing the rate of ErbB1 Y1173 dephosphorylation in the model does not strongly influence dynamics after EGF only, but significantly alters the response to gefitinib.

Experimental data of ErbB1 phosphorylation at Y1173 from Fig. 2.9B and used for fitting are shown here as solid curves, along with error bars derived from an error model (see Chapter 4 for details). Decreasing the parameter describing dephosphorylation of that site when ErbB1 is phosphatase-bound ("k2Poff") by 100-fold leads to the *higher* dashed curves, and increasing the rate by 100-fold leads to the *lower* dashed curves.

Exploring mechanisms for sustained ErbB1 signaling following treatment with low doses of gefitinib

Even when the dephosphorylation rate of ErbB1 Y1173 was decreased in the model, which led to very high levels of sustained phosphorylation after simulated gefitinib treatment, ErbB1 was still not degraded (not shown). It is generally thought that the degree of ErbB1 phosphorylation (including phosphorylation on specific phosphotyrosine sites such as Y1173) correlates with the degree of receptor degradation (Roepstorff et al., 2009). We explored potential mechanisms for this discrepancy between receptor phosphorylation and degradation in the model.

The E3 ubiquitin ligase Cbl is known to be recruited to phosphorylated Y1045 on ErbB1 (or indirectly through Grb2) after ligand stimulation (Levkowitz et al., 1998), and promote ubiquitination and degradation of the receptor. Therefore, our model describes two phosphotyrosine sites on ErbB1 that are regulated separately, one that represents Y1173 to which the adaptor protein Shc binds and transmits signals to downstream pathways, and another that represents Y1045 where Cbl binds and promotes downregulation of the receptor (see Chapter 4 for details). We hypothesized that the sustained phosphorylation on Y1173 is a result of altered receptor trafficking and inhibited degradation due to a difference in the ErbB1-Cbl-ubiquitination pathway.

Phosphorylation of ErbB1 at the Shc and Cbl-binding sites exhibit identical dynamics following stimulation with EGF alone in the model (Fig. 2.18, *top, blue curves*). However, phosphorylation of ErbB1 on the Cbl-binding site was inhibited after even 0.5μM gefitinib due to a larger (faster) fitted value for the dephosphorylation rate of this site ("k5Poff") compared to the dephosphorylation rate of Y1173 (73/min versus 2.5/min, respectively). Indeed, decreasing this rate to be equivalent to the dephosphorylation rate of Y1173 led to higher levels of Y1045 phosphorylation following gefitinib treatment, Cbl binding to ErbB1, trafficking and degradation

of the receptor, and therefore downregulation of Y1173 phosphorylation (Fig. 2.18, *bottom*).

However, faster dephosphorylation of the Cbl-binding site on ErbB1 compared to the Shc-binding site is only one way to explain our experimental data. If we force these two rates to be equivalent in the model, parameter values can still be found through fitting that match our experimental data of Y1173 phosphorylation and receptor degradation (not shown). This clearly highlights the issue of model non-identifiability, since other parameter sets and therefore model behaviors can also reproduce the observable data. Additional explanations for the sustained signaling on Y1173 without degradation could be other mechanisms regulating receptor trafficking, such as parameters controlling Cbl binding, ErbB1 internalization or receptor ubiquitination. Nonetheless, these modeling results emphasize decoupling between the pathways promoting downstream signal propagation and receptor downregulation, and again illustrate the importance of pulse-chase experiments to detect this decoupling.

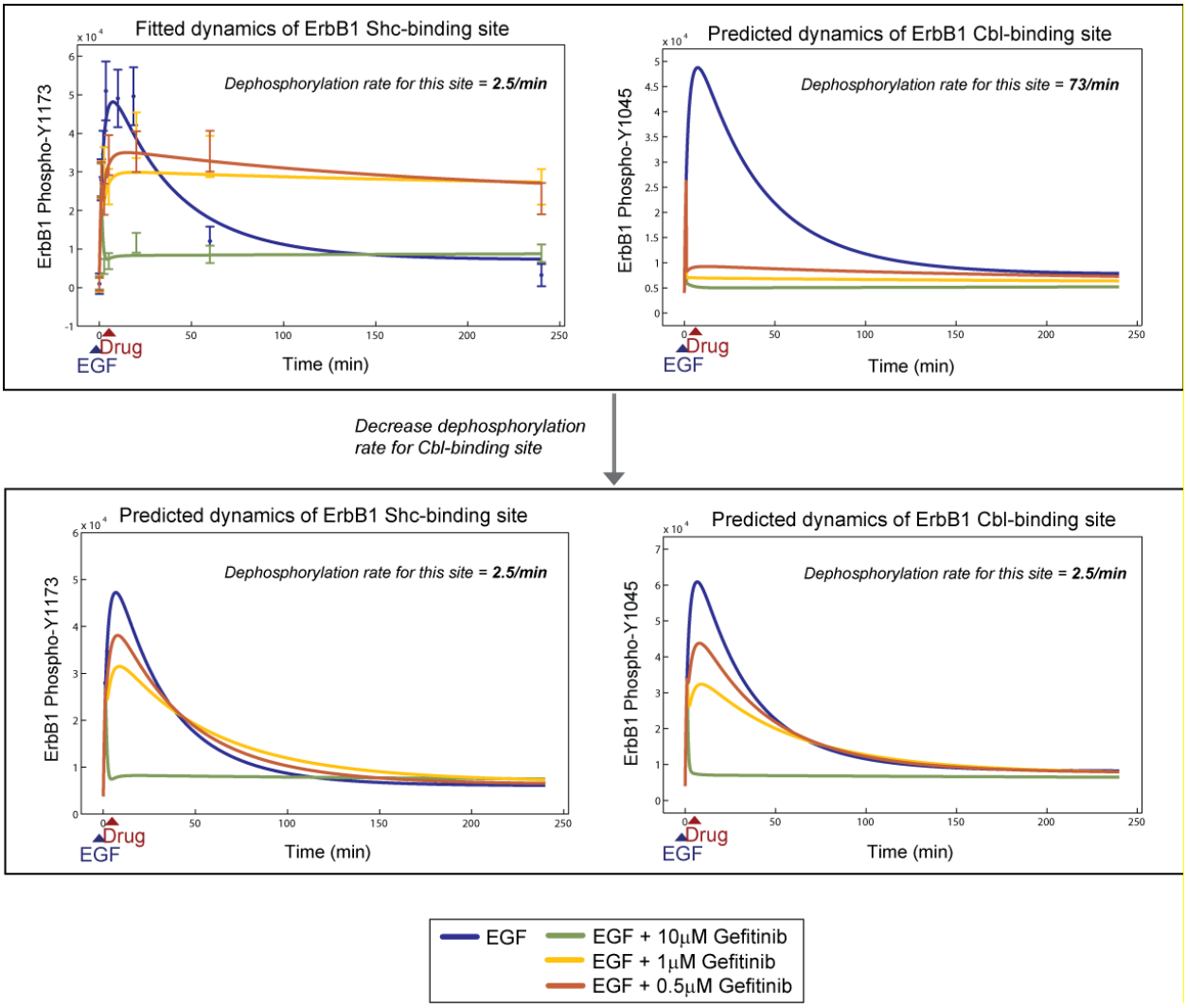

Figure 2.18 – Model prediction that sustained phosphorylation of ErbB1 Y1173 after low doses of gefitinib results from a faster dephosphorylation rate of the Cbl-binding site.

Top left: same as the solid curves and data shown in Figure 2.17. *Top right*: Predicted dynamics of ErbB1 at the Cbl-binding site based on the fitted parameter values. Even low doses of gefitinib lead to dephosphorylation. *Bottom*: Effects of decreasing the dephosphorylation rate of the Cbl-binding site ("k5Poff") to be equivalent to the Shc-binding site. Now Y1173 is dephosphorylated after low doses of gefitinib.

CHAPTER 3: Discussion and Future Directions

Summary of approach and key results

Protein phosphorylation networks play an essential role in the control of almost all physiologic processes, including cell growth, differentiation, migration and oncogenesis. The ErbB pathway, a prototypical signaling network regulated by phosphorylation cascades, is frequently hyperactive in cancer and is being aggressively targeted in the clinic with various therapeutic antibodies and small molecule kinase inhibitors. However, fundamental questions about the regulation of this pathway and the effects of the drugs remain unaddressed. This thesis describes experimental and computational methods that were developed to examine how ErbB1 kinases and phosphatases work in concert to control the dynamics of receptor phosphorylation and downstream signaling and to understand how ErbB1-targeting drugs alter this regulation.

We discovered that individual proteins undergo extremely rapid phosphorylation cycling and that these fast dynamics play a crucial role in determining the response to ErbB1-targeting cancer therapies, which we found to vary significantly between drugs with different mechanisms of action. We showed that treatment with some of these drugs results in sustained signaling, instead of inhibition, and thus may actually promote tumor proliferation or invasion. Beyond therapeutics, we elucidated the importance of teasing out the time scales of different events regulating cell signaling. We found that signals are rapidly propagated through some pathways but slowly through others, leading to prolonged activation in the absence of upstream signal, and that fast phosphorylation and dephosphorylation may provide cells with the flexibility necessary to rapidly detect and respond to changes in their extracellular environment. Importantly, we formulate a general strategy for analyzing biochemical signaling networks that integrates pulse-chase experiments where one node within a pathway is very rapidly inhibited, with a hierarchy of computational models that each allow different biochemical aspects to be addressed.

Rapid ErbB1 dephosphorylation following sequential ligand and gefitinib treatment

Once activated by ligand, cell surface receptors could theoretically remain active for a long time and continue to transduce signals to downstream pathways, or they could quickly turn off and require detection of upstream signal for further activation. Based on population-level measurements, ErbB1 receptors appear to remain phosphorylated for many minutes or hours after exogenous growth factor stimulation. Signal downregulation is primarily thought to result from dephosphorylation by phosphatases that are brought into close proximity after receptor endocytosis, ligand removal from endosomes (Burke et al., 2001), or ErbB1 degradation. We investigated the frequency with which proteins in the ErbB1 signaling pathway are phosphorylated in response to growth factors to address whether these dynamics are representative of the phosphorylation and dephosphorylation rates of individual proteins. Since it is not feasible to directly measure phosphorylation of a single protein over time, we deduced these individual molecule dynamics from population measurements.

To this end, we performed the simple experiment of inactivating receptor catalytic activity after ligand addition with a panel of ATP-competitive ErbB1 kinase inhibitors (pulse-chase experiments) and measured receptor dephosphorylation kinetics. If receptors become phosphorylated and then remain phosphorylated until degradation (~30-120 min), addition of kinase inhibitors after receptor phosphorylation should not significantly alter the degree of phosphorylation. However, the results were striking: we found that drugs such as gefitinib result in dephosphorylation of nearly all ErbB1 receptors within 10 seconds after addition to cells, suggesting that individual receptors undergo multiple rounds of phosphorylation and dephosphorylation each minute, even though the overall level of phosphorylation changes very slowly. Yet our explanation of the data was complicated by the fact that drugs with different mechanisms of action result in remarkably different dephosphorylation kinetics and dose-response behaviors.

Previous evidence indicating an important role for phosphatases

Over the past few decades, the field has begun to appreciate the importance of phosphatases in regulating the activity of signaling pathways. Heinrich and colleagues (Heinrich et al., 2002) developed a simple mathematical model of the kinetics of protein kinase signaling pathways and computationally analyzed the effects of kinases and phosphatases on signaling rate, duration and amplitude. The authors found that signaling rate and duration are primarily controlled by phosphatases (less so by kinases), and they considered the balance between the two opposing entities. Yet their analysis did not include any experimental verification of their model predictions.

Early indications of the role of phosphatases in regulating ErbB1 activity came from experimental observations that after receptor phosphorylation by ligand stimulation, the addition of inhibitors of the catalytic activity of ErbB1 led to faster ErbB1 dephosphorylation than in the presence of ligand alone (Bohmer et al., 1995; Offterdinger et al., 2004). However, a detailed study of the dynamics and the seemingly profound implications of these findings had not been performed until now. Here we integrated computation with experiments to improve our understanding of the underlying biochemistry.

Computational models of ErbB1 regulation

Models previously developed to study the ErbB system were inadequate for our purposes. Some models do not accurately describe competition of kinase inhibitors with ATP for binding to ErbB1 and are only useful to simulate pre-incubation with inhibitors (e.g. (Chen et al., 2009)), and others assume that ErbB phosphatases do not play an important role in receptor and downstream regulation so therefore do not consider them (e.g. (Orton et al., 2009)). Furthermore, we found it necessary to develop a succession of mathematical models of varying biochemical resolution to help guide our interpretations of the data, each one useful for a

different question we wanted to address. These models ranged from simple (one ordinary differential equation (ODE)) to quite elaborate and realistic (hundreds of ODEs).

We estimated lower bounds for phospho-ErbB1 turnover using a small model describing receptor phosphorylation and dephosphorylation (the only one of these models with identifiable parameters) by fitting to phosphorylation measurements of dense temporal sampling following inhibitor addition. While parameters of the larger models were not identifiable, the phosphorylation and dephosphorylation rate constants estimated with these models by considering many different fits of the model to data were only slightly higher. These more detailed models were used to analyze properties of ErbB1 receptors and drugs that give rise to the different drug responses and to understand the somewhat non-intuitive effects of the drugs in the presence of decreased phosphatase activity. The models fit the data well and we could accurately predict the results of new experiments, suggesting that our assumptions and those in the literature are consistent and reasonable and that we have a good biochemical understanding of how the receptors and drugs function.

Phosphatase activity regulating ErbB1

ErbB1 is rapidly dephosphorylated regardless of subcellular localization

We found fast phosphorylation/dephosphorylation cycling regardless of ErbB1 subcellular localization. Our results challenge the classical notion that ErbB1 is phosphorylated at the plasma membrane after ligand binding and then remains phosphorylated until receptor degradation or dephosphorylation when the receptor co-localizes with PTP1B near the ER. Evidence of long-term EGF treatment resulting in accumulation of dephosphorylated receptor in the perinuclear region (Offterdinger et al., 2004) suggests that phosphatases may be more active at intracellular sites and play a significant role in overall ErbB1 signal attenuation. However, a recent paper showed that the phosphatase DEP-1 acts on ErbB1 only at the cell

surface and does not internalize along with ErbB1 (Tarcic et al., 2009). After EGF stimulation, more receptors were bound by substrate-trapping mutants of DEP-1 than wild-type DEP-1, suggesting that phosphatases may bind in a reversible manner to dephosphorylate ErbB1. We conclude that ErbB1 phosphatases are always localized near the receptors and are continually acting on them, although different phosphatases are likely to be important over a time course of ErbB1 stimulation and trafficking.

Identification of PTPs responsible for rapid ErbB1 dephosphorylation

We do not know the full spectrum of phosphatases acting on ErbB1 or which tyrosine residues on the receptor are targets of specific PTPs. It is also unclear if and when PTPs directly bind to the receptor and how that regulates their activity, and if different phosphatases can act on one receptor and if they can do so simultaneously. We asked whether the best studied ErbB1 phosphatase, PTP1B, plays a role in rapid gefitinib-induced ErbB1 dephosphorylation and found that knocking down PTP1B had no effect in H1666 cells when gefitinib was added after 10 minutes of EGF treatment. It is possible that at this time ErbB1 and PTP1B are unable to interact due to their subcellular localizations and that their interaction only occurs at later times during receptor trafficking. However, we could not find any evidence in the literature for PTPs that might act on ErbB1 while the receptor is being internalized and shuttled to early endosomes.

Either way, our PTP1B knockdown results are not very surprising since, depending on the local concentration of kinases and phosphatases, basically all phosphatases capable of contributing to the fast dephosphorylation may have to be depleted to see any effect. There are many potential candidates for the relevant PTP(s) (there are more than 100 different PTPs in the mammalian genome (Alonso et al., 2004)), and it is possible that chronic depletion of one could result in compensation by others. Furthermore, phosphatase activity may be dynamically

regulated following ligand stimulation. For all of these reasons, it will be very challenging, if not impossible, to identify the specific phosphatase(s) that contribute to rapid ErbB1 phosphorylation cycling, and doing so is beyond the scope of this thesis. Nonetheless, the pan-specific tyrosine phosphatase inhibitor pervanadate blocked the gefitinib-induced ErbB1 dephosphorylation, demonstrating that phosphatases are indeed responsible for this behavior.

Chemical inhibitors of ErbB1 phosphatases

Potent and selective phosphatase inhibitors could facilitate the search for PTPs that regulate fast phosphorylation cycling, as well as help identify PTPs that regulate specific ErbB1 phosphotyrosine sites and ErbB1 in different subcellular localizations. Unfortunately, commercially available inhibitors seem to be of poor quality. A key challenge in developing PTP inhibitors is the issue of selectivity due to the highly conserved PTP active site (the phosphotyrosine binding site). To address this problem, bidentate PTP inhibitors that simultaneously bind both the active site and a unique adjacent site for enhanced affinity and specificity are under development (Zhang, 2002).

However, there may be fewer incentives to develop PTP inhibitors than PTK inhibitors since it is unclear whether these represent good targets for therapeutic drugs. Intuitively, decreasing the activity of a PTP should lead to increased phosphorylation of the PTP substrate and hyperactivation of its downstream signaling pathway. In this case, a potential method to curb overactive ErbB1 signaling could include activating or recruiting PTPs that dephosphorylate and inactivate the receptor. Yet the effects of modulating phosphatase activity can be complex for multiple reasons: phosphatases can be positive (e.g. Shp-2) or negative (e.g. Shp-1) effectors of RTK signaling, phosphatases can dephosphorylate inhibitory sites, and each PTP can have multiple substrates and might regulate the activity of the various substrates in different ways. The functions of PTPs in cell signaling are still being unraveled and will likely

influence the decision of whether to try to modulate their activity therapeutically.

Future study: PTP siRNA screen

Attempts could be made to identify PTPs that regulate the rapid phosphorylation cycling of ErbB1 using an RNAi screen of the potential phosphatases. Following knockdown, similar experiments to the ones described in this thesis could be performed, where cells are stimulated with ligand and then ErbB1 catalytic activity inhibited with gefitinib. ErbB1 phosphorylation measurements would then elucidate whether the knockdown blocked ErbB1 dephosphorylation. These measurements could be done for different ErbB1 phosphotyrosine sites and at different times during receptor trafficking. In one recently published siRNA screen, the authors knocked down all PTPs and then measured the effect on ErbB1 phosphorylation (Tarcic et al., 2009). Another group screened the effects of knocking down 244 phosphatases (tyrosine-, serine- and threonine-specific phosphatases) on ERK and Akt phosphorylation (Omerovic et al., 2010). These two studies monitored the steady state effects of decreasing phosphatase activity, while the experiments proposed here would instead ask how important each phosphatase is under the particular pulse-chase conditions.

Transient phosphorylation and binding events are likely general regulatory mechanisms

Prior indications that other proteins may also undergo rapid phosphorylation cycling

Fast cycling has been observed for the aggregation and phosphorylation of high affinity IgE receptors on rat basophilic leukemia cells (Mao and Metzger, 1997). IgE receptors normally mediate inflammatory reactions such as allergic responses. In this study, cells were stimulated with multivalent antigen (antigen-activated cells) followed by disaggregation with monomeric

hapten. The receptors, which do not have intrinsic kinase activity and are phosphorylated by other cytosolic proteins, were rapidly dephosphorylated, suggesting that fast phosphorylation cycling may not be specific for ErbB1.

It is also possible that the same PTPs that regulate phospho-ErbB1 cycling also regulate other proteins using similar mechanisms. Each PTP can have multiple substrates and ErbB1 PTPs have been shown to dephosphorylate other receptors. For example, DEP-1 suppresses signaling emanating from other RTKs, such as PDGF β-receptors and HGF/Met receptors (Kovalenko et al., 2000; Palka et al., 2003). Indeed, after sequential ligand and drug treatment specific for PDGF receptors, these receptors were dephosphorylated more rapidly than in the presence of ligand alone (Bohmer et al., 1995).

All proteins measured in the ErbB network undergo fast phosphorylation cycling

We measured activation of the canonical ErbB1 immediate-early downstream pathways after sequential exposure of cells to ligand and gefitinib, and reasoned that the rapid shut-off of other proteins would imply that the proteins also undergo fast phosphorylation cycling. This approach of activating the ErbB1 network with ligand and then instantly turning off the receptor with gefitinib is analogous to applying a step function and allowed us to investigate how these rapid receptor dynamics propagate downstream. We found that a fast dissociation rate of the adaptor protein Shc for binding to ErbB1 leads to a dynamic equilibrium with low stability of the ErbB1-Shc complex such that phosphatases can rapidly dephosphorylate ErbB1 sites that are Shc-bound at the time of gefitinib addition. These results corroborate *in vitro* measurements showing that interactions of SH2 domains with phosphotyrosines can occur with a half life around 6 seconds (Felder et al., 1993), similar to our estimates for the ErbB1 dephosphorylation rate.

Proteins within the ErbB3-PI3K-Akt pathway were immediately dephosphorylated once ErbB1 activity was terminated, suggesting that activation of these proteins is closely linked to continued upstream signal. However, there was a delay in attenuation of the Shc-Ras-MAPK (Raf-MEK-ERK) pathway, where gefitinib led to fast Shc dephosphorylation but slow ERK phosphorylation, which we determined was not due to slow ERK phosphatase activity since a MEK inhibitor led to rapid ERK dephosphorylation. This delay was variable between cell types and correlated with the presence of activating mutations within the pathway that may prolong signaling (H1666 cells harbor a B-Raf G466V low-activity mutation (Pratilas et al., 2008)). Slower dephosphorylation of the ERK pathway in general could be attributed to more steps in the cascade between ErbB1 and ERK versus ErbB1 and Akt, therefore taking more time, or to GAP-mediated inactivation of Ras, which may be slower than the dephosphorylation reactions.

Additional measurements of pathway activity between Shc and ERK (e.g. measurements of Ras activity, Raf phosphorylation or MEK phosphorylation) and additional inhibitors (e.g. Raf inhibitors) could be helpful to narrow down the position(s) within the pathway where the delay arises. All proteins we measured were rapidly shut off when either ErbB1 or MEK were inhibited, which implies that they are undergoing rapid phosphorylation cycling and require upstream activation to remain phosphorylated. Very little is known about the regulation of these other proteins by phosphatases and this would be interesting to explore using similar methods as those described above for ErbB1 PTPs. These studies confirmed the notion that phosphorylation cycling not a property limited to ErbB1. Moreover, we provide *in vivo* evidence that a single cell line under the same culture conditions exhibits transient ligand binding, protein-protein interactions and phosphorylation, making it somewhat surprising that signals can still be effectively propagated through this pathway.

Binding affinities of adaptor proteins for ErbB1 may be dynamically regulated

Several studies have suggested that binding affinities for ErbB1 adaptor proteins decrease upon phosphorylation of the adaptor proteins, which in some cases is mediated directly by ErbB1 catalytic activity. For example, using molecular dynamics simulations phosphorylation of Shc on Y317 was shown to decrease its affinity for ErbB1 (Suenaga et al., 2009). Shc Y317 is phosphorylated by ErbB1 and acts as a major site for binding the Grb2 adaptor and the Grb2-SOS complex, which triggers Ras activation. The effects of this decrease in affinity are unclear. We have shown rapid phosphorylation and dephosphorylation cycling of this phospho-site on Shc, so presumably if phospho-Shc could no longer bind ErbB1 it would be rapidly dephosphorylated. However, Shc was phosphorylated with almost identical dynamics to ErbB1 in our measurements, and through co-immunoprecipitation we showed the ErbB1-Shc association to persist for at least 30 minutes after ligand stimulation. This diminished binding may play a role in terminating signals emanating from ErbB1 on longer time scales.

Future study: Broad signaling analysis of deactivation kinetics

We found different time scales of propagation through the two canonical ErbB downstream pathways, where signals were transmitted through the Akt pathway very rapidly, but there was a delay between ErbB1 and Shc dephosphorylation and ERK dephosphorylation. This study served as a proof of principle for stimulating a signaling pathway and then immediately inhibiting a node of the pathway to measure deactivation kinetics. Interestingly, this approach is not limited to gefitinib-induced dephosphorylation but could potentially be applied with any fast binding drug. For example, the MEK inhibitor PD0325901 used in Chapter 2 resulted in very rapid ERK dephosphorylation.

This approach could be used in a broad signaling study where cells are treated with different combinations of ligand and then drug, and time courses of deactivation kinetics are

measured throughout the pathway. This study would benefit from high-throughput methods for measuring protein phosphorylation, such as Luminex (bead-based multiplexed ELISAs) (Du et al., 2009; Saez-Rodriguez et al., 2009), mass spectrometry (Wolf-Yadlin et al., 2006) or reverse-phase protein lysate arrays (Gujral and MacBeath, 2009; Sevecka and MacBeath, 2006). Many positive and negative feedback loops regulate signal transduction networks and insight could be gained by inhibiting downstream nodes and measuring the effects on upstream nodes. The breadth of this study will widen as more potent and selective inhibitors become available.

Rewiring of signaling networks

A comparison of different cell types in a study of this nature could reveal how signaling pathways are rewired during disease (for example, if the cell types being compared are normal versus cancer tissue) or as an effect of a certain genetic mutation (if isogenic cells differing only in the expression of that mutation were used). Sophisticated computational modeling methods have recently been developed to analyze and interpret large datasets of this kind and deconstruct differential pathway usage (Saez-Rodriguez et al., 2009). In addition to increasing our understanding of signal transduction networks, this study would provide crucial information about the effects of drugs and could be a way to screen for and identify promising therapeutics. Short-term effects of drugs, which presumably influence and perhaps determine the long-term response, cannot be revealed using the typical method of pretreating cells with drugs prior to ligand stimulation.

Phosphatase regulation of ErbB2 and ErbB3

Since ErbB1 signaling can be shut off through internalization and degradation, it will be interesting to understand how receptors that are not internalized are regulated by phosphatases, as it is possible that phosphatases play a more pertinent role in overall signal

attenuation from these receptors. Downregulation of ErbB2 and ErbB3 following growth factor stimulation is not thought to be mediated by endocytosis (Baulida et al., 1996). In Chapter 2 we showed that ErbB2 and ErbB3 are phosphorylated after EGF stimulation, and then rapidly dephosphorylated after addition of gefitinib with similar half lives as ErbB1. These results suggest that ErbB2 and ErbB3 are also subject to rapid phosphorylation and dephosphorylation cycling, although very little is known about phosphatases for these receptors.

Examining whether phosphatases are activated following ligand stimulation to promote overall phospho-ErbB downregulation

We tried to address whether ErbB1 phosphatase activity changes over time by monitoring ErbB1 dephosphorylation after EGF pulses of different durations followed by addition of 1μM gefitinib. This treatment immediately reduces ErbB1 phosphorylation levels by ~50% and results in a new steady state level. We hypothesized that the new steady state reached after gefitinib would be representative of the ratio of kinases and phosphatases that can act on the receptor at that time, and if we could assume that the kinase activity remains constant it would provide clues to the phosphatase activity. Of course, the concentration of active kinases for ErbB1 is expected to change over a time course of ligand stimulation, first increased due to receptor dimerization and then decreased due to receptor degradation. Indeed, the steady state level decreased slightly as gefitinib was added at later times once the receptor was internalized, and our mathematical modeling suggested that this decrease could be attributed to receptor degradation alone and did not require an increase in phosphatase activity. This experiment of adding 1μM gefitinib after different durations of EGF stimulation could be repeated and phospho-ErbB2 and ErbB3 measured. These receptors are likely not degraded during this time and our measurements show ErbB3 becoming phosphorylated and then dephosphorylated within minutes of EGF stimulation. Adding pervanadate at different times after EGF exposure and measuring phosphorylation of these two receptors could also be informative.

Stimulation of ErbB3 by EGF and HRG

We wondered whether ErbB3 was also only transiently activated after stimulation with the growth factor heregulin (HRG), which binds to ErbB3 directly. In contrast to stimulation with the ErbB1-ligand EGF, we found that ErbB3 phosphorylation was sustained following exposure to HRG. Moreover, when gefitinib was added to cells after 10 minutes of HRG stimulation, ErbB3 was dephosphorylated slowly in comparison to when gefitinib was added after EGF. These intriguing results can be explained by a number of possibilities.

The differences may indicate more potent phosphatase activity following EGF stimulation, perhaps triggered by different dimers that form and contribute to the level of ErbB3 phosphorylation after exposure to the growth factors (likely ErbB1-ErbB3 dimers after EGF and ErbB2-ErbB3 dimers after HRG). It is conceivable that different phosphatases are recruited to different dimers and that potent ErbB1 phosphatases recruited to ErbB1-ErbB3 dimers are more likely to act on ErbB3 as well due to close proximity. Assuming that dimerization is a transient and continuous process, an alternative explanation for the different dynamics of ErbB3 phosphorylation following EGF and HRG stimulation is that ErbB1 is internalized and therefore depleted from the pool of receptors available to bind ErbB3 at the cell surface after EGF stimulation. This may lead to a decrease in the number of ErbB1-ErbB3 heterodimers and therefore a decrease in the number of phosphorylated ErbB3 receptors.

If ErbB2-ErbB3 dimers are indeed dominant after HRG stimulation, the slow dephosphorylation of ErbB3 following HRG and then gefitinib addition could be a function of gefitinib binding to ErbB2. Since gefitinib binds with lower affinity (higher K_d) to ErbB2, the slow dephosphorylation of ErbB3 could be due to the time it takes for gefitinib to inhibit ErbB2 catalytic activity. One way to address this could be to use a fast binding and specific small molecule kinase inhibitor of ErbB2 instead of gefitinib, which was not possible here since we are currently unaware of the existence of such an inhibitor. HRG stimulation and gefitinib addition have been shown to promote the dissociation of ErbB2-ErbB3 dimers and formation of inactive,

gefitinib-bound ErbB1-ErbB2 and ErbB1-ErbB3 dimers (Anido et al., 2003). This process could also contribute to the slow dephosphorylation of ErbB3 that we measured.

ErbB3 relevance in cancer

ErbB3 plays an important role in resistance to ErbB1- and ErbB2-targeting drugs. Resistance to gefitinib and erlotinib in lung cancer has been attributed to MET amplification-driven activation of ErbB3 (Engelman et al., 2007). In addition, ErbB3 has been found to be transcriptionally upregulated in breast cancer after lapatinib treatment (Amin et al., 2010). Prolonged gefitinib treatment of breast cancer cells was shown to cause resistance to ErbB3 dephosphorylation following an additional pulse of gefitinib. This resistance was explained by an increase in cell surface ErbB3 receptors and a decrease in ErbB3 phosphatase activity resulting from production of cellular reactive oxygen species, which are known to inhibit PTPs (Sergina et al., 2007). Accordingly, attempts to target ErbB3 by blocking ligand binding are underway and the first therapeutic anti-ErbB3 antibody is in clinical development (Schoeberl et al., 2009). The phospho-ErbB ELISA assays developed in this thesis and discussed in Chapter 4 will be useful for future studies to dissect the regulation of ErbB2 and ErbB3 by phosphatases, since they are more specific, sensitive and quantitative than the typical methods used to measure receptor phosphorylation.

Physiological consequences of rapid phosphorylation cycling

It is typically assumed that the specific kinetics of phosphorylation reactions play a role in controlling the physiological behavior of cells, but this connection had not been fully established. We discovered that fast phosphorylation cycling and signal propagation allows for rapid responses at the phenotypic level. ErbB1 phosphorylation dynamics were intimately linked to protrusion of lamellipodia, an early event in the process of cell migration, such that

lamellipodia stopped protruding and began to retract almost immediately after shutting off the receptors with 10μM gefitinib, following an initial EGF pulse. The short time difference between receptor dephosphorylation and lamellipodia retraction is likely attributed to how long it takes for intermediates (e.g. ERK and Akt) to be inhibited under these conditions.

Interestingly, we found that adding 1μM gefitinib shortly after EGF blocks the typical EGF-induced increase in receptor phosphorylation and instead results in lower but sustained phosphorylation; however, short-term protrusion dynamics were unaffected. Continued extension of lamellipodia therefore requires continued, but not necessarily increasing, receptor phosphorylation. We conclude that fast phosphorylation and dephosphorylation may provide cells with the flexibility necessary to rapidly detect and respond to changes in their extracellular environment. To our knowledge, this is the first study showing the dependency of short-term receptor signaling on lamellipodia extension and retraction following ligand stimulation.

To more accurately determine whether rapid phosphorylation cycling allows ErbB1 to act as an immediate sensor, it is important to understand the effects of a decrease in the actual ligand concentration as opposed to a decrease in receptor catalytic activity. Following EGF stimulation, removal of EGF by either washing away ligand or using the monoclonal antibody 225 to compete with ligand binding led to slow receptor dephosphorylation (although faster than in the continued presence of ligand). This dephosphorylation rate when removing ligand likely depends on the additional rates of ligand dissociation and the dissociation of ErbB1 oligomers. By measuring the effects of blocking phosphorylation directly with drugs like gefitinib, we eliminated these potentially slower time scales from the analysis (e.g. EGF is known to have a slow dissociation rate). Many different ligands can bind to ErbB1, and ligands with faster off rates such as growth factor receptor ligands immobilized in the extracellular matrix (Iyer et al., 2007; Tran et al., 2004) may have similar effects as gefitinib on ErbB1 dephosphorylation and retraction of membrane protrusions. We therefore speculate that the rate of response to a decrease in ligand concentration is dominated by the specific ligand dissociation rate.

Future studies to relate receptor activity to membrane protrusion dynamics

Ligands with faster dissociation rates could be used to test the relationship between a decrease in the extracellular growth factor concentration and the protrusion of lamellipodia. For example, amphiregulin is a physiologically relevant ErbB1 ligand with low affinity for the receptor and is thought to have a fast off rate (Neelam et al., 1998; Roepstorff et al., 2009). Thus, the fraction of ErbB1 receptors bound by amphiregulin after exposure to the ligand and then washing it away should diminish quickly, and a faster decrease in ErbB1 phosphorylation may be detected compared to our results with EGF. If this is the case, experiments using a microfluidics device could explore the kinetics of and relationship between amphiregulin washout and retraction of lamellipodia.

To more precisely determine the role of fast ErbB1 phosphorylation and dephosphorylation in regulating protrusion dynamics, modulation of these rates is necessary. If specific PTPs responsible for the fast ErbB1 phosphorylation cycling are later identified, it would be interesting to inhibit (e.g. by knock down or chemical inhibition) or activate (e.g. by PTP overexpression) the PTP activity and correlate membrane protrusion dynamics with varying dephosphorylation rates.

Investigating the striking differences in the responses to ErbB1-targeting drugs

Pulse-chase experiments reveal transient drug effects

The search for effective drugs targeting the ErbB receptors has exploded over the past 10 years (Knight et al., 2010). Although some drugs are already being used to treat patients, several basic properties of the drugs and their cellular targets are still only poorly understood. The typical method used to determine drug efficacy in cell culture is to measure whether signaling is inhibited after treating cells with a drug for many hours or days, or pretreating with

the drug before challenging cells with exogenous ligand. These experiments report on the steady state effects of drug treatment and may be useful for understanding the potential long-term effects of drugs *in vivo*. However, steady state signaling levels *in vivo* following drug treatment may also be modulated by factors that are not applicable in cell culture, so the relevancy of measuring steady state drug effects in cell culture is unclear.

We find that there is a large amount of information contained in the early drug response. Here we illustrate the importance of understanding the transient (short-term) response to drugs and show that this approach can elucidate drug mechanism of action and immediate effects of inhibition. We activated the ErbB signaling pathway with exogenous ligand before drug treatment ("pulse-chase" experiments) to be able to measure the dynamics of deactivation in the presence of various drugs.

Differences between drugs with various mechanisms of action

We evaluated the kinetics of ErbB1 dephosphorylation following EGF stimulation and then addition of gefitinib, erlotinib, lapatinib or canertinib and found very different dose-response behaviors. We developed a computational model to quantitatively explore properties of the receptors and drugs that give rise to these striking differences, specifically between gefitinib and lapatinib. We initially tried to explain these differences in the model by only taking into account their different binding velocities to ErbB1, but found that the model could not explain the experimental data without also accounting for the different conformations of ErbB1 to which the drugs bind, suggesting that this is important in determining their behavior. Since it is unclear how to test this experimentally, using the model we showed that these distinct drug responses are caused by rapid ErbB1 phosphorylation cycling, and that slower phosphorylation and dephosphorylation rates generate similar ErbB1 dynamics in the presence of the two drugs.

For gefitinib or erlotinib, which bind reversibly to an active ErbB1 conformation with fast kinetics, dosing at the mean patient plasma concentration (~1μM (Baselga et al., 2002)) in pulse-chase experiments led to only partial receptor inhibition and surprisingly sustained signaling. However, treatment at this concentration with lapatinib, which binds reversibly to an inactive ErbB1 conformation with slow kinetics, resulted in complete receptor inhibition. Interestingly, the irreversible inhibitor canertinib had an intermediate dose-response behavior where high doses resulted in rapid ErbB1 dephosphorylation and low doses resulted in slow but complete dephosphorylation. Lapatinib is currently only approved to treat breast cancers overexpressing ErbB2, but our results suggest that it may also be effective for other tumors.

The time course dose-response behaviors shown in Chapter 2 for gefitinib, lapatinib and canertinib are very different and it would be difficult to make sense of these data if only the typically IC50 curves had been obtained, where one time point of receptor phosphorylation is measured for each concentration of drug. These IC50 curves would vary based on the time point chosen, and the results would be especially uninformative if this time point was taken after ~1 hour of drug treatment, when even low doses of lapatinib and canertinib result in complete receptor dephosphorylation. IC50 curves after treatment with gefitinib should be relatively time-independent since different doses result in a quite stable new steady state phosphorylation level. IC50 curves generated after long durations of drug treatment (e.g. multiple days) may report on indirect effects of the drug binding to ErbB1, such as subsequent activation of drug resistance pathways or protein degradation. Nonetheless, the variation measured here between these three drugs strongly advocates for dynamic measurements to be able to understand their direct effects.

Increased steady state inhibition of ErbB1 by lapatinib is likely due to its mode of binding to ErbB1

In addition to binding to ErbB1, lapatinib has a high affinity for ErbB2 and a relatively high affinity for ErbB4. ErbB1 phosphorylation following lapatinib treatment could be inhibited by lapatinib-bound ErbB2 or ErbB4 receptors that interact with ErbB1 in heterodimers and would normally phosphorylate ErbB1. Therefore, at similar concentrations lapatinib could potentially lead to more steady state inhibition of ErbB1 than gefitinib, which only binds with high affinity to ErbB1 and thus should only inhibit ErbB1 homodimers. However, we do not believe that binding of lapatinib to ErbB2 or ErbB4 is relevant to our results. H1666 and MCF-10A cells express low or undetectable levels of ErbB receptors other than ErbB1, so ErbB1 homodimers are likely the predominant dimers formed following EGF stimulation. Furthermore, our computational models could explain our experimental data without taking into account lapatinib binding to ErbB2 or ErbB4, and the lower steady states reached with lapatinib make sense based on its slow dissociation rate and ability to stabilize the inactive-like ErbB1 conformation (Wood et al., 2004). The irreversible inhibitor canertinib also eventually led to complete ErbB1 dephosphorylation at low doses and does not bind as strongly to ErbB2, suggesting that the effects of lapatinib can be explained based solely on mechanism of action of drug binding. An additional possibility is that ErbB1 is efficiently degraded following lapatinib but not gefitinib treatment. However, ErbB1 was not found to be degraded after treatment with either of these drugs (Wood et al., 2004).

Subsaturating doses of gefitinib turn a transient response to ligand into a sustained ErbB1 signal

We propose that gefitinib treatment leads to a rapid equilibrium of drug-bound receptors and phosphorylated receptors due to both fast drug binding and fast phosphorylation and dephosphorylation rates. When gefitinib was added while ErbB1 was at the plasma membrane, normal receptor trafficking following EGF stimulation was altered such that internalization may

have been partially blocked and receptors were not degraded. Receptors that were dephosphorylated due to gefitinib treatment would presumably be unable to recruit and bind the E3 ubiquitin ligase Cbl, which interacts with ErbB1 via phosphotyrosine residues to mediate its internalization and downregulation (Fry et al., 2009). Indeed, gefitinib is known to inhibit ErbB1 internalization and receptor trafficking (Nishimura et al., 2007).

This straightforward explanation of the 10μM gefitinib data was brought into question by experiments where we treated cells with lower doses of gefitinib (0.5 or 1μM), which resulted in a fraction of receptors still phosphorylated on Y1173 but trafficking and degradation blocked. We examined this discrepancy using a very detailed mathematical model describing normal EGF-induced ErbB1 regulation, including activation by ligand binding and receptor dimerization, and downregulation by ErbB1 internalization, ubiquitination and degradation. We found a disconnect between the pathways emanating from ErbB1 that lead to signal propagation (in our model, via binding of Shc to ErbB1) and receptor downregulation (via binding of Cbl to ErbB1) which was only detectable following subsaturating gefitinib treatments.

After fitting the model to ErbB1 phospho-Y1173 and total ErbB1 data following treatment with different concentrations of gefitinib added after 1 minute of EGF stimulation, the model predicted that the sustained signaling after 1μM gefitinib was due to a faster dephosphorylation rate of the Cbl-binding site on ErbB1, compared to the Shc-binding site. This results in Cbl being unable to bind to ErbB1 and promote its degradation, leading to sustained phosphorylation of the Shc-binding site since its normal downregulation by receptor degradation is now blocked. However, the data could still be explained in the model by imposing the same dephosphorylation rates for the two phosphotyrosine sites on ErbB1, illustrating the basic non-identifiability problem of these models (discussed in Chapters 2 and 4). In Chapter 2 we measured dephosphorylation of multiple ErbB1 phospho-sites after sequential EGF and 10μM gefitinib treatment, including Y1045 where Cbl binds to ErbB1 directly. We found that all sites were rapidly dephosphorylated and concluded that rapid phosphorylation cycling occurs at all

sites. Nonetheless, it is still possible that there are different dephosphorylation rates for the sites that is undetectable under these conditions but may become apparent after treatment with various gefitinib doses.

ErbB1vIII mutants are hypophosphorylated on the Y1045 Cbl-binding site

ErbB1vIII (normally referred to as EGFRvIII, but for consistency we use the nomenclature ErbB1) is a truncation mutant of ErbB1 that is expressed in about 40-50% of human glioblastomas (Gan et al., 2009). A portion of the extracellular domain is deleted in this mutant such that the receptor cannot bind ligand yet it is constitutively active. ErbB1vIII is internalized at a much slower rate than wild-type ErbB1 and is inefficiently ubiquitinated and degraded (Grandal et al., 2007). This seems to cause internalized ErbB1vIII in early endosomes to be recycled back to the plasma membrane instead of being delivered to lysosomes. Direct binding of Cbl to phosphorylated Y1045 on ErbB1vIII has been found to be limited, and instead Cbl primarily binds to ErbB1vIII indirectly via Grb2. Interestingly, this may be caused by negligible phosphorylation of Y1045 in comparison to other phosphotyrosine residues on ErbB1vIII such as Y1173 (Han et al., 2006; Pedersen et al., 2005), and thus Cbl would be unable to bind at that site. This could promote sustained signaling from some phospho-sites while inhibiting downregulation, similar to what might occur in cells expressing wild-type ErbB1 after treatment with low doses of gefitinib.

In fact, long-term exposure of ErbB1vIII-expressing cells to low concentrations of gefitinib has been found to result in sustained phosphorylation of ErbB1vIII Y1173 and ERK, and promote cell proliferation and anchorage-independent growth (Pedersen et al., 2005). The phosphorylation sites Y992 and Y1173 required higher concentrations of gefitinib to be inhibited compared to other sites on the receptor. While mechanisms leading to this sustained signaling have not yet been elucidated, the authors propose that the effect is due to an increase in ErbB1vIII dimerization and a slow decrease in the gefitinib concentration, such that at after a

while the receptors are able to *trans*-phosphorylate one another.

It will be interesting to test for different dephosphorylation rates of Y1045 and Y1173 in the wild-type ErbB1 cells used in this thesis and cells expressing ErbB1vIII and see whether this can explain the sustained signaling. Since 10μM gefitinib resulted in rapid dephosphorylation of both of these sites in H1666 cells as shown in Chapter 2, cells should be treated with various concentrations of gefitinib to better estimate the rates. While an attractive possibility, a faster dephosphorylation rate of Y1045 is clearly not the only explanation of the data. If true, though, it would hint at increased phosphatase activity directed at that site, and potentially provide for novel mechanisms to induce downregulation of ErbB1vIII as a therapeutic strategy.

Future study: Effects of sustained receptor phosphorylation on downstream signaling

Even though we found that phosphorylation of ErbB1 Y1173 remained constant for many hours following one or two minutes of EGF stimulation and then addition of low concentrations of gefitinib, ERK and Akt phosphorylation were still shut off over this time (data not shown). Therefore, receptors may become decoupled to their downstream kinases, which can still be efficiently turned off by their phosphatases to prevent aberrant signaling. However, some of our preliminary data suggests that this might not always be the case, and that certain conditions such as adding drug after longer durations of ligand stimulation may lead to increased downstream signaling.

A large-scale study to measure the phosphorylation states of many signaling proteins, for example, by mass spectrometry-based approaches, would be informative to better understand how signaling is altered by subsaturating concentrations of gefitinib and to determine whether activation of some downstream pathways could be prolonged by sustained receptor signaling. The ability of ErbB1 to signal to certain pathways may be influenced by its localization, which may be relevant here if ErbB1 is stuck in a particular cellular compartment under these conditions. Additional experiments to measure gene expression and physiological

changes such as proliferation and invasion would be revealing. Finally, the drug effects could be tested in mice or in patients receiving gefitinib treatment if it were possible to obtain biopsy samples before and after treatment for signaling analysis.

ErbB1 phosphorylation cycling in the presence of constitutive receptor activation

Do ErbB1 dephosphorylation dynamics following pulse-chase experiments or after drug treatment alone look similar in the case of constitutive ErbB1 activation? In this thesis, to lay the groundwork for this type of analysis we focused our studies on cell lines expressing wild-type ErbB1 at moderate levels and stimulated cells with exogenous ligand to activate ErbB1. Since ErbB1 is often mutated or overexpressed in cancer, or activated by autocrine ligand stimulation, future studies should investigate the effects of these alterations on ErbB1 phosphorylation/dephosphorylation cycling. It will be important to measure the dose-response behavior to various drugs in these cellular contexts and address whether gefitinib and erlotinib result in sustained receptor signaling and, if so, at which concentrations. We expect there to be a range of concentrations that give rise to sustained receptor signaling based on the results discussed above using ErbB1vIII-expressing cells (Pedersen et al., 2005). ErbB1 mutations such as the L858R point mutation confer sensitivity to drugs such as gefitinib and erlotinib (Gazdar, 2009), and therefore, we may detect very similar dose-response behaviors just with the receptor being inhibited at lower concentrations of drug. However, these mutations alter endocytosis (Shtiegman et al., 2007) and could potentially alter phosphatase activity, and it is therefore unclear what to expect.

Conclusions

This work has revealed the importance of teasing out the time scales of different events regulating cell signaling. Whereas phosphorylation and dephosphorylation happen within

seconds, initial ErbB1 activation following exposure to growth factors can take a few minutes (primarily regulated by the kinetics of ligand binding and receptor dimerization) and desensitization by receptor endocytosis and degradation occurs on the order of minutes or hours. Furthermore, oncogenesis induced by prolonged receptor activation may develop over months or years. A key challenge in the future will be to better understand these relevant time scale separations.

CHAPTER 4: Methods

The material in this thesis is an extended version of a manuscript to be submitted for publication:

Coupled fast and slow dynamics regulate ErbB1 signaling
Laura B. Kleiman, Holger Conzelmann, Thomas Maiwald, Douglas A. Lauffenburger and Peter K. Sorger

(All experiments were performed by Laura Kleiman. Mathematical modeling was done by Laura Kleiman in collaboration with Holger Conzelmann and Thomas Maiwald.)

Detailed experimental materials and methods

Cell culture, reagents and general experimental protocols

H1666 human lung carcinoma cells were maintained in ACL-4 media: RPMI supplemented with 0.5% BSA (2g/L), 10% fetal bovine serum, 100units/ml penicillin, 100µg/mL streptomycin, 4.5mM L-glutamine, 1x ITES, 50nM hydrocortisone, 0.1nM tri-iodothyronine, 10µM phosphorylethanolamine, 10mM HEPES, 0.5mM sodium pyruvate and 1ng/ml epidermal growth factor (EGF). Serum starvation medium consisted of RPMI with penicillin/streptomycin and glutamine. MCF-10A human mammary epithelial cells were maintained in DMEM/F12 supplemented with 5% horse serum, 20ng/ml EGF, 0.5mg/ml hydrocortisone, 100ng/ml cholera toxin, 10ug/ml insulin, and penicillin/streptomycin. MCF-10A cells were cultured and passaged using standard protocols (Debnath et al., 2003). Serum starvation medium consisted of DMEM/F12 with penicillin/streptomycin and L-glutamine.

Recombinant human EGF and Heregulin-β1 (HRG) were purchased from PeproTech, recombinant human amphiregulin (AR) from R&D Systems, gefitinib, erlotinib and canertinib from WuXi PharmaTech, lapatinib from LC Laboratories, and PD0325901 from Selleck. Ligands were dissolved in water and drugs in DMSO. Mouse monoclonal antibody 225 was a gift from J. Spangler and D. Wittrup. Pervanadate was prepared by mixing equal amounts of activated Na_3VO_4 (Sigma) and H_2O_2 (Sigma) in water 10 minutes before addition to cells.

After seeding cells for an experiment in normal media, they were allowed to grow for one day and then switched to serum starvation medium for one additional day. Cells were ~70-80% confluent at the time of treatment. Ligands and inhibitors were diluted in serum starvation medium (10x the final concentration) and 10% of the final volume was added to cells to minimize changes to the cell culture medium that may alter short-term signaling. For EGF washout experiments, EGF was added to cells and after 10 minutes was removed and replaced

with conditioned medium from another plate of identically growing cells that had not been exposed to EGF. Data was typically normalized between 0 and 1 for visualization of the trends in signaling.

High-throughput fluorescence microscopy

Cells were seeded in Costar #3603 96-well optical plates (7,500 MCF-10A cells/well or 9,000 H1666 cells/well) with 200µl of medium per well. Edge wells were typically not used due to lower cell density at the time of the experiment. At the end of the time course cells were fixed for 10 minutes with 2% paraformaldehyde, washed with PBS-T (0.1% Tween-20 in PBS) three times, permeabilized with 100% methanol for 10 minutes, washed with PBS-T, and blocked for 1 hour with Odyssey Blocking Buffer (OBB; LI-COR Biosciences). Primary antibodies, typically at 1:100 dilutions, were diluted in OBB and cells were incubated with the antibodies overnight at 4°C. The next day cells were washed again with PBS-T, incubated with secondary antibodies (Invitrogen Alexa Fluor 647 goat anti-rabbit IgG #A21245 or 488 donkey anti-mouse IgG #A21202 diluted 1:500 in OBB) for 1 hour in the dark at room temperature, washed with PBS-T and then with PBS. To stain nuclei and cytoplasm, cells were then incubated with Hoeschst-33342 (Molecular Probes #H1399 at 1:40,000 dilution in PBS) and Whole Cell Dye blue protein dye (Pierce Biotech at 1:1000 dilution in PBS) for 30 minutes in the dark at room temperature, washed with PBS and imaged with an Applied Precision cellWoRx scanner. Images were analyzed using the custom segmentation software ImageRail (B. Millard and P.K. Sorger, Harvard Medical School) and intensity values were plotted as the mean ± standard deviation from triplicate wells. Higher resolution images (all images shown in this thesis) were taken at 20x magnification with a DeltaVision RT microscope (Applied Precision, Inc., Issaquah, WA, www.appliedprecision.com).

The following primary antibodies were used in these imaging experiments: ErbB1 pY1173 (Epitomics #1124-1), ERK1 pT202/Y204 + ERK2 pT185/Y187 (Cell Signaling Technologies #4377), Akt pS473 (Cell Signaling Technologies #4058), Shc pY317 (Upstate/Millipore #07-206) and total ErbB1 (Thermo Scientific Ab-12 #MS-400). The permeabilization step was skipped for cell surface ErbB1 measurements and an ErbB1 antibody (Thermo Scientific Ab-3 #MS-311) that binds to the extracellular domain of the receptor was used.

ELISA assays for ErbB receptor phosphorylation

Rational for developing new assays

There are a few issues with the typical methods for measuring phosphorylation of ErbB receptors. The receptors are highly homologous and therefore antibodies sometimes cross-react. Since the receptors are all a similar size, detection by Western blotting is problematic. Furthermore, in many cell types ErbB receptors (especially ErbB3 and ErbB4) are expressed at very low levels, which may not be detectable by methods like Western blotting or microscopy. Sandwich enzyme-linked immunosorbent assays (ELISAs) have high sensitivity and specificity due to the use of two antibodies that recognize the same protein. However, most commercial ELISAs for ErbB receptor phosphorylation use a pan-phosphotyrosine antibody for detection following capture with an antibody specific to one of the receptors. We found that due to having to use a weak detergent in the lysis buffer, complexes are still present in the lysate prepared for these assays. Thus, using a pan-phosphotyrosine antibody may actually detect phosphorylation of other proteins bound to the specific protein captured (e.g. other ErbB receptors present in heterodimers). To get around these issues, we developed and optimized novel ELISA assays where one receptor is captured and a detection antibody recognizing a specific phosphorylation site on that same receptor is then used. This approach also allows us to compare dynamics

between different phospho-sites on one receptor with increased sensitivity and specificity.

ELISA Protocol

Following treatment cells were quickly washed with cold PBS and lysed in 1% NP-40, 20mM Tris, 137mM NaCl, 10% glycerol, 2mM EDTA and 1mM activated sodium orthovanadate supplemented with Halt Phosphatase Inhibitor Cocktail (1:100 dilution, Pierce/Thermo), 10ug/ml LPC (leupeptin, pepstatin A and chymostatin), 10ug/ml aprotinin and 1mM PMSF. Lysates were incubated on ice rocking gently for 30 minutes followed by centrifugation, and the supernatant was stored at -80°C. Total protein concentrations were determined using a Bicinchoninic Acid (BCA) protein assay kit (Pierce #23225).

Capture antibodies were immobilized on 96-well plates (Costar #3601 purchased from Corning) overnight at room temperature. The next day, plates were washed with PBS-T (0.05% Tween-20 in PBS), blocked for 1-2 hours with 1% BSA and 0.05% NaN_3 in PBS, and then washed again. Lysates were diluted in lysis buffer and incubated in the 96-well plates for 2 hours at room temperature. The amount of H1666 cell lysate that was used depended on the protein to be measured (100µl/well): pErbB1 = 2µg/well, pErbB2 = 40µg/well and pErbB3 = 80µg/well. After incubation with lysate the plates were washed again and detection antibodies were added in 20mM Tris, 137mM NaCl, 0.05% Tween-20 and 0.1% BSA and incubated overnight at 4°C. The following day, plates were washed and incubated for 2 hours at room temperature in the dark with Peroxidase AffiniPure donkey anti-rabbit IgG (Jackson ImmunoResearch #711-035-152, 1:40,000 for pErbB1 and 1:5,000 for pErbB2 and pErbB3) diluted in 20mM Tris, 137mM NaCl, 0.05% Tween-20 and 0.1% BSA. Plates were washed again and then incubated with substrate solution (1:1 Substrate Reagents A (H_2O_2) & B (Tetramethylbenzidine), R&D Systems #DY999) for ~20 minutes in the dark, followed by addition of stop solution (2N H_2SO_4, R&D Systems #DY994). Optical density was determined at 450nm and 560nm using a microplate reader, and readings at 560nm were subtracted from

450nm to correct for optical imperfections in the plate. For each detection antibody, lysis buffer only controls were subtracted from measurements of wells with lysate.

Capture antibodies that bind to the extracellular domains of the ErbB receptors were purchased from R&D Systems and used in 100µl/well: ErbB1 #AF231 goat IgG (used at 0.4µg/ml), ErbB2 #MAB1129 mouse monoclonal IgG_{2B} (used at 7µg/ml) and ErbB3 #MAB3481 mouse monoclonal IgG_1 (used at 2µg/ml). The following rabbit detection antibodies were diluted 1:200 and used in 100µl/well: ErbB1 pY845 (Cell Signaling Technologies (CST) #2231), pY992 (Invitrogen #44-786G), pY1045 (CST #2237), pY1068 (Epitomics #1138-1), pY1148 (CST #4404), and pY1173 (Epitomics #1124-1), ErbB2 pY1221/1222 (CST #2243), and ErbB3 pY1289 (CST #4791).

ELISA assays for total ErbB expression

The following human DuoSet IC ELISA kits were purchased from R&D Systems and used to measure total ErbB protein expression levels using the manufacturer's protocols: ErbB1 #DYC1854, ErbB2 #DYC1129, ErbB3 #DYC234 and ErbB4 #DYC1133. To calculate the number of receptors per cell, we first estimated the concentration of the target protein in the whole cell lysate based on recombinant protein standards provided with the kits. A replicate plate of cells was trypsinized and counted so that the total number of cells could be estimated, from which we then calculated the amount (picograms) of target protein per cell. Using the molecular weight of the ErbB proteins, we obtained the following estimates for serum starved H1666 cells: ErbB1 ~60,000/cell, ErbB2 ~7,000/cell and ErbB3 ~1,000/cell (ErbB4 levels were not detectable). In this thesis we assume that H1666 cells express ~100,000 ErbB1 molecules per cell.

Co-immunoprecipitation (co-IP) and Western blotting

Following treatment cells were quickly washed with cold PBS and lysed in 50mM Tris, 150mM NaCl, 2.5mM EDTA, 0.25% NP-40, and 1% Triton X-100 supplemented with Halt Phosphatase Inhibitor Cocktail (1:100, Pierce/Thermo), 10ug/ml LPC, 10ug/ml aprotinin and 1mM PMSF. Lysates were incubated on ice rocking gently for 30 minutes, and following centrifugation, the supernatant was retained for Western blotting (as whole cell lysate) or used for IP. To IP ErbB1, cell lysates were incubated with an ErbB1 antibody-agarose bead conjugate (Santa Cruz #sc-120AC) overnight at 4°C with gentle mixing. The next day the lysate and beads mixture was centrifuged and the pellet was washed gently with lysis buffer. Captured lysate proteins were eluted with 1% SDS at room temperature for 30 minutes.

Lysates were diluted in 3x SDS sample buffer (187.5mM Tris-HCl, 6% w/v SDS, 30% glycerol, 150mM DTT, 0.03% w/v bromophenol blue) before boiling, separated by SDS-PAGE, and transferred to PVDF or nitrocellulose membranes. Membranes were blocked with Odyssey Blocking Buffer (LI-COR Biosciences) and cut to enable proteins of different sizes to simultaneously be probed with different antibodies. The following primary antibodies were used: total ErbB1 (Thermo Scientific Ab-12 #MS-400), ErbB1 pY1173 (Epitomics #1124-1), total Shc (Upstate #06-203) and GAPDH (Abcam #ab8245). Membranes were then probed with IRDye 800 conjugated anti-rabbit IgG (Rockland Immunochemicals) and/or Alexa Fluor 680 anti-mouse IgG (Invitrogen) at 1:5000, detected using an Odyssey Infrared Scanner (LI-COR Biosciences) and analyzed using Odyssey 2.1 software. Integrated pixel intensities were calculated for uniformly-sized rectangular regions framing individual bands, and background correction was performed by subtracting the integrated pixel intensity for equally-sized regions within the same lane. For Western blots with whole cell lysate, the background-corrected band intensity for the protein of interest was subsequently normalized by GAPDH from the same lane on the membrane. For quantification of the ErbB1 and Shc co-IP, the Shc band was normalized by the ErbB1 band.

Live-cell microscopy for membrane protrusions

MCF-10A cells were seeded in 96-well 0.17mm low glass bottom plates with square wells (Matrical #MGB096-1-2-LG) at 30,000 cells/well in 400µl/well, allowed to grow for one day and then switched to serum starvation medium for an additional day. Before imaging, the medium was changed to phenol-red free CO_2-independent medium (Invitrogen) supplemented with penicillin/streptomycin and L-glutamine, and ligands and inhibitors were prepared in the CO_2-independent medium. Cells were treated and imaged on a Nikon TE2000E with DIC optics and a 20x objective in a 37°C chamber. Frames were taken every ~10 seconds, starting 5-20 minutes before EGF was added. Images were calibrated so that pixels were converted to distances (e.g. 1 pixel = X µm) based on the microscope and objective used. To quantify short-term membrane protrusion dynamics, kymographs were constructed in MetaMorph (Molecular Devices) and analyzed in MATLAB. Kymograph analysis tracks pixel intensity along an arbitrary line over time, say one that is drawn from the edge of a cell before treatment in the direction of a lamellipod extension, as a measure of protrusion distance. Data are represented as the average ± standard error of the mean for 5-10 cells that began extending lamellipodia in response to EGF stimulation.

Only a fraction of cells extended lamellipodia in response to EGF stimulation, typically those located at the edge of a cluster of cells and not those lacking cell-cell contact (this has been previously observed for MCF-10A cells; (Debnath et al., 2003)). The data shown in this thesis focus on the first few minutes after EGF stimulation and lamellipodia normally retract by ~15 minutes. However, cells usually extend additional lamellipodia at later times in the continued presence of ligand; interestingly, these later protrusions exhibit more variability with respect to timing and protrusion distance.

siRNA for PTPs

The following siRNA oligos were purchased from Dharmacon (Thermo Scientific): ON-TARGETplus SMARTpool siRNA for PTPN1/PTP1B (#L-003529-00), PTPN6/Shp-1 (#L-009778-00) and PTPN11/Shp-2 (#L-003947-00), ON-TARGETplus GAPDH siRNA Control Pool (Human) (#D-001830-10-05), and ON-TARGETplus Non-targeting Pool (#D-001810-10-05). siRNA treatment was performed in antibiotic-free complete medium that was replaced with normal growth medium the following day. DharmaFECT #1, 2, 3 and 4 Transfection Reagents (Dharmacon #T-2005-01) were tested for H1666 cells based on GAPDH and PTP1B knockdown and all worked well except for #3. PTP1B, Shp-1 and Shp-2 siRNAs at concentrations of 10, 50 or 100nM after treatment for 48 or 72 hours were optimized for maximal knockdown. Maximal PTP1B knockdown was detected at 100nM after 72 hours, whereas all concentrations of Shp-2 siRNA produced good knockdowns after 72 hours. The faint band thought to be Shp-1 did not diminish upon any siRNA treatment.

To test the effects of PTP1B knockdown on fast gefitinib-induced dephosphorylation, DharmaFECT #4 was used at 3µl/well, and PTP1B and non-targeting control siRNAs were used at 100nM for 72 hours (including one day of serum starvation). Samples were collected and analyzed following the ELISA and Western blotting protocols described above. The following antibodies were used to analyze the effects of the knockdowns by Western blotting: PTP1B (Calbiochem Ab-1 #PH01), Shp-1 (Santa Cruz D-11 #sc-7289), Shp-2 (Epitomics #1590-1), GAPDH (Abcam #ab8245), total ErbB1 (Thermo Scientific Ab-12 #MS-400), ErbB1 pY1173 (Epitomics #1124-1), and ERK1 pT202/Y204 + ERK2 pT185/Y187 (Cell Signaling Technologies #4377).

Chemical inhibitors of PTPs

The following chemical inhibitors of PTP1B, Shp-1 and/or Shp-2 were tested: NSC-

87877 (Calbiochem #565851), CinnGel 2Me (Enzo #PR-115) and PTP1B inhibitor (Calbiochem #539741). H1666 cells were unaffected by the inhibitors and we could not reproduce results reported in the literature with different cell lines. For example, Shp-2 is thought to mediate EGF-induced activation of ERK1/2, and therefore, Shp-2 inhibition could be detected indirectly by measuring ERK1/2. H1666 cells were pretreated with 0-50μM NSC-87877 (supposedly a Shp-2 inhibitor) for 3 hours and then stimulated with EGF for 10 minutes before fixation and immunofluorescence. Although Chen et al. (Chen et al., 2006) showed that this drug inhibited ERK1/2 phosphorylation in a dose-dependent manner in HEK293 cells, pERK1/2 levels were not altered by this drug in H1666 cells under our conditions (data not shown). However, a control treatment with a MEK inhibitor did lead to ERK1/2 dephosphorylation. We were unable to find any better commercial PTP inhibitors or obtain more specific inhibitors synthesized by other academic laboratories.

Computational models of ErbB1 phosphorylation dynamics

Overview

In Chapter 2, various mathematical models were used to interpret the experimental data and explore ErbB1 phosphorylation/dephosphorylation cycling, and many details of the modeling were omitted. In this chapter, we describe in detail the development and analysis of a succession of mathematical models that all focus on ErbB1 phosphorylation dynamics but incorporate varying degrees of biochemical resolution.

General comments

Mass action kinetics based on elementary reactions was used to construct all mathematical models. No Michaelis-Menten approximations or other simplifications were made since their assumptions are often not appropriate for biochemical signaling networks *in vivo*. We assume compartments where proteins are located to be well mixed. Protein concentrations were high (>1000 molecules per cell), so deterministic approaches were used. Even though measurements of some kinetic parameters are available in the literature, they are usually from *in vitro* measurements and may not be relevant in the crowded environment of a cell (Schnell and Turner, 2004). Therefore, instead of forcing these values that may be unreasonable, we typically allowed them to be fitted. Equilibrium constants (keq) are always expressed as association equilibrium constants (kon/koff; therefore, higher values mean higher binding affinity), and on rates can be calculated directly as kon=keq x koff.

Exponential decay model for half life estimates

We constructed the most simple ordinary differential equation (ODE) model to describe the decrease in the fraction of ErbB1 receptors that are phosphorylated (x_p, which can also be thought of as the total number of receptors that can then be degraded) over time by assuming that the fraction of phosphorylated receptors decreases at a rate proportional to its value: $\dot{x}_p = -k_{-1}x_p$. The solution to this equation is $x_p = e^{-k_{-1}\cdot t}$ (exponential decay) when $x_p(t=0) = 1$, where k_{-1} is the dephosphorylation or degradation rate constant. To estimate half lives we scaled the experimental data (using the average of replicate data points) such that t=0 was the maximum signal before starting to decline and had a value of 1, and the minimum signal was 0, and the model parameter k_{-1} was fitted using the function NMinimize in Mathematica. The half life ($t_{1/2}$), or the time required for the decaying quantity to fall to one half of its initial value, was then calculated as $\ln 2 / k_{-1}$.

Since $x_p = e^{-k_{-1}\cdot t}$ is equivalent to $\ln x_p = -k_{-1}t$, a common way to estimate k_{-1} and the half life is by plotting $\ln x_p$ vs. t and performing linear regression to calculate the slope ($-k_{-1}$). We obtain similar estimates using this method, but it is more accurate to fit the exponential decay directly instead of taking the logarithms of the data, so this is what we report on throughout the thesis. Linear regression assumes normally distributed (Gaussian) noise, but since it is being used on a log scale it should really be log-normally distributed.

If we consider the decline in ErbB1 phosphorylation after only EGF stimulation in Figure 2.1A (starting at t=10 min after EGF is added), k_{-1} = 0.026/min and $t_{1/2}$= 27 min. The decline in total ErbB1 (receptor degradation) starts at t=30 min after EGF addition here, and fitting to this data results in k_{-1} = 0.022/min and $t_{1/2}$= 31.5 min. The decrease in ErbB1 phosphorylation after

EGF stimulation followed by addition of 10μM gefitinib was extremely fast with k_{-1}~7/min. Assuming that 40% of the receptors are phosphorylated after 10 minutes of EGF stimulation (40,000 molecules per cell; see below), this corresponds to ~5,000 receptors per cell dephosphorylated within the first second after drug addition, compared to ~10 receptors in the presence of EGF only.

ErbB1 dephosphorylation is nearly complete after stimulation of cells with EGF for 10 minutes and then 10μM gefitinib for one minute, so the fitted dephosphorylation rate constant (k_{-1}~2/min) is an underestimate when this is the first time point measured. To better constrain this value we measured ErbB1 dephosphorylation after treatment with various concentrations of gefitinib where measurements were taken at 10, 20 and 30 seconds after drug addition (Fig. 2.5B), and we obtained the following estimates: for 20μM gefitinib, k_{-1}~8/min and $t_{1/2}$ ~5 sec; for 10μM, k_{-1}~6.5/min and $t_{1/2}$ ~6.5 sec; for 1μM, k_{-1}~4.2/min and $t_{1/2}$ ~10 sec.

Following 20 minutes of 10μM gefitinib treatment of H1666 cells, ERK dephosphorylation still had not reached basal levels. However, 15-20 minutes after addition of 10μM erlotinib or canertinib, ERK phosphorylation was down to the basal level and continued to decrease a little more over the next ~30 minutes (data not shown). Assuming that after 20 minutes of 10μM gefitinib treatment ERK is completely dephosphorylated, we can estimate a lower bound for its half life ($t_{1/2}$ > 9.4 min).

Table 4.1 – Summary of decay rates and half lives.

*The first time point measured following addition of inhibitor (e.g. at t=10 min) was typically 1 minute (e.g. at t=11 min).

Measurement	Cell line	Time after EGF that inhibitor is added*	Inhibitor and concentration	Decay rate	$t_{1/2}$
Total ErbB1	H1666	– (EGF only)	–	0.022/min	31.5 min
pErbB1 Y1173	H1666	– (EGF only)	–	0.026/min	27 min
		10 min (first measurement after 10 sec)	20μM Gefitinib	8/min	5 sec
		10 min (first measurement after 10 sec)	10μM Gefitinib	6.5/min	6.5 sec
		10 min (first measurement after 10 sec)	1μM Gefitinib	4.2/min	10 sec
		10 min (first measurement after 1 min)	10μM Gefitinib	2.04/min	20 sec
		2 min	10μM Gefitinib	0.96/min	43 sec
		30 min	10μM Gefitinib	2.21/min	19 sec
		10 min	10μM Canertinib	2.95/min	14 sec
		10 min	10μM Lapatinib	0.09/min	7.7 min
		10 min	10μg/ml mAb 225	0.093/min	7.5 min
pErbB2 Y1221/1222	H1666	10 min	10μM Gefitinib	2.74/min	15 sec
pErbB3 Y1289	H1666	10 min	10μM Gefitinib	1.32/min	32 sec
ErbB1:Shc association	H1666	10 min	10μM Gefitinib	2.92/min	14 sec
pShc Y317	H1666	10 min	10μM Gefitinib	1.63/min	26 sec
pERK1/2	H1666	10 min	10μM Gefitinib	< 0.074/min	> 9.4 min
	H1666	10 min	1μM PD0325901	0.97/min	43 sec
	MCF-10A	10 min	10μM Gefitinib	0.197/min	3.5 min
pAkt S473	H1666	10 min	10μM Gefitinib	0.678/min	61 sec
	MCF-10A	10 min	10μM Gefitinib	0.42/min	99 sec

Small model describing ErbB1 phosphorylation and dephosphorylation

The exponential decay model does not take into account phosphorylation reactions. Since we wanted to understand how the phosphorylation reactions compete with dephosphorylation and to estimate the corresponding rate constants, we developed a slightly more detailed biochemical model that describes how the concentration of phosphorylated receptors changes over time in the presence and absence of gefitinib. We aimed to characterize the fast dephosphorylation of ErbB1 immediately following gefitinib addition, and therefore, in this scheme we considered reactions we believed to be important for t=10-20 min after EGF stimulation of H1666 cells. The ODE describing the change in the fraction of phosphorylated receptors (x_p) with respect to time is given as described in the main text as:

$$\dot{x}_p = \frac{k_1}{1 + K_{eqG} G}(1 - x_p) - k_{-1} x_p$$

where k_1 is the phosphorylation rate constant, k_{-1} is the dephosphorylation rate constant, the term $1 - x_p$ represents the fraction of all ErbB1 receptors that are not phosphorylated, K_{eqG} is association constant for gefitinib binding to ErbB1, and G is the gefitinib concentration.

The solution to the ODE was calculated analytically, resulting in an analytic solution for the concentration of phosphorylated receptors that depends on the three parameters (rates of ErbB1 phosphorylation and dephosphorylation and the association constant for gefitinib binding), the gefitinib concentration, and the initial concentration of phosphorylated species. The solution when $x_p(t = 0) = \frac{2}{5}$ (40% of ErbB1 receptors are phosphorylated at t=0; see below for details) is:

$$x_p = \frac{\frac{5k_1}{1+K_{eqG}G} + e^{-(k_{-1}+\frac{k_1}{1+K_{eqG}G})t}(2k_{-1} - \frac{3k_1}{1+K_{eqG}G})}{5(k_{-1} + \frac{k_1}{1+K_{eqG}G})}.$$

To test whether the parameters of the model are identifiable (i.e. exact values of the parameters can be obtained with exact data), we generated random values for the three parameters to obtain a fully parameterized model, from which we produced simulated exact data of time courses for two different concentrations of gefitinib. We then numerically minimized the difference between these data points and the algebraic equations (without knowledge of the parameter values used to generate the data) and obtained the original parameter values. Alternatively, using three exact measurements (random parameter values and three different concentrations of gefitinib and time points) the algebraic equations could be solved uniquely and the original parameters exactly retrieved (direct calculation with no optimization). Therefore, the model parameters are identifiable using three data points with no measurement error.

We performed Monte Carlo simulations to obtain probabilistic estimates of the three parameters (k_1, k_{-1} and K_{eqG}) from the variance in the experimental data. To do this, we generated 1,000 artificial time courses by choosing random values from log-normal distributions with the same mean and standard deviation as the experimental measurements (similar results were obtained using normal distributions, but using log-normal distributions avoided negative concentrations), for each time point and concentration of gefitinib. For each artificial time course the parameters of the model were fit using the following procedure. The time point and gefitinib concentration were substituted into the analytical solution to the ODE, resulting in an algebraic equation with three unknown parameter values, and optimization was then performed. To simultaneously minimize the objective function for all concentrations of gefitinib with different artificial data but the same parameters, we defined an objective function that calculated the difference between the algebraic equation and the artificial data, and then took the sum of the

squared values for each time point and the sum for each concentration of gefitinib (least squares method). We minimized the objective function using NMinimize in Mathematica.

For this model it was necessary to estimate the fraction of receptors that were phosphorylated at any given time. Since this is difficult to measure experimentally, we tested different normalizations of the 1, 10 and 20μM gefitinib data (these drugs were added after 10 minutes of EGF stimulation) to see which normalization fit the model best. Pervanadate treatment inhibits phosphatase activity and results in an increase in ErbB1 phosphorylation to levels significantly above those reached after EGF stimulation, and we reasoned that after EGF treatment fewer than half of the receptors may become phosphorylated. Therefore, we tested normalization for the fraction of receptors phosphorylated after 10 minutes of EGF treatment (the model steady state) between 25-50%, and normalization for the steady state after 20μM gefitinib treatment between 0.5-10%; these values define the range of receptor phosphorylation since 1 and 10μM gefitinib treatments result in intermediate levels. We found that the model fit the experimental data best when the 20μM gefitinib data was normalized such that 0.5% of the receptors were phosphorylated after treatment. However, normalization of the data for 10 minutes of EGF treatment (the upper bound) was less sensitive and we got similar fits with the different normalizations; thus, we set the level of ErbB1 phosphorylation after 10 minutes of EGF to be 40%. The data used for this model was therefore normalized to range between 0.5-40% ErbB1 receptors phosphorylated under conditions of EGF stimulation and gefitinib treatment.

Estimates for the values of the ErbB1 dephosphorylation rate and the association constant for gefitinib binding were similar for the different normalizations of the 10min EGF treatment (median values of 7.70-7.85/min and 0.91-1.55/μM, respectively). Fitted values for the association constant for gefitinib binding differ from literature estimates due to the lack of ATP competition with drug for binding to ErbB1 in this model (discussed in Chapter 2). Broader estimates were obtained for the ErbB1 phosphorylation rate based on the normalization of the

10min EGF treatment (median values of 2.15-6.57/min). Median values were used instead of mean values because outliers sometimes resulted in enormous values for the average.

In the main text we derived the following equation to describe the fraction of receptors gefitinib-bound at steady state: $f_G = \frac{K_{eqG}G}{1+K_{eqG}G}$. Therefore, since we estimated K_{eqG} ~ 1.3/μM, after treatment with 1μM gefitinib ~56% of receptors are gefitinib-bound, and after treatment with 20μM gefitinib ~96% are gefitinib-bound.

The phosphorylation and dephosphorylation rate constants that we estimated represent lower bounds for these parameters since in this model these reactions are basically only dependent on the catalytic rates. This reasoning can be more easily understood with an example. In this model we do not account for adaptor protein binding to ErbB1 phosphotyrosine sites, which would protect these adaptor-bound sites from dephosphorylation and decrease the overall fraction of receptors that are able to become dephosphorylated. Consider a modified ODE where f_a equals the fraction of receptors that are not adaptor bound and therefore able to become dephosphorylated:

$$\dot{x}_p = \frac{k_1}{1+K_{eqG}G}(1-x_p) - k_{-1}f_a x_p$$

We can think of our estimate of the dephosphorylation rate constant (k_{-1}~8/min, as described in the main text) as $k_{-1}f_a$ ~8/min where f_a = 1. If f_a would now take on a value between 0 and 1, k_{-1} would be estimated to be greater than 8/min. However, we cannot estimate f_a because we do not have experimental data for the effects of modulating the adaptor protein concentration on receptor phosphorylation levels, like we have for gefitinib. Other processes can also slow down receptor phosphorylation or dephosphorylation (thereby increasing our estimates of these rate constants), such as phosphatase binding and ATP and gefitinib competition for binding to ErbB1.

We asked whether the model could explain the lapatinib-induced dynamics where even low concentrations of drug result in complete ErbB1 dephosphorylation. We tried to fit the model to data of ErbB1 phosphorylation levels following treatment with 0.5, 1 and 10μM lapatinib when the drug was added 10 minutes after EGF stimulation in H1666 cells. We first tested different normalizations of the data, where the steady state phosphorylation level was taken to be 40% (10 min after addition of EGF) and the minimum level of phosphorylation reached with the drug was varied between 0.5-10%. The phosphorylation rate constant and association constant for lapatinib binding could not be identified unless this minimum phosphorylation level was set to be greater than ~6%, but the dephosphorylation rate constant was not dependent on this value. However, all of these parameter sets produced dose-response behavior that looked more like the response to gefitinib than lapatinib, and therefore produced very poor fits when compared to the experimental data. Lower concentrations of drug still led to a lower steady state level of receptor phosphorylation (as for gefitinib), although it took much longer to reach this new steady state than with parameter values found from fitting to gefitinib data due to the much slower phosphorylation and dephosphorylation rate constants estimated here.

From this fitting exercise we draw two conclusions. First, if we only had the lapatinib data we would estimate a much slower rate of receptor phosphorylation cycling due to the slow phosphorylation and dephosphorylation rate constants. Thus, very fast binding drugs are needed to get closer to the actual rates of phosphorylation cycling. Second, this model is insufficient to explain the response to lapatinib. This is an issue we explore with our extended models that incorporate more biochemical information about these receptors and drugs.

Stochastic model describing the intervals between switching events

Instead of considering the average behavior of a large population of ErbB1 receptors that can be phosphorylated or dephosphorylated over time (for example using the small deterministic ODE model depicted in Figure 2.5) we considered individual molecules independently switching between phosphorylated and dephosphorylated states. We were interested in calculating the waiting time between phosphorylation and dephosphorylation events and constructing time courses of state fluctuations for individual ErbB1 molecules. Similar to the ODE model, we considered these events to be a result of monomolecular reactions that are dependent on the catalytic rates of phosphorylation and dephosphorylation only (e.g. no explicit binding of gefitinib or adaptor proteins). These events can be described as Poisson processes, stochastic processes in which events occur continuously and independently at a constant average rate (probability per unit time). The time between events in a Poisson process is given by an exponential distribution. We therefore took the probability that a certain ErbB1 molecule switches from being phosphorylated to dephosphorylated or vice versa (with each molecule having the same probability) to be described by an exponential distribution with a rate parameter equivalent to the dephosphorylation or phosphorylation rate constant, respectively.

The relative likelihood of a switching event at a certain time is given by the probability density function ke^{-kt} where k is the rate parameter. The probability that the switching time falls within the interval from 0 to t is given by the integral of its density over the interval, also known as the cumulative distribution function (CDF), $1-e^{-kt}$. Thus, the probability that the receptor is still in the same state at time t is given by e^{-kt}. Using the inverse of the CDF we can describe switching times in terms of these probabilities. We generated exponential variates for switching times based on the inverse transform sampling method by choosing probabilities

(p) from a uniform distribution with an interval [0,1] and computing the inverse CDF (the quantile function), $\frac{-\ln(1-p)}{k}$. We used the median values for the three parameters estimated with our small ODE model in Figure 2.5D (phosphorylation rate constant k_1 = 4.4/min, dephosphorylation rate constant k_{-1} = 7.8/min, and association constant for gefitinib binding to ErbB1 K_{eqG} = 1.3/μM) and calculated the phosphorylation rate in the presence of 10μM gefitinib using $\frac{k_1}{1+K_{eqG}G}$, as derived in equations (2) and (3) in the main text. The average switching times (times between events) calculated using this procedure are equivalent to $\frac{1}{k}$, the mean or expected value of an exponentially distributed random variable with rate parameter k.

Using the approach described above, we generated lists of the varying amounts of time it can take for ErbB1 receptors that are not phosphorylated to become phosphorylated (in the presence or absence of 10μM gefitinib), as well as for phosphorylated receptors to become dephosphorylated. Time courses of phosphorylation and dephosphorylation cycling of individual ErbB1 molecules were constructed by combining these waiting times and setting the phosphorylated and unphosphorylated receptor state to 1 and 0, respectively. The sum of all receptors phosphorylated over time was normalized by the total number of molecules simulated and plotted over time as an estimate of the average population behavior. Only 1000 ErbB1 molecules were simulated to illustrate noise in the stochastic simulation, which scales with $\frac{1}{\sqrt{\#molecules}}$.

Similar to the ODE formalism, this stochastic model does not account for the slow processes that normally regulate overall levels of ErbB1 phosphorylation after EGF stimulation (e.g. ligand binding, receptor dimerization and degradation) and therefore is most accurate ~10-30 minutes after adding EGF.

To generate the green curve in Fig. 2.12A, the fraction of receptors phosphorylated over time as described in ODE formalism is defined as $\dot{x}_p = k_1(1 - x_p) - k_{-1}x_p$ and we assume that $x_p(t = 0) = 0$. The analytical solution for x_p was plotted with k_1 being the phosphorylation rate constant in the absence of gefitinib for the first 10 minutes of the simulation and in the presence of 10μM gefitinib afterward.

An extension of this stochastic simulation to take into account bimolecular events such as ErbB1 phosphorylation/dephosphorylation as a function of whether the adaptor protein Shc is bound to the ErbB1 phosphotyrosine site is not as straightforward. The probability that a receptor is dephosphorylated would depend on whether Shc is bound to that site, and the probability of the receptor binding Shc would be dependent on the absolute concentration of Shc. Therefore, once one ErbB1 molecule bound Shc, the concentration of free Shc would change so that the probability of another ErbB1 molecule binding Shc would also change.

Model describing different ErbB1 conformations and drug responses

We constructed a more detailed model of ErbB1 phosphorylation dynamics that also describes gefitinib and lapatinib binding to different receptor conformations. This model describes how binding of the following molecules to ErbB1 affects ErbB1 phosphorylation dynamics: ATP or drug (and competition between the two), phosphatases and adaptor proteins. This model does not explicitly include the dynamics of ligand binding, dimerization, internalization or degradation, and we assume that EGF is bound and stays bound and that the receptor species represent monomers that exist in stable ErbB1 homodimers (similar assumptions as for the small ODE model). ErbB1 can switch between active and inactive conformations. The active conformation is likely dominant in the presence of high concentrations of EGF and is therefore the dominant conformation in our model at steady state. The ErbB1 phospho-site described in this model and measured in the corresponding experiments is Y1173, a high affinity binding site for the adaptor protein Shc. When in the inactive conformation the receptor remains bound to EGF (implicitly), and can still be phosphorylated, Shc, ATP or gefitinib bound, although these are unlikely events. We assume that phosphorylation is irreversible if ATP is bound because ATP is consumed in the process and is then no longer bound to the receptor, and that dephosphorylation is irreversible if a phosphatase is bound (no dephosphorylation is allowed if a phosphatase is not bound). We assume that ATP and gefitinib bind much better to ErbB1 when in the active conformation but that they can still bind although with much lower affinity to the inactive conformation. On the other hand, lapatinib is only allowed to bind to ErbB1 when it is in the inactive conformation (and binds with slower on and off rates than gefitinib), and once lapatinib-bound the receptor cannot switch conformations. These assumptions are supported by structural data (Wood et al., 2004) and reduce the complexity of the model.

The model consists of 46 dynamic variables/species that primarily represent different ErbB1 receptor states. These are represented by the notation: "ac/in_0/ATP/G/L_0/Phos_0/P/Shc" and describe the following about a given ErbB1 receptor: 1) whether it is in an active ("ac") or inactive ("in") conformation, 2) not bound by ATP or drug ("0"), or bound by ATP ("ATP"), gefitinib ("G") or lapatinib ("L"), 3) not bound by phosphatase ("0") or bound by phosphatase ("Phos"), and 4) not phosphorylated ("0"), phosphorylated ("P") or phosphorylated and Shc bound (just represented by being Shc bound) ("Shc"). All 48 combinatorial possibilities are allowed except that lapatinib cannot be bound to ErbB1 when it is in an active conformation (leaving a total of 42 receptor species). In addition to the receptor species, we consider a family of free phosphatases that are available to bind to and dephosphorylate ErbB1 ("Phos") as well as a family of free adaptor proteins that can bind to ErbB1 pY1173 (the only ErbB1 phospho-site modeled here), thought to primarily be comprised of Shc and is therefore termed "Shc". We consider the effects of pervanadate, a tyrosine phosphatase inhibitor, in this model. To do so, we consider free pervanadate ("Van") and pervanadate-bound phosphatases ("PhosVan"), which are unable to bind ErbB1 and are therefore inhibited. We assume that only free phosphatases (not receptor-bound) can be inhibited by pervanadate. An illustration of the combinatorial complexity of this model is shown in Figure 4.1, which is complementary to the model depiction in Figure 2.7A that details the different ErbB1 conformations to which the drugs can bind but not the combinatorial binding events. A complete list of all species can be found in Table 4.2.

We modeled pervanadate activity as a time dependent variable because literature results show that its activity decreases rapidly after addition to cells (Mikalsen and Kaalhus, 1998), although making this assumption does not seem to significantly alter our results. We consider pervanadate as an "injection" such that after adding it at a certain time its concentration value evolves within the differential equation as any other dynamical species. Two parameters describe the injection of pervanadate with exponential decay, one regulates the

decay/degradation time ('koff2Van'; this value is fixed since we found it not to make much of a difference to our results) and another regulates the steady state level that is reached ('keq2Van'; the receptor phosphorylation level goes down to ~20% after 7-10 minutes).

We assign three non-zero initial species concentrations. ErbB1 in the inactive conformation with no ATP or drug bound, no phosphatase bound and not phosphorylated (therefore also not Shc bound), "inR_0_0_0", is 74nM. ErbB1 phosphatases and Shc are both assumed to be in excess of ErbB1 and are assigned the concentration 740nM. We assume that the ATP concentration within cells is very high and stays constant. Therefore, we consider ATP to be a fixed parameter with a value 2.5mM (Lehninger et al., 2000).

The model was implemented in a rule-based format in the MATLAB toolbox PottersWheel (Maiwald and Timmer, 2008) to account for the combinatorial complexity (Hlavacek et al., 2006). Instead of manually enumerating ~100 reaction rates individually, the reactions are defined using only 17 rules. As an example of one rule, consider the reaction rule describing lapatinib binding to ErbB1 when the receptor is in the inactive conformation and not bound by ATP or drug. We assume that lapatinib binds similarly regardless of whether a phosphatase is bound or the receptor is phosphorylated or Shc bound. The reactant ('r1') is 'inR_O _<1:+>_<2:+>' and the product ('p1') is 'inR_Lap _<1>_<2>', where <1> and <2> are placeholders for phosphatase and Shc binding, which are irrelevant for lapatinib binding. Lapatinib is considered to be a modifier ('m1') of this reaction. The rate signature is given by 'k1*k2*m1*r1 - k2*p1' where the parameters are keqLap ('k1') and koffLap ('k2'). Since keqLap=konLap/koffLap, the aggregate reaction rate describing lapatinib binding to the inactive conformation of ErbB1 is equivalent to:

$$konLap \times [Lap] \times [inR\_0\_+\_+] - koffLap \times [inR\_Lap\_+\_+]$$

The individual rules, reactions and ODEs are then automatically enumerated. A complete list of the rules can be found in Table 4.3.

There are 24 kinetic parameters in the model, primarily equilibrium constants and off rates. Equilibrium constants (keq) are defined as kon/off and have units 1/nM, koff values have units 1/min and kon have units 1/(nM x min). It is important to keep in mind that dissociation constants (K_d), which are normally reported in the literature, are given by 1/keq. For example, the K_d for lapatinib binding to ErbB1 has been measured to be 3nM (Karaman et al., 2008), so here the keq value is (1/3)nM. Inhibitor concentrations are given in nM. The following parameter values were obtained from the literature or estimated and were not fitted: keqGefitinib (1/nM) (Karaman et al., 2008), keqLapatinib (1/3nM), koff2Van (0.1/min). We set these parameters to have equivalent values since we have no evidence that they are different: koffATP= koffATP2, koffAct=koffAct2=koffAct3, and koffGefitinib=koffGefitinib2. 17 unknown parameters remain and are estimated through fitting. Descriptions of all parameters and their fitted values are detailed in Table 4.4.

To normalize across many datasets collected at different times, we assume that 10% of the receptors are phosphorylated in serum starved cells and 40% after 10 minutes of 100ng/ml EGF stimulation. All datasets were normalized to these values. They were chosen so that the maximum phosphorylation we ever measured (in the presence of pervanadate) was ~95% and the minimum phosphorylation measured (in the presence of lapatinib) was ~5%.

Since in this model we do not take into account an increase in ErbB1 phosphorylation caused by EGF binding and receptor dimerization, or a decrease in ErbB1 phosphorylation caused by internalization and degradation, the steady state of the model can be thought of as the pseudo-steady state of ErbB1 phosphorylation ~10-30 minutes after EGF addition to cells. We assume that 40% of ErbB1 receptors are phosphorylated after 10 minutes of EGF stimulation and force this steady state to be reached by adding artificial data points for fitting. An experimental time course of EGF treatment only was not used here. We consider the effects of kinase and phosphatase inhibitors only after steady state is reached.

We performed parameter estimation in PottersWheel, where we simultaneously fit the model to a large dataset consisting of ErbB1 phosphorylation dynamics following treatment of H1666 cells with 100ng/ml EGF (at t=0) and then various gefitinib or lapatinib concentrations or the phosphatase inhibitor pervanadate (all single inhibitor treatments added at t=10 min). The pervanadate experimental data was weighed more heavily since we used data of treatment with only one concentration as opposed to various concentrations of gefitinib and lapatinib.

Error bars for model calibration were estimated using an error model. We took the treatment condition where we had the most repeated measurements of ErbB1 phosphorylation (treatment with 10μM gefitinib on separate days; 4-6 independent measurements per time point after addition of drug) and calculated the average and standard deviation for each time point. We then plotted the average (x) vs. standard deviation (y) and performed linear regression to obtain the error model: y = 0.127x + 0.66, a 12.7% relative error with 0.66 offset.

The Fortran integrator RADAU5 was used to numerically solve the system of ODEs. We used a trust-region optimization approach in logarithmic parameter space and a chi-square tolerance and fit parameters tolerance of 1e-8. We minimized the chi-square value, the sum of weighted and squared residuals between the model trajectories and our experimental time course measurements. 2000 fits were carried out, each time varying all parameters (p) before fitting with a disturbance strength s of 0.3, corresponding to $p_{new} = p_{old} \times 10^{s \times \varepsilon}$, with ε being normally distributed with mean 0 and variance 1 and p_{old} being the initial guess for the parameter value.

Simulations started at t = -60 min to allow for reaching basal steady state levels at t=0 min and inhibitors were added to the system at t = 10 min. Gefitinib and lapatinib were considered as step functions. The sum of all species that were phosphorylated (including those that were phosphorylated and Shc bound) was compared to the experimental ErbB1 pY1173 measurements. ErbB1 phosphorylation was normalized to the total number of receptors so that

the percentage of receptors phosphorylated was plotted.

To reveal the dependency of the different trends of ErbB1 dephosphorylation by 10μM gefitinib or lapatinib on the fitted ErbB1 phosphorylation and dephosphorylation rate constants, the rate constants from the best fit model (fit with the lowest chi-square value) were both decreased while keeping the ratio of the two parameters constant (Fig. 2.7D). The model steady state level was rescaled to 40% to be able to compare the trends in dephosphorylation. Overall, kPhos was decreased from 209/min to 0.33/min and kDephos was decreased from 37.5/min to 0.06/min.

As already mentioned, this model is only applicable to analyze events occurring ~10-30 min after EGF stimulation, since the model represents the steady state ErbB1 phosphorylation levels reached following EGF treatment and does not describe receptor degradation (which begins ~30 min). Therefore, caution should be taken when comparing the model trajectories to experimental data after this time. Furthermore, treatment of H1666 cells with pervanadate resulted in cell loss (likely detachment due to the effects of pervanadate on adhesion molecules) and therefore pervanadate data could only be plotted before 30 min.

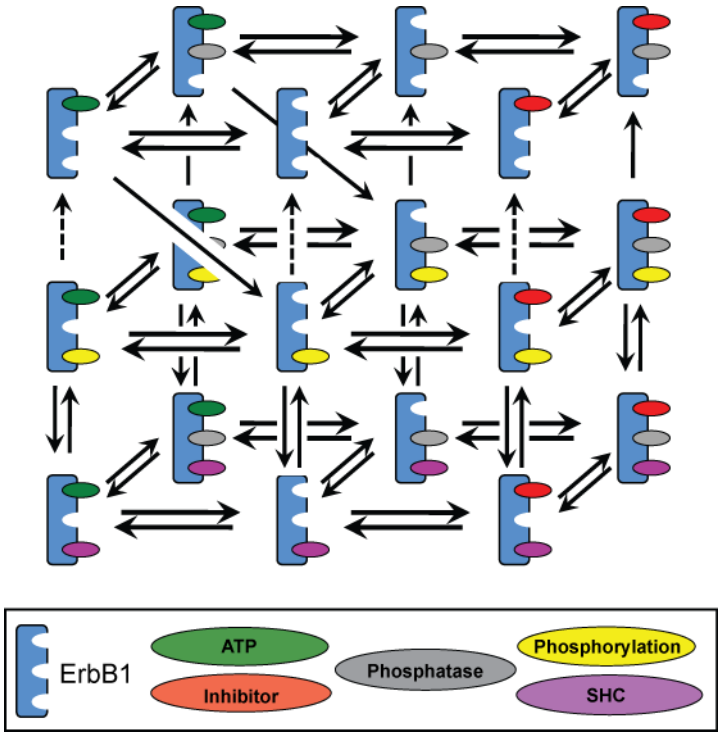

Figure 4.1 - An illustration of the combinatorial complexity of binding events described in the 46 ODE model.

This figure is complementary to Figure 2.7A since it does not show the difference between the active and inactive ErbB1 conformations but instead focuses on the combinatorial complexity of the basic binding events. The reactions shown here describe gefitinib binding to the active ErbB1 conformation.

Table 4.2 – Species and initial protein concentrations in the 46 ODE model.

If no initial concentration is specified it is given a value of zero. Iressa = Gefitinib, Van = pervanadate.

Species	Initial Concentration	Species	Initial Concentration
Phos	740nM	inR_O _Phos _O	
PhosVan		inR_O _Phos _Shc	
acR_O _O _O		inR_O _Phos _P	
acR_O _O _Shc		inR_ATP _O _O	
acR_O _O _P		inR_ATP _O _Shc	
acR_O _Phos _O		inR_ATP _O _P	
acR_O _Phos _Shc		inR_ATP _Phos _O	
acR_O _Phos _P		inR_ATP _Phos _Shc	
acR_ATP _O _O		inR_ATP _Phos _P	
acR_ATP _O _Shc		inR_Iressa _O _O	
acR_ATP _O _P		inR_Iressa _O _Shc	
acR_ATP _Phos _O		inR_Iressa _O _P	
acR_ATP _Phos _Shc		inR_Iressa _Phos _O	
acR_ATP _Phos _P		inR_Iressa _Phos _Shc	
acR_Iressa _O _O		inR_Iressa _Phos _P	
acR_Iressa _O _Shc		inR_Lap _O _O	
acR_Iressa _O _P		inR_Lap _O _Shc	
acR_Iressa _Phos _O		inR_Lap _O _P	
acR_Iressa _Phos _Shc		inR_Lap _Phos _O	740nM
acR_Iressa _Phos _P		inR_Lap _Phos _Shc	
inR_O _O _O	74nM	inR_Lap _Phos _P	
inR_O _O _Shc		Shc	
inR_O _O _P		Van	

Table 4.3 – Reaction rules describing the 46 ODE model.

Reactions are in PottersWheel notation: reactants, products, modifiers, rateSignature, parameters.

{'inR_O _<1:+>_<2:+>'}, {'inR_ATP _<1>_<2>'}, {}, 'k1/k2*k3*k4*r1 - k3*p1', {'keqATP', 'aATP', 'koffATP','ATP'}
{'inR_O _<1:+>_<2:+>'}, {'inR_Iressa _<1>_<2>'}, {'Iressa'}, 'k1/k2*k3*m1*r1 - k3*p1', {'keqIressa', 'aIressa', 'koffIressa'}
{'inR_O _<1:+>_<2:+>'}, {'inR_Lap _<1>_<2>'}, {'Lap'}, 'k1*k2*m1*r1 - k2*p1', {'keqLap', 'koffLap'}
{'acR_O _<1:+>_<2:+>'}, {'acR_ATP _<1>_<2>'}, {}, 'k1*k2*k3*r1 - k2*p1', {'keqATP', 'koffATP2','ATP'}
{'acR_O _<1:+>_<2:+>'}, {'acR_Iressa _<1>_<2>'}, {'Iressa'}, 'k1*k2*m1*r1 - k2*p1', {'keqIressa', 'koffIressa2'}
{'inR_O _<1:+>_<2:+>'}, {'acR_O _<1>_<2>'}, {}, 'k1*k2*r1 - k2*p1', {'keqAct','koffAct'}
{'inR_ATP _<1:+>_<2:+>'}, {'acR_ATP _<1>_<2>'}, {}, 'k1*k2*k3*r1 - k2*p1', {'keqAct','koffAct2', 'aATP'}
{'inR_Iressa _<1:+>_<2:+>'}, {'acR_Iressa _<1>_<2>'}, {}, 'k1*k2*k3*r1 - k2*p1', {'keqAct','koffAct3', 'aIressa'}
{'acR_<1:O|Iressa|ATP>_O _<2:+>', 'Phos'}, {'acR_<1>_Phos _<2>'}, {}, 'k1*k2*r1*r2 - k2*p1', {'keqPhos','koffPhos'}
{'inR_<1:+>_O _<2:+>', 'Phos'}, {'inR_<1>_Phos _<2>'}, {}, 'k1*k2*r1*r2 - k2*p1', {'keqPhos','koffPhos'}
{'<1:acR|inR>_ATP _<2:O|Phos>_O'}, {'<1>_O _<2>_P'}, {}, 'k1*r1', {'kPhos'}
{'acR_<1:O|Iressa|ATP>_Phos _P'}, {'acR_<1>_Phos _O'}, {}, 'k1*r1', {'kDephos'}
{'inR_<1:+>_Phos _P'}, {'inR_<1>_Phos _O'}, {}, 'k1*r1', {'kDephos'}
{'acR_<1:O|Iressa|ATP>_<2:O|Phos>_P', 'Shc'}, {'acR_<1>_<2>_Shc'}, {}, 'k1*k2*r1*r2-k2*p1', {'keqShc', 'koffShc'}
{'inR_<1:+>_<2:O|Phos>_P', 'Shc'}, {'inR_<1>_<2>_Shc'}, {}, 'k1*k2*r1*r2-k2*p1', {'keqShc', 'koffShc'}
{'Phos'}, {'PhosVan'}, {'Van'}, 'k1*k2*r1*m1 - k2*p1', {'keqVan','koffVan'}
{'Van'}, {'inVan'}, {}, 'k1*k2*r1-k2*p1', {'keq2Van','koff2Van'}

Table 4.4 – Description of parameters in the 46 ODE model and their fitted values.

Below are the parameter values from the parameter set that resulted in the best fit of the model to the experimental data. Not every parameter was fitted but if the parameter was fitted it was given the indicated range (note: 1e3 = 103). The reason for choosing those ranges is described. keqAct is the equilibrium constant describing the switch between active and inactive conformations and has no units. "a" factors follow from thermodynamic considerations (principle of detailed balance). Iressa = Gefitinib, Lap = lapatinib, Van = pervanadate.

Dynamical Parameters	Value	Min Value	Max Value	Units	Description
ATP	2.5e6			nM	ATP concentration
aATP	49200	1e3	1e5		Factor by which the equilibrium constant of ATP binding is increased in the ErbB1 active conformation and activation of receptor is increased if ATP is bound. Has to be a strong effect otherwise the receptor would be active all the time
aIressa	165	1.5e2	1e5		Factor by which Iressa binding is increased in active state, factor by which activation of receptor is increased if Iressa is bound. Should be in a similar range as for ATP
kDephos	37.5	1	1e3	1/min	From the smallest ODE model we estimated values somewhere between 1 and 10 and we know that in this model the values have to be higher
kPhos	209	1	1e3	1/min	Same argument as for kDephos
keqATP	0.0004402	1e-7	1e-3	1/nM	We assume that the binding affinity of ATP for the inactive ErbB1 conformation is low. The affinity for the active receptor is higher by the factor aATP
keqAct	0.00109	1e-6	1		Activation if neither ATP nor Iressa are bound is very unlikely (therefore 1e-6), however very little is known about this process. Thus we assumed a quite large range. This equilibrium constant is increased by the factor aATP if ATP binds the receptor. Very low chance of switching to inactive if ATP is bound
keqIressa	1			1/nM	(Karaman et al., 2008)
keqLap	1/3			1/nM	(Karaman et al., 2008)

keqPhos	0.01006	1e-2	10	1/nM	Allows phosphatase binding to be a little higher or lower compared to Iressa
keqShc	0.00607	1/200	1/40	1/nM	(Jones et al., 2006)
keqVan	0.00188	1e-4	1e3	1/nM	
koffATP	65.3	1	1e4	1/min	Assumed to be fast because Iressa can compete with ATP very rapidly
koffATP2	Same as koffATP				
koffAct	0.0472	1e-2	1e4	1/min	A conformational change should be very fast (monomolecular, no diffusion limit), thus a similar range as for ATP binding
koffAct2	Same as koffAct				
koffAct3	Same as koffAct				
koffIressa	12.4	1	1e2	1/min	Fast on rate so has to have fast off rate; would expect it to be slower than the dephosphorylation rate
koffIressa2	Same as koffIressa				Same reasoning as for ATP
koffLap	0.000458	1e-4	1e-1	1/min	Much slower than Iressa
koffPhos	0.497	1e-2	1e2	1/min	
koffShc	165	1	1e3	1/min	Has to be fast too according to our Shc measurements, thus same parameters as for phosphorylation
koffVan	0.367	1e-4	1	1/min	Should be fast since pervanadate has a fast effect. However, the pervan concentration is enormous thus the reaction might be a bit slower than others
keq2Van	8.14	1	9	1/nM	This determines the new steady state (goes down to 20% after 7-10min)
koff2Van	0.1			1/min	This determines how fast it goes down; injection of vanadate with exponential decay

Model incorporating mechanisms for kinase activation and receptor trafficking

To study ErbB1 dephosphorylation dynamics in a larger context and the effects of gefitinib (Iressa) in the presence of normal receptor trafficking, we constructed a more complete model that describes the relevant processes. Ligand binding, ErbB dimerization and phosphorylation, adaptor protein and phosphatase binding, ubiquitination, internalization and degradation of the receptors are modeled here. Lapatinib binding to an inactive ErbB1 conformation is not described in this model since the size of the model would explode due to the combinatorial character of rule-based models.

Specifically, our most detailed model of ErbB receptor signaling comprises the receptors ErbB1-3 which all can form homodimers as well as heterodimers; to simplify the model we do not include ErbB4 since many cell types including H1666 cells do not express detectable levels. The model also includes the two ErbB1 ligands EGF and amphiregulin (AR or Areg) as well as HRG, which is known to bind ErbB3. Furthermore, we explicitly account for one ATP and one phosphatase binding domain at each of the three receptors. We assume that the different receptors can recruit different phosphatases ("ErbB1/2/3 phosphatase" can be considered to be the family of phosphatases that can act on ErbB1/2/3 at that given time, with an average affinity, etc.), and that the small molecule inhibitor gefitinib competes with ATP for the mentioned ATP binding domain. The ErbB1 receptor in our model provides three additional binding domains: (1) the phospho-domain Y1173, which can recruit Shc, (2) the phospho-domain Y1045, which, after phosphorylation and Cbl binding, plays an important role in internalization and degradation of the receptor, and (3) a domain at which ErbB1 can be labeled with ubiquitin for degradation. The model also comprises the Shc-recruiting phospho-domain Y1221/1222 on ErbB2 and the PI3K recruiting phospho-domain Y1289 on ErbB3. These binding events can also be thought of as the binding of the family of adaptor proteins that can bind to these phospho-sites. Finally, internalization as well as receptor synthesis and degradation are accounted for. For sake of

simplicity, it is assumed that when the receptor is degraded, all proteins that are recruited to that receptor are released into the cytosol.

A complete mechanistic description of all the mentioned processes would result in a model composed of more than 100,000 ordinary differential equations (ODEs). Using the model reduction techniques of Conzelmann et al. (Conzelmann et al., 2008) and Koschorreck et al. (Koschorreck et al., 2007), which had to be partly extended, the model could be reduced to 648 ODEs. Details about the extension of the approximate reduction approach of Koschorreck et al. can be found below. Since the model is still too complex for intensive simulation studies or automated parameter estimation, it has to be reduced further. By focusing on the interplay of EGF and gefitinib, it is possible to further reduce the model eliminating all states required to describe signal propagation induced by Amphiregulin and HRG. Due to the relatively low concentration of ErbB2 and ErbB3 in H1666 cells, another reasonable reduction step is the complete elimination of ErbB2 and ErbB3 from the model. MCF-10A cells express low levels of ErbB1 and no detectable levels of ErbB2-4 by Western blotting (Neve et al., 2006). The resulting model consists of 203 ODEs and allows us to study the phosphorylation dynamics of ErbB1 after EGF stimulation and drug inhibition in greater detail.

We use a rule-based approach to formulate the model equations. Tools that support rule-based modeling are, for instance, BioNetGen, ALC, PottersWheel and *little b* (Blinov et al., 2004; Koschorreck and Gilles, 2008; Maiwald and Timmer, 2008; Mallavarapu et al., 2009). However, considerable model reduction is necessary in order to get a model of manageable size. Unfortunately, neither the application of the exact reduction approach by Conzelmann et al. (Conzelmann et al., 2008) nor the usage of Koschorreck's layer based reduction approach (Koschorreck et al., 2007) are very helpful in this case. The structure of the highly complex ErbB receptor system would not allow us to eliminate more than a few states using these approaches. Therefore, we had to develop a new reduction technique, which can be considered a generalization of Koschorreck's layer-based approach. The layer-based approach

uses the special properties of so-called all-or-none interactions as they usually occur between the phosphorylation of a domain and its subsequent adaptor recruitment. Usually, it is assumed that an adaptor protein such as Shc can only bind to a domain if this domain is phosphorylated. The other way around, the same domain will only get dephosphorylated if the adaptor dissociates first. The same assumptions are made in our model for Shc, Cbl and PI3K binding. However, since we do not consider further adaptor recruitment, the benefits from solely using the layer-based approach would have been negligible.

Interestingly, it is possible to show that the same method can easily be extended and applied to a set of consecutive, unidirectional interactions. One of the simplest examples is shown in Figure 4.2. The receptor R possesses three binding domains. If domain 1 gets occupied by a ligand, the binding affinity of domain 2 towards its ligand changes. However, binding of ligand 2 has no effect on the recruitment of ligand 1, but changes the binding affinity of domain 3. If one accounts for mass conversation relations, a complete mechanistic model of this system will consist of seven ordinary differential equations. To generate a reduced model version, the system is split up into two modules. The first module only describes the domains 1 and 2, while the second module describes the domains 2 and 3. Since ligand binding to domain 3 has no effect on the other two domains, the first module accurately describes the dynamics of domains 1 and 2. A problem occurs when we model the second module. Domain 1 is not part of this module and therefore will in a first step not be accounted for. As a result domain 2 appears to be completely uninfluenced in this module, and therefore all reactions describing ligand recruitment to domain 2 have to be parameterized by the same kinetic parameters. It is not obvious which parameters can be used to describe this seemingly independent process, since we know that domain 2 does not always have the same affinity for its ligand, and that a switch in affinity is caused by domain 1. This problem can be solved by assuming that the unknown kinetic parameters k_Y and k_{-Y} correspond to the weighted mean value of the true parameter values k_2, k_4 and k_{-2}, k_{-4}:

$$k_Y = k_2 \frac{R[0,0,X]}{R[X,0,X]} + k_4 \frac{R[1,0,X]}{R[X,0,X]} \qquad k_{-Y} = k_{-2} \frac{R[0,1,X]}{R[X,1,X]} + k_{-4} \frac{R[1,1,X]}{R[X,1,X]}$$

The used weights correspond to the fractions of receptors that can undergo the respective reaction step. For instance, the binding process of ligand to the second receptor domain requires that this domain is unoccupied (R[X,0,X]). The 'X's here represent placeholders and indicate that the state of that domain is irrelevant. Now, one fraction of all these species recruit the ligand with k_2, namely all species with an unoccupied first domain (R[0,0,X]), while the remaining fraction (R[1,0,X]) binds the ligand with k_3. The same reasoning is used to formulate the expression for k_{-Y}. The new parameters are concentration dependent and therefore vary over time.

The described modeling approach yields two small models both consisting of three ordinary differential equations, if we again account for all mass conservation relations. One more state can be eliminated due to the redundant information about process two in both models when these are integrated into one model. One can mathematically prove that the reduced model provides the same convergence properties as the ones introduced by Koschorreck et al. (Koschorreck et al., 2007).

Analogously, the large ErbB receptor network is split into modules that are modeled separately. The model consists of five modules describing: 1) ligand binding (EGF, AR, HRG) to ErbB1 and ErbB3, dimerization (homo and heterodimerization of ErbB1-3), ubiquitination, internalization and degradation of the receptors, 2) phosphorylation of ErbB1-3, 3) Shc binding, 4) Cbl binding, and 5) PI3K binding. Some of the resulting modules can be further reduced by using the exact model reduction approach as it has been introduced in Conzelmann et al. (Conzelmann et al., 2008). The connections between the different modules are established by using the same kind of concentration dependent kinetic parameters as shown in the example above.

The ALC (Automated Layer Construction) computer program written in Perl supports rules, macrostates and modularity (Koschorreck and Gilles, 2008). ALC was used to convert model definitions given in a rule-based syntax into computational model files in different formats, including Mathematica and MATLAB.

We provide an example of how the reaction rules are translated into reaction rates and ODEs for the very small Cbl-binding module that contains three species: free Cbl (**Cbl**), ErbB1 phosphorylated at the Cbl-binding site and not bound by Cbl (**ErbB1[X,X,X,X,X,X,p]**) and ErbB1 phosphorylated and bound by Cbl at that site (**ErbB1[X,X,X,X,X,X,Cbl]**). While these species are represented as monomers here, they are taken to be all ErbB1 species phosphorylated at the Cbl-binding site (monomers and dimers). The X's mean that it is irrelevant what happens at those sites for the reaction being described, so all possibilities are allowed. There are three reaction rules in this module:

(1) Cbl binds to ErbB1 that is phosphorylated at the Cbl-binding site with the equilibrium constant (always defined as on rate/off rate) **kCbleq** and the off rate **kCbloff**:

ErbB1[X,X,X,X,X,X,p]+Cbl↔ErbB1[X,X,X,X,X,X,Cbl].

(2)-(3) ErbB1 degradation reactions depend on whether or not Cbl is bound. We assume that when ErbB1 is degraded, all other proteins bound are released into the cytosol. These degradation reactions are irreversible. Recall that the full model was developed and then reduced to the 203 ODE version, which is why there are ErbB12 and ErbB13 terms here that indicate ErbB1:ErbB2 and ErbB1:ErbB3 heterodimers, respectively:

ErbB1[X,X,X,X,X,X,p]→0

ErbB1[X,X,X,X,X,X,Cbl]→Cbl

The same rate constant describes both of these reactions, where the "fac" variables correspond to the earlier mentioned weights and the information to calculate the weights comes from the

other modules not discussed here:

kdegErbB1*fac1degInttot1+kdegErbB1ub*fac1degIntubtot1+kdegErbB11*fac11degInttot1+kdegErbB11ub1*fac11degIntub1tot1+kdegErbB11ub2*fac11degIntub2tot1+kdegErbB12*fac12degInttot1+kdegErbB12ub*fac12degIntubtot1+kdegErbB13*fac13degInttot1+kdegErbB13ub*fac13degIntubtot1

The reaction rates are given by:

r1=kCbleq*kCbloff*ErbB1[X,X,X,X,X,X,p]*Cbl-kCbloff*ErbB1[X,X,X,X,X,X,Cbl]

r2=(kdegErbB1*fac1degInttot1+kdegErbB1ub*fac1degIntubtot1+kdegErbB11*fac11degInttot1+kdegErbB11ub1*fac11degIntub1tot1+kdegErbB11ub2*fac11degIntub2tot1+kdegErbB12*fac12degInttot1+kdegErbB12ub*fac12degIntubtot1+kdegErbB13*fac13degInttot1+kdegErbB13ub*fac13degIntubtot1)*ErbB1[X,X,X,X,X,X,p]

r3=(kdegErbB1*fac1degInttot1+kdegErbB1ub*fac1degIntubtot1+kdegErbB11*fac11degInttot1+kdegErbB11ub1*fac11degIntub1tot1+kdegErbB11ub2*fac11degIntub2tot1+kdegErbB12*fac12degInttot1+kdegErbB12ub*fac12degIntubtot1+kdegErbB13*fac13degInttot1+kdegErbB13ub*fac13degIntubtot1)*ErbB1[X,X,X,X,X,X,Cbl]

The three ODEs are therefore:

Cbl' = -r1+r3

ErbB1[X,X,X,X,X,X,Cbl]' = r1-r3

ErbB1[X,X,X,X,X,X,p]' = -r1-r2

The following modification factor (weights described above) for the Cbl module describes the fraction of receptors that are not Cbl bound:

facCbl=ErbB1[X, X, X, X, X, X, p]/(ErbB1[X, X, X, X, X, X, p]+ErbB1[X, X, X, X, X, X, Cbl])

This modification factor is used, for example, when defining the phosphorylation reaction of the Cbl-binding site on ErbB1 in the module describing ErbB1 phosphorylation events. Only receptors that are phosphorylated at that site and not Cbl bound can be dephosphorylated.

The macrostates in this modification factor are:

ErbB1[X, X, X, X, X, X, Cbl], ErbB1[X, X, X, X, X, X, p]

Macrostates are then generated by the transformation of the individual species concentrations (microstates), and all species discussed from here on out will refer to the macrostates. The notation ErbB1[ ].X or ErbB1_X (MATLAB notation) means that the macrostate comprises both monomers and dimers. Phosphorylated species include those that are adaptor bound. For example, the variable ErbB1[X,X,X,X,X,p,X].X comprises all receptors that are phosphorylated at the Shc binding site, including those that are bound by Shc, regardless of the states of the other sites. Calculating ErbB1[X,X,X,X,X,p,X].X - ErbB1[X,X,X,X,X,Shc,X].X will produce the number of receptors that are phosphorylated at that site but not Shc bound.

A list of species comprising the 203 ODE model can be found in Tables 4.5 and 4.6. The complete set of ODEs is enormous since each ODE has hundreds of algebraic expressions, and even the rules used to generate the ODEs (following model reduction) are too long to report here. The 203 ODE model was imported into PottersWheel for parameter estimation and analysis. Initial protein concentrations are given in molecules per cell, gefitinib concentrations are in nM, and EGF is given in ng/ml. Off rates are in 1/min. Rate parameters were assigned to the reaction classes (rules) rather than specific reactions. There are 55 parameters including scaling parameters for both phosphorylated and total ErbB1. A complete list of all parameters as well as their fitted values is shown in Table 4.7.

The data was normalized for fitting in the following way: we assumed that MCF-10A cells express 100,000 ErbB1 receptors per cell and that 50% of receptors are degraded after 4 hours of EGF treatment. Although it is unclear how much signal can be attributed to background staining using methods such as microscopy, Western blotting and ELISAs, our results suggest that a significant fraction of receptors is not degraded over this time (data not shown). We

normalized data of pY1173-ErbB1 such that 1% of the receptors were phosphorylated before EGF stimulation and a maximum of ~50% were phosphorylated after EGF stimulation.

Scaling parameters were fit since the experimental measurements were in arbitrary units (relative, not absolute amounts). A default error model of 10% error plus 5% of the maximum signal was used (yStd(i) 0.1*y(i) + 0.05*max(y), for data point i with max(y) denoting the maximum over all data points).

The following non-zero initial conditions were used: ErbB1 ("ErbB1XXXXXXX_X") = 10^5 molecules per cell (as measured for H1666 cells, also reasonable for MCF-10A cells (Neve Cancer Cell 2006)), Shc = $3.5x10^6$ molecules per cell, Cbl = 10^6 molecules per cell and ErbB1 phosphatases ("Phos1") = 10^6 molecules per cell. Shc, Cbl and the phosphatases were assumed to be in excess of the receptor. To get a reasonable estimate for a steady state without EGF, which corresponds to the start scenario of the model, the model was run to steady state with no EGF or drug using these initial protein concentrations and values of 10^{-12} for the other species. The steady state values for the protein concentrations were then used as the initial conditions to simulate the effects of ligand stimulation.

Due to the large number of parameters we expected the model to be non-identifiable and the landscape of the objective function to contain multiple local minima. We therefore used simulated annealing for broad searches through parameter space, spanning 10-fold above and below *a priori* parameter values. We performed two rounds of simulated annealing followed by trust region optimization. The model state describing ErbB1 phosphorylated at the Shc-binding site (ErbB1XXXXXpX_X) was compared to measurements of ErbB1 pY1173 and the model state describing the overall level of ErbB1 (ErbB1XXXXXXX_X) to total ErbB1 measurements.

Sensitivity analysis was performed by making the following calculations: sens = (x(k=1.01) - x(k=1))/x(k=1)/0.1, where the individual parameter values (k) were increased by 1% and the effects on the model species concentrations were determined. We asked how the various parameter values influence ErbB1 Y1173 phosphorylation and total receptor levels after

20 and 240 minutes of EGF stimulation or EGF stimulation for one minute followed by 1μM gefitinib treatment.

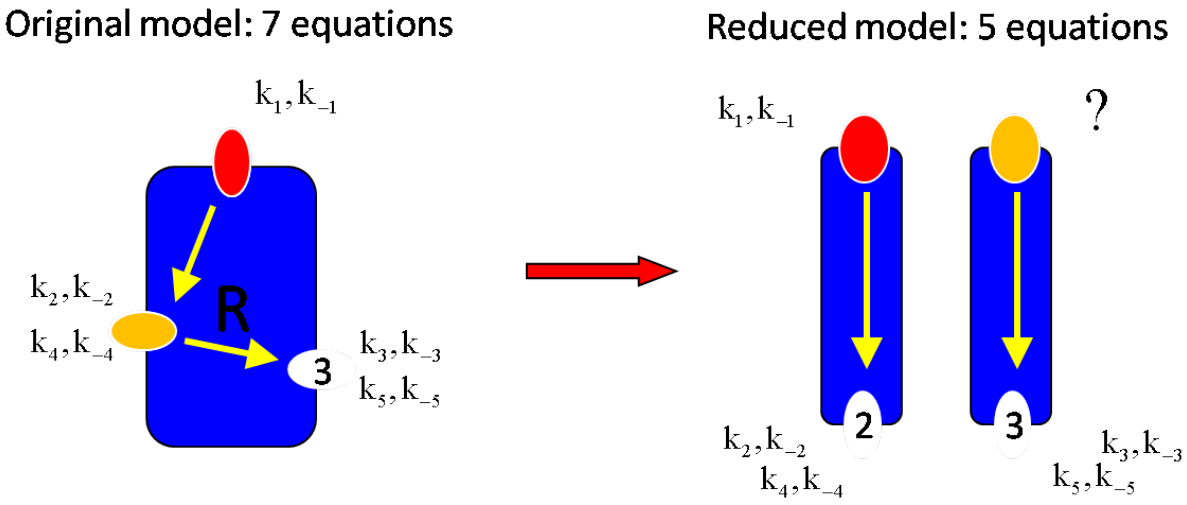

Figure 4.2 – Simple example of how the model reduction approach was applied by separation into modules.

Table 4.5 – Macrospecies in the 203 ODE model.

Key for the different possibilities for the binding sites on ErbB1 monomers and homodimers:
ErbB1{0,Int}{0,EGF}{0,ATP,Inh}{0,ub}{0,Phos1}{0,p,Shc}{0,p,Cbl}
ErbB11{0,Int}{0,EGF}{0,ATP,Inh}{0,ub}{0,Phos1}{0,p}{0,p,Cbl}{0,EGF}{0,ATP,Inh}
{0,ub}{0,Phos1}{0,p,Shc}{0,p,Cbl}

Species	Species	Species
ErbB1XXXXXXp_X	ErbB1XEGFXXXXX_X	ErbB11symIntEGFXubXXCblEGFXubXXX
ErbB1XXXXXpX_X	ErbB1XEGFXXXXCbl_X	ErbB11symIntEGFXubXXCblEGFXXXXCbl
ErbB1XXXXXpp_X	ErbB1XEGFXXXXp_X	ErbB11symIntEGFXubXXCblEGFXXXXp
ErbB1XXXXPhos1XX_X	ErbB1XEGFXubXXX_X	ErbB11symIntEGFXubXXCblEGFXXXXX
ErbB1XXXXPhos1Xp_X	ErbB1XEGFXubXXCbl_X	ErbB11symIntEGFXubXXCblXXubXXCbl
ErbB1XXXXPhos1pX_X	ErbB1XEGFXubXXp_X	ErbB11symIntEGFXubXXCblXXubXXp
ErbB1XXXXPhos1pp_X	ErbB1IntXXXXXX_X	ErbB11symIntEGFXubXXCblXXubXXX
ErbB1XXATPXXXX_X	ErbB1IntXXubXXX_X	ErbB11symIntEGFXubXXCblXXXXXCbl
ErbB1XXInhXXXX_X	ErbB1IntXXubXXCbl_X	ErbB11symIntEGFXubXXCblXXXXXp
ErbB11symXXATPXXXXXXXPhos1pp	ErbB1IntXXubXXp_X	ErbB11symIntEGFXubXXCblXXXXXX
ErbB11symXXATPXXXXXXXPhos1pX	ErbB1IntEGFXXXXX_X	ErbB11symIntEGFXubXXpEGFXubXXX
ErbB11symXXATPXXXXXXXPhos1Xp	ErbB1IntEGFXXXXCbl_X	ErbB11symIntEGFXubXXpEGFXXXXCbl
ErbB11symXXATPXXXXXXXPhos1XX	ErbB1IntEGFXXXXp_X	ErbB11symIntEGFXubXXpEGFXXXXp
ErbB11symXXATPXXXXXXXXpp	ErbB1IntEGFXubXXX_X	ErbB11symIntEGFXubXXpEGFXXXXX
ErbB11symXXATPXXXXXXXXpX	ErbB1IntEGFXubXXCbl_X	ErbB11symIntEGFXubXXpXXubXXCbl
ErbB11symXXATPXXXXXXXXXp	ErbB1IntEGFXubXXp_X	ErbB11symIntEGFXubXXpXXubXXp
ErbB11symXXATPXXXXXXXXXX	ErbB11IntEGFXubXXCblEGFXubXXCbl	ErbB11symIntEGFXubXXpXXubXXX
ErbB11symXXInhXXXXXXXPhos1pp	ErbB11IntEGFXubXXpEGFXubXXp	ErbB11symIntEGFXubXXpXXXXXCbl
ErbB11symXXInhXXXXXXXPhos1pX	ErbB11IntEGFXubXXXEGFXubXXX	ErbB11symIntEGFXubXXpXXXXXp
ErbB11symXXInhXXXXXXXPhos1Xp	ErbB11IntEGFXXXXCblEGFXXXXCbl	ErbB11symIntEGFXubXXpXXXXXX
ErbB11symXXInhXXXXXXXPhos1XX	ErbB11IntEGFXXXXpEGFXXXXp	ErbB11symIntEGFXubXXXEGFXXXXCbl
ErbB11symXXInhXXXXXXXXpp	ErbB11IntEGFXXXXXEGFXXXXX	ErbB11symIntEGFXubXXXEGFXXXXp
ErbB11symXXInhXXXXXXXXpX	ErbB11IntXXubXXCblXXubXXCbl	ErbB11symIntEGFXubXXXEGFXXXXX
ErbB11symXXInhXXXXXXXXXp	ErbB11IntXXubXXpXXubXXp	ErbB11symIntEGFXubXXXXXubXXCbl
ErbB11symXXInhXXXXXXXXXX	ErbB11IntXXubXXXXXubXXX	ErbB11symIntEGFXubXXXXXubXXp
ErbB11symXXXXPhos1ppXXXXXX	ErbB11IntXXXXXXXXXXX	ErbB11symIntEGFXubXXXXXubXXX
ErbB11symXXXXPhos1pXXXXXXX	ErbB11XEGFXubXXCblEGFXubXXCbl	ErbB11symIntEGFXubXXXXXXXXCbl
ErbB11symXXXXPhos1XpXXXXXX	ErbB11XEGFXubXXpEGFXubXXp	ErbB11symIntEGFXubXXXXXXXXp
ErbB11symXXXXPhos1XXXXXXXX	ErbB11XEGFXubXXXEGFXubXXX	ErbB11symIntEGFXubXXXXXXXXX
ErbB11symXXXXXppXXXXXX	ErbB11XEGFXXXXCblEGFXXXXCbl	ErbB11symIntEGFXXXXCblEGFXXXXp
ErbB11symXXXXXpXXXXXXX	ErbB11XEGFXXXXpEGFXXXXp	ErbB11symIntEGFXXXXCblEGFXXXXX
ErbB11symXXXXXXpXXXXXX	ErbB11XEGFXXXXXEGFXXXXX	ErbB11symIntEGFXXXXCblXXubXXCbl
Phos1	ErbB11XXXubXXCblXXubXXCbl	ErbB11symIntEGFXXXXCblXXubXXp
ErbB1XXXXXXX_X	ErbB11XXXubXXpXXubXXp	ErbB11symIntEGFXXXXCblXXubXXX
ErbB1XXXubXXX_X	ErbB11XXXubXXXXXubXXX	ErbB11symIntEGFXXXXCblXXXXXCbl
ErbB1XXXubXXCbl_X	ErbB11XXXXXXXXXXXXX	ErbB11symIntEGFXXXXCblXXXXXp
ErbB1XXXubXXp_X	ErbB11symIntEGFXubXXCblEGFXubXXp	ErbB11symIntEGFXXXXCblXXXXXX

Table 4.6 – Macrospecies in the 203 ODE model (continued).

Species	Species	Species
ErbB11symIntEGFXXXXpEGFXXXXX	ErbB11symXEGFXubXXCblXXubXXp	ErbB11symXEGFXXXXCblXXXXXX
ErbB11symIntEGFXXXXpXXubXXCbl	ErbB11symXEGFXubXXCblXXubXXX	ErbB11symXEGFXXXXpEGFXXXXX
ErbB11symIntEGFXXXXpXXubXXp	ErbB11symXEGFXubXXCblXXXXXCbl	ErbB11symXEGFXXXXpXXubXXCbl
ErbB11symIntEGFXXXXpXXubXXX	ErbB11symXEGFXubXXCblXXXXXp	ErbB11symXEGFXXXXpXXubXXp
ErbB11symIntEGFXXXXpXXXXXCbl	ErbB11symXEGFXubXXCblXXXXXX	ErbB11symXEGFXXXXpXXubXXX
ErbB11symIntEGFXXXXpXXXXXp	ErbB11symXEGFXubXXpEGFXubXXX	ErbB11symXEGFXXXXpXXXXXCbl
ErbB11symIntEGFXXXXpXXXXXX	ErbB11symXEGFXubXXpEGFXXXXCbl	ErbB11symXEGFXXXXpXXXXXp
ErbB11symIntEGFXXXXXXXubXXCbl	ErbB11symXEGFXubXXpEGFXXXXp	ErbB11symXEGFXXXXpXXXXXX
ErbB11symIntEGFXXXXXXXubXXp	ErbB11symXEGFXubXXpEGFXXXXX	ErbB11symXEGFXXXXXXXubXXCbl
ErbB11symIntEGFXXXXXXXubXXX	ErbB11symXEGFXubXXpXXubXXCbl	ErbB11symXEGFXXXXXXXubXXp
ErbB11symIntEGFXXXXXXXXXXCbl	ErbB11symXEGFXubXXpXXubXXp	ErbB11symXEGFXXXXXXXubXXX
ErbB11symIntEGFXXXXXXXXXXp	ErbB11symXEGFXubXXpXXubXXX	ErbB11symXEGFXXXXXXXXXXCbl
ErbB11symIntEGFXXXXXXXXXXX	ErbB11symXEGFXubXXpXXXXXCbl	ErbB11symXEGFXXXXXXXXXXp
ErbB11symIntXXubXXCblXXubXXp	ErbB11symXEGFXubXXpXXXXXp	ErbB11symXEGFXXXXXXXXXXX
ErbB11symIntXXubXXCblXXubXXX	ErbB11symXEGFXubXXpXXXXXX	ErbB11symXXXubXXCblXXubXXp
ErbB11symIntXXubXXCblXXXXXCbl	ErbB11symXEGFXubXXXEGFXXXXCbl	ErbB11symXXXubXXCblXXubXXX
ErbB11symIntXXubXXCblXXXXXp	ErbB11symXEGFXubXXXEGFXXXXp	ErbB11symXXXubXXCblXXXXXCbl
ErbB11symIntXXubXXCblXXXXXX	ErbB11symXEGFXubXXXEGFXXXXX	ErbB11symXXXubXXCblXXXXXp
ErbB11symIntXXubXXpXXubXXX	ErbB11symXEGFXubXXXXXubXXCbl	ErbB11symXXXubXXCblXXXXXX
ErbB11symIntXXubXXpXXXXXCbl	ErbB11symXEGFXubXXXXXubXXp	ErbB11symXXXubXXpXXubXXX
ErbB11symIntXXubXXpXXXXXp	ErbB11symXEGFXubXXXXXubXXX	ErbB11symXXXubXXpXXXXXCbl
ErbB11symIntXXubXXpXXXXXX	ErbB11symXEGFXubXXXXXXXXCbl	ErbB11symXXXubXXpXXXXXp
ErbB11symIntXXubXXXXXXXXCbl	ErbB11symXEGFXubXXXXXXXXp	ErbB11symXXXubXXpXXXXXX
ErbB11symIntXXubXXXXXXXXp	ErbB11symXEGFXubXXXXXXXXX	ErbB11symXXXubXXXXXXXXCbl
ErbB11symIntXXubXXXXXXXXX	ErbB11symXEGFXXXXCblEGFXXXXp	ErbB11symXXXubXXXXXXXXp
ErbB11symXEGFXubXXCblEGFXubXXp	ErbB11symXEGFXXXXCblEGFXXXXX	ErbB11symXXXubXXXXXXXXX
ErbB11symXEGFXubXXCblEGFXubXXX	ErbB11symXEGFXXXXCblXXubXXCbl	ErbB1XXXXXShcX_X
ErbB11symXEGFXubXXCblEGFXXXXCbl	ErbB11symXEGFXXXXCblXXubXXp	Shc
ErbB11symXEGFXubXXCblEGFXXXXp	ErbB11symXEGFXXXXCblXXubXXX	ErbB1XXXXXCbl_X
ErbB11symXEGFXubXXCblEGFXXXXX	ErbB11symXEGFXXXXCblXXXXXCbl	Cbl
ErbB11symXEGFXubXXCblXXubXXCbl	ErbB11symXEGFXXXXCblXXXXXp	

Table 4.7 – Parameters in the 203 ODE model and their fitted values.

Below are the parameter values from the parameter set that resulted in the best fit of the model to the experimental data after two rounds of simulated annealing (in log space) and one round of trust region optimization. Parameters were given the indicated range (note: 1e3 = 10^3). koff values are given in units 1/min.

Dynamical Parameters	Value	Min Value	Max Value	Units	Description
kDim11eq	1.6e-7	5.24e-9	4.71e-6		
aEGFDim11	15.7	0.511	460		how much the affinity changes for EGF when ErbB1 is dimerized – thermodynamic constraint, dimerized because conformation is such that ligand can bind more easily
k1Dim11off	0.0367	0.00124	1.12		
k2Dim11off	0.03604	0.00119	1.07		
k3Dim11off	0.0645	0.00217	1.96		
k1EGFeq	6.04	0.12	180		
k2EGFeq	7.21e-7	2.38e-8	2.14e-5		
k1EGFoff	1.4	0.0467	42		
k2EGFoff	0.01805	0.000612	0.551		
k5EGFoff	0.436	0.0146	13.2		
k6EGFoff	0.367	0.0121	10.9		
k1ATPeq	0.814	0.0273	24.5		
k1ATPoff	1.68	0.0563	50.6		

k1Inheq	3.98	0.133	119	
k1Inhoff	4.05	0.133	119	
k1Phos1eq	0.0239	0.000775	0.697	
k1Phos1off	5.38	0.18	162	
k1PShceq	0.000909	3.04e-5	0.0274	phosphatase driven not ATP
k1ATPShceq	86.9	3.004	2700	phosphorylation reaction driven by ATP, Shc binding site
k1Poff	0.00196	6.63e-5	0.0597	
k2Poff	2.54	0.0854	76.9	
k3Poff	20.03	0.670	602	
k1PCbleq	0.0428	0.0014005	1.26	
k1ATPCbleq	46.8	1.57	1420	
k4Poff	2.93e-5	9.43e-7	0.000849	
k5Poff	72.6	2.31	2080	
k6Poff	4.92	0.162	146	
k1ErbB1IntOn	0.002006	7.23e-5	0.06503	
k1ErbB1IntOff	0.0674	0.00225	2.022	
k2ErbB1IntOn	0.0317	0.00105	0.942	
k2ErbB1IntOff	0.00427	0.000139	0.125	
k1ErbB11IntOn	0.00282	9.4e-5	0.0846	

k1ErbB11IntOff	0.0839	0.00281	2.53
k2ErbB11IntOn	0.12	0.004011	3.61
k2ErbB11IntOff	0.00735	0.000241	0.217
k3ErbB11IntOn	0.0498	0.00165	1.48
k3ErbB11IntOff	0.0112	0.000369	0.332
kCbleq	2.98e-7	1.077e-8	9.69e-6
kCbloff	0.245	0.008068	7.26
k1ubeq	0.0219	0.000753	0.678
k1uboff	6.74	0.224	202
k2ubeq	7.32	0.245	220
k2uboff	68.9	2.34	2107
kdegErbB1	0.115	0.00372	3.35
kdegErbB1ub	0.198	0.00667	6.004
kdegErbB11	0.00785	0.000263	0.237
kdegErbB11ub1	2.12	0.0706	63.6
kdegErbB11ub2	0.116	0.00391	3.52
kShc1eq	6.006e-5	2.03e-6	0.00183
kShc1off	0.755	0.0258	23.2
ksyn1	288	8.95	8056

ATP	7831	266	240000	
EGFInt	0.00146	4.84e-5	0.0435	internalized free ligand in endosomes
scale_pR_C1	0.776	0.0287	25.8	
scale_tR_C1	0.929	0.0317	28.5	

CHAPTER 5: References

Agazie, Y.M., and Hayman, M.J. (2003a). Development of an efficient "substrate-trapping" mutant of Src homology phosphotyrosine phosphatase 2 and identification of the epidermal growth factor receptor, Gab1, and three other proteins as target substrates. J Biol Chem *278*, 13952-13958.

Agazie, Y.M., and Hayman, M.J. (2003b). Molecular mechanism for a role of SHP2 in epidermal growth factor receptor signaling. Mol Cell Biol *23*, 7875-7886.

Alonso, A., Sasin, J., Bottini, N., Friedberg, I., Osterman, A., Godzik, A., Hunter, T., Dixon, J., and Mustelin, T. (2004). Protein tyrosine phosphatases in the human genome. Cell *117*, 699-711.

Amin, D.N., Sergina, N., Ahuja, D., McMahon, M., Blair, J.A., Wang, D., Hann, B., Koch, K.M., Shokat, K.M., and Moasser, M.M. (2010). Resiliency and Vulnerability in the HER2-HER3 Tumorigenic Driver. Science Translational Medicine *2*, 16ra17-16ra17.

Amit, I., Citri, A., Shay, T., Lu, Y., Katz, M., Zhang, F., Tarcic, G., Siwak, D., Lahad, J., and Jacob-Hirsch, J. (2007). A module of negative feedback regulators defines growth factor signaling. Nature genetics *39*, 503-512.

Anido, J., Matar, P., Albanell, J., Guzman, M., Rojo, F., Arribas, J., Averbuch, S., and Baselga, J. (2003). ZD1839, a specific epidermal growth factor receptor (EGFR) tyrosine kinase inhibitor, induces the formation of inactive EGFR/HER2 and EGFR/HER3 heterodimers and prevents heregulin signaling in HER2-overexpressing breast cancer cells. Clin Cancer Res *9*, 1274-1283.

Baselga, J., Rischin, D., Ranson, M., Calvert, H., Raymond, E., Kieback, D.G., Kaye, S.B., Gianni, L., Harris, A., Bjork, T.*, et al.* (2002). Phase I safety, pharmacokinetic, and pharmacodynamic trial of ZD1839, a selective oral epidermal growth factor receptor tyrosine kinase inhibitor, in patients with five selected solid tumor types. J Clin Oncol *20*, 4292-4302.

Baulida, J., Kraus, M.H., Alimandi, M., Di Fiore, P.P., and Carpenter, G. (1996). All ErbB receptors other than the epidermal growth factor receptor are endocytosis impaired. J Biol Chem *271*, 5251-5257.

Blinov, M., Faeder, J., Goldstein, B., and Hlavacek, W. (2006). A network model of early events in epidermal growth factor receptor signaling that accounts for combinatorial complexity. Biosystems *83*, 136-151.

Blinov, M.L., Faeder, J.R., Goldstein, B., and Hlavacek, W.S. (2004). BioNetGen: software for rule-based modeling of signal transduction based on the interactions of molecular domains. Bioinformatics *20*, 3289-3291.

Bohmer, F., Bohmer, A., Obermeier, A., and Ullrich, A. (1995). Use of selective tyrosine kinase blockers to monitor growth factor receptor dephosphorylation in intact cells. Analytical biochemistry *228*, 267-273.

Brunati, A., Pinna, L., Bergantino, E., Ruzzene, M., Cirri, P., Ramponi, G., and Donella-Deana, A. (1998). Src homology-2 domains protect phosphotyrosyl residues against enzymatic dephosphorylation. Biochemical and Biophysical Research Communications *243*, 700-705.

Bublil, E.M., and Yarden, Y. (2007). The EGF receptor family: spearheading a merger of signaling and therapeutics. Curr Opin Cell Biol *19*, 124-134.

Burke, P., Schooler, K., and Wiley, H.S. (2001). Regulation of epidermal growth factor receptor signaling by endocytosis and intracellular trafficking. Mol Biol Cell *12*, 1897-1910.

Burnett, G., and Kennedy, E.P. (1954). The enzymatic phosphorylation of proteins. J Biol Chem *211*, 969-980.

Butler, M.T., Ziemiecki, A., Groner, B., and Friis, R.R. (1989). Characterization of a membrane-associated phosphotyrosyl protein phosphatase from the A431 human epidermoid carcinoma cell line. Eur J Biochem *185*, 475-483.

Capdeville, R., Buchdunger, E., Zimmermann, J., and Matter, A. (2002). Glivec (STI571, imatinib), a rationally developed, targeted anticancer drug. Nat Rev Drug Discov *1*, 493-502.

Chen, C.H., Cheng, T.H., Lin, H., Shih, N.L., Chen, Y.L., Chen, Y.S., Cheng, C.F., Lian, W.S., Meng, T.C., Chiu, W.T.*, et al.* (2006). Reactive oxygen species generation is involved in epidermal growth factor receptor transactivation through the transient oxidization of Src homology 2-containing tyrosine phosphatase in endothelin-1 signaling pathway in rat cardiac fibroblasts. Mol Pharmacol *69*, 1347-1355.

Chen, W., Schoeberl, B., Jasper, P., Niepel, M., Nielsen, U., Lauffenburger, D., and Sorger, P. (2009). Input–output behavior of ErbB signaling pathways as revealed by a mass action model trained against dynamic data. Molecular Systems Biology *5*.

Citri, A., and Yarden, Y. (2006). EGF-ERBB signalling: towards the systems level. Nat Rev Mol Cell Biol *7*, 505-516.

Clayton, A.H., Orchard, S.G., Nice, E.C., Posner, R.G., and Burgess, A.W. (2008). Predominance of activated EGFR higher-order oligomers on the cell surface. Growth Factors *26*, 316-324.

Cohen, P. (2000). The regulation of protein function by multisite phosphorylation--a 25 year update. Trends Biochem Sci *25*, 596-601.

Conzelmann, H., Fey, D., and Gilles, E.D. (2008). Exact model reduction of combinatorial reaction networks. BMC Syst Biol *2*, 78.

Debnath, J., Muthuswamy, S.K., and Brugge, J.S. (2003). Morphogenesis and oncogenesis of MCF-10A mammary epithelial acini grown in three-dimensional basement membrane cultures. Methods *30*, 256-268.

Du, J., Bernasconi, P., Clauser, K.R., Mani, D.R., Finn, S.P., Beroukhim, R., Burns, M., Julian, B., Peng, X.P., Hieronymus, H.*, et al.* (2009). Bead-based profiling of tyrosine kinase phosphorylation identifies SRC as a potential target for glioblastoma therapy. Nat Biotechnol *27*, 77-83.

Eck, M.J., and Yun, C.H. (2009). Structural and mechanistic underpinnings of the differential drug sensitivity of EGFR mutations in non-small cell lung cancer. Biochim Biophys Acta.

Eden, E.R., White, I.J., Tsapara, A., and Futter, C.E. (2010). Membrane contacts between endosomes and ER provide sites for PTP1B-epidermal growth factor receptor interaction. Nat Cell Biol *12*, 267-272.

Engelman, J.A., Zejnullahu, K., Mitsudomi, T., Song, Y., Hyland, C., Park, J.O., Lindeman, N., Gale, C.M., Zhao, X., Christensen, J.*, et al.* (2007). MET amplification leads to gefitinib resistance in lung cancer by activating ERBB3 signaling. Science *316*, 1039-1043.

Felder, S., Zhou, M., Hu, P., Urena, J., Ullrich, A., Chaudhuri, M., White, M., Shoelson, S.E., and Schlessinger, J. (1993). SH2 domains exhibit high-affinity binding to tyrosine-phosphorylated peptides yet also exhibit rapid dissociation and exchange. Mol Cell Biol *13*, 1449-1455.

Feng, G.S. (1999). Shp-2 tyrosine phosphatase: signaling one cell or many. Exp Cell Res *253*, 47-54.

Fischer, E.H., and Krebs, E.G. (1955). Conversion of phosphorylase b to phosphorylase a in muscle extracts. J Biol Chem *216*, 121-132.

Flint, A.J., Tiganis, T., Barford, D., and Tonks, N.K. (1997). Development of "substrate-trapping" mutants to identify physiological substrates of protein tyrosine phosphatases. Proc Natl Acad Sci U S A *94*, 1680-1685.

Fragale, A., Tartaglia, M., Wu, J., and Gelb, B.D. (2004). Noonan syndrome-associated SHP2/PTPN11 mutants cause EGF-dependent prolonged GAB1 binding and sustained ERK2/MAPK1 activation. Hum Mutat *23*, 267-277.

Frangioni, J.V., Beahm, P.H., Shifrin, V., Jost, C.A., and Neel, B.G. (1992). The nontransmembrane tyrosine phosphatase PTP-1B localizes to the endoplasmic reticulum via its 35 amino acid C-terminal sequence. Cell *68*, 545-560.

Fry, D.W., Bridges, A.J., Denny, W.A., Doherty, A., Greis, K.D., Hicks, J.L., Hook, K.E., Keller, P.R., Leopold, W.R., Loo, J.A.*, et al.* (1998). Specific, irreversible inactivation of the epidermal growth factor receptor and erbB2, by a new class of tyrosine kinase inhibitor. Proc Natl Acad Sci U S A *95*, 12022-12027.

Fry, W., Kotelawala, L., Sweeney, C., and Carraway, K. (2009). Mechanisms of ErbB receptor negative regulation and relevance in cancer. Experimental Cell Research *315*, 697-706.

Gan, H.K., Kaye, A.H., and Luwor, R.B. (2009). The EGFRvIII variant in glioblastoma multiforme. J Clin Neurosci *16*, 748-754.

Garrett, T.P., McKern, N.M., Lou, M., Elleman, T.C., Adams, T.E., Lovrecz, G.O., Kofler, M., Jorissen, R.N., Nice, E.C., Burgess, A.W.*, et al.* (2003). The crystal structure of a truncated ErbB2 ectodomain reveals an active conformation, poised to interact with other ErbB receptors. Mol Cell *11*, 495-505.

Gazdar, A.F. (2009). Activating and resistance mutations of EGFR in non-small-cell lung cancer: role in clinical response to EGFR tyrosine kinase inhibitors. Oncogene *28 Suppl 1*, S24-31.

Gebbia, V., Giuliani, F., Valori, V.M., Agueli, R., Colucci, G., and Maiello, E. (2007). Cetuximab in squamous cell head and neck carcinomas. Ann Oncol *18 Suppl 6*, vi5-7.

Gilmer, T.M., Cable, L., Alligood, K., Rusnak, D., Spehar, G., Gallagher, K.T., Woldu, E., Carter, H.L., Truesdale, A.T., Shewchuk, L.*, et al.* (2008). Impact of common epidermal growth factor receptor and HER2 variants on receptor activity and inhibition by lapatinib. Cancer Res *68*, 571-579.

Gordon, J.A. (1991). Use of vanadate as protein-phosphotyrosine phosphatase inhibitor. Methods Enzymol *201*, 477-482.

Grandal, M.V., Zandi, R., Pedersen, M.W., Willumsen, B.M., van Deurs, B., and Poulsen, H.S. (2007). EGFRvIII escapes down-regulation due to impaired internalization and sorting to lysosomes. Carcinogenesis *28*, 1408-1417.

Gujral, T.S., and MacBeath, G. (2009). Emerging miniaturized proteomic technologies to study cell signaling in clinical samples. Sci Signal *2*, pe65.

Haj, F.G., Verveer, P.J., Squire, A., Neel, B.G., and Bastiaens, P.I. (2002). Imaging sites of receptor dephosphorylation by PTP1B on the surface of the endoplasmic reticulum. Science *295*, 1708-1711.

Han, W., Zhang, T., Yu, H., Foulke, J.G., and Tang, C.K. (2006). Hypophosphorylation of residue Y1045 leads to defective downregulation of EGFRvIII. Cancer Biol Ther *5*, 1361-1368.

Heinrich, R., Neel, B.G., and Rapoport, T.A. (2002). Mathematical models of protein kinase signal transduction. Mol Cell *9*, 957-970.

Hirsch, D., Shen, Y., and Wu, W. (2006). Growth and motility inhibition of breast cancer cells by epidermal growth factor receptor degradation is correlated with inactivation of Cdc42. Cancer research *66*, 3523.

Hlavacek, W.S., Faeder, J.R., Blinov, M.L., Posner, R.G., Hucka, M., and Fontana, W. (2006). Rules for modeling signal-transduction systems. Sci STKE *2006*, re6.

Hof, P., Pluskey, S., Dhe-Paganon, S., Eck, M.J., and Shoelson, S.E. (1998). Crystal structure of the tyrosine phosphatase SHP-2. Cell *92*, 441-450.

Holbro, T., and Hynes, N.E. (2004). ErbB receptors: directing key signaling networks throughout life. Annu Rev Pharmacol Toxicol *44*, 195-217.

Huse, M., and Kuriyan, J. (2002). The conformational plasticity of protein kinases. Cell *109*, 275-282.

Huyer, G., Liu, S., Kelly, J., Moffat, J., Payette, P., Kennedy, B., Tsaprailis, G., Gresser, M., and Ramachandran, C. (1997). Mechanism of inhibition of protein-tyrosine phosphatases by vanadate and pervanadate. Journal of Biological Chemistry *272*, 843.

Hynes, N.E., and Lane, H.A. (2005). ERBB receptors and cancer: the complexity of targeted inhibitors. Nat Rev Cancer *5*, 341-354.

Iyer, A.K., Tran, K.T., Borysenko, C.W., Cascio, M., Camacho, C.J., Blair, H.C., Bahar, I., and Wells, A. (2007). Tenascin cytotactin epidermal growth factor-like repeat binds epidermal growth factor receptor with low affinity. J Cell Physiol *211*, 748-758.

Jecklin, M.C., Touboul, D., Jain, R., Toole, E.N., Tallarico, J., Drueckes, P., Ramage, P., and Zenobi, R. (2009). Affinity classification of kinase inhibitors by mass spectrometric methods and validation using standard IC(50) measurements. Anal Chem *81*, 408-419.

Johnson, L.N. (2009). Protein kinase inhibitors: contributions from structure to clinical compounds. Q Rev Biophys *42*, 1-40.

Johnson, T.O., Ermolieff, J., and Jirousek, M.R. (2002). Protein tyrosine phosphatase 1B inhibitors for diabetes. Nat Rev Drug Discov *1*, 696-709.

Jones, R.B., Gordus, A., Krall, J.A., and MacBeath, G. (2006). A quantitative protein interaction network for the ErbB receptors using protein microarrays. Nature *439*, 168-174.

Jorissen, R.N., Walker, F., Pouliot, N., Garrett, T.P., Ward, C.W., and Burgess, A.W. (2003). Epidermal growth factor receptor: mechanisms of activation and signalling. Exp Cell Res *284*, 31-53.

Jura, N., Shan, Y., Cao, X., Shaw, D., and Kuriyan, J. (2009). Structural analysis of the catalytically inactive kinase domain of the human EGF receptor 3. Proceedings of the National Academy of Sciences *106*, 21608.

Karaman, M.W., Herrgard, S., Treiber, D.K., Gallant, P., Atteridge, C.E., Campbell, B.T., Chan, K.W., Ciceri, P., Davis, M.I., Edeen, P.T.*, et al.* (2008). A quantitative analysis of kinase inhibitor selectivity. Nat Biotechnol *26*, 127-132.

Kaushansky, A., Gordus, A., Chang, B., Rush, J., and MacBeath, G. (2008). A quantitative study of the recruitment potential of all intracellular tyrosine residues on EGFR, FGFR1 and IGF1R. Mol Biosyst *4*, 643-653.

Keilhack, H., Tenev, T., Nyakatura, E., Godovac-Zimmermann, J., Nielsen, L., Seedorf, K., and Bohmer, F.D. (1998). Phosphotyrosine 1173 mediates binding of the protein-tyrosine phosphatase SHP-1 to the epidermal growth factor receptor and attenuation of receptor signaling. J Biol Chem *273*, 24839-24846.

Kholodenko, B., Demin, O., Moehren, G., and Hoek, J. (1999). Quantification of short term signaling by the epidermal growth factor receptor. Journal of Biological Chemistry *274*, 30169.

Klapper, L.N., Glathe, S., Vaisman, N., Hynes, N.E., Andrews, G.C., Sela, M., and Yarden, Y. (1999). The ErbB-2/HER2 oncoprotein of human carcinomas may function solely as a shared coreceptor for multiple stroma-derived growth factors. Proc Natl Acad Sci U S A *96*, 4995-5000.

Knight, Z.A., Lin, H., and Shokat, K.M. (2010). Targeting the cancer kinome through polypharmacology. Nat Rev Cancer *10*, 130-137.

Kontaridis, M.I., Eminaga, S., Fornaro, M., Zito, C.I., Sordella, R., Settleman, J., and Bennett, A.M. (2004). SHP-2 positively regulates myogenesis by coupling to the Rho GTPase signaling pathway. Mol Cell Biol *24*, 5340-5352.

Koschorreck, M., Conzelmann, H., Ebert, S., Ederer, M., and Gilles, E.D. (2007). Reduced modeling of signal transduction - a modular approach. BMC Bioinformatics *8*, 336.

Koschorreck, M., and Gilles, E.D. (2008). ALC: automated reduction of rule-based models. BMC Syst Biol *2*, 91.

Kovalenko, M., Denner, K., Sandstrom, J., Persson, C., Gross, S., Jandt, E., Vilella, R., Bohmer, F., and Ostman, A. (2000). Site-selective dephosphorylation of the platelet-derived growth factor beta-receptor by the receptor-like protein-tyrosine phosphatase DEP-1. J Biol Chem *275*, 16219-16226.

Kulas, D.T., Goldstein, B.J., and Mooney, R.A. (1996). The transmembrane protein-tyrosine phosphatase LAR modulates signaling by multiple receptor tyrosine kinases. J Biol Chem *271*, 748-754.

Kwok, T.T., and Sutherland, R.M. (1991). Differences in EGF related radiosensitisation of human squamous carcinoma cells with high and low numbers of EGF receptors. Br J Cancer *64*, 251-254.

Lammers, R., Bossenmaier, B., Cool, D., Tonks, N., Schlessinger, J., Fischer, E., and Ullrich, A. (1993). Differential activities of protein tyrosine phosphatases in intact cells. Journal of Biological Chemistry *268*, 22456.

Lee, S., Kwon, K., Kim, S., and Rhee, S. (1998). Reversible inactivation of protein-tyrosine phosphatase 1B in A431 cells stimulated with epidermal growth factor. Journal of Biological Chemistry *273*, 15366.

Lehninger, A.L., Nelson, D.L., and Cox, M.M. (2000). Lehninger principles of biochemistry, 3rd edn (New York, Worth Publishers).

Levkowitz, G., Waterman, H., Zamir, E., Kam, Z., Oved, S., Langdon, W.Y., Beguinot, L., Geiger, B., and Yarden, Y. (1998). c-Cbl/Sli-1 regulates endocytic sorting and ubiquitination of the epidermal growth factor receptor. Genes Dev *12*, 3663-3674.

Li, X., Huang, Y., Jiang, J., and Frank, S.J. (2008). ERK-dependent threonine phosphorylation of EGF receptor modulates receptor downregulation and signaling. Cell Signal *20*, 2145-2155.

Linggi, B., and Carpenter, G. (2006). ErbB receptors: new insights on mechanisms and biology. Trends Cell Biol *16*, 649-656.

Liu, F., and Chernoff, J. (1997). Protein tyrosine phosphatase 1B interacts with and is tyrosine phosphorylated by the epidermal growth factor receptor. Biochem J *327 (Pt 1)*, 139-145.

Liu, Y., and Gray, N.S. (2006). Rational design of inhibitors that bind to inactive kinase conformations. Nat Chem Biol *2*, 358-364.

Lu, W., Gong, D., Bar-Sagi, D., and Cole, P.A. (2001). Site-specific incorporation of a phosphotyrosine mimetic reveals a role for tyrosine phosphorylation of SHP-2 in cell signaling. Mol Cell *8*, 759-769.

Maiello, E., Giuliani, F., Gebbia, V., Piano, A., Agueli, R., and Colucci, G. (2007). Cetuximab: clinical results in colorectal cancer. Ann Oncol *18 Suppl 6*, vi8-10.

Maiwald, T., and Timmer, J. (2008). Dynamical modeling and multi-experiment fitting with PottersWheel. Bioinformatics *24*, 2037.

Mallavarapu, A., Thomson, M., Ullian, B., and Gunawardena, J. (2009). Programming with models: modularity and abstraction provide powerful capabilities for systems biology. J R Soc Interface *6*, 257-270.

Manning, G., Whyte, D.B., Martinez, R., Hunter, T., and Sudarsanam, S. (2002). The protein kinase complement of the human genome. Science *298*, 1912-1934.

Mao, S.Y., and Metzger, H. (1997). Characterization of protein-tyrosine phosphatases that dephosphorylate the high affinity IgE receptor. J Biol Chem *272*, 14067-14073.

Mattila, E., Pellinen, T., Nevo, J., Vuoriluoto, K., Arjonen, A., and Ivaska, J. (2005). Negative regulation of EGFR signalling through integrin-alpha1beta1-mediated activation of protein tyrosine phosphatase TCPTP. Nat Cell Biol *7*, 78-85.

Mikalsen, S.O., and Kaalhus, O. (1998). Properties of pervanadate and permolybdate. Connexin43, phosphatase inhibition, and thiol reactivity as model systems. J Biol Chem *273*, 10036-10045.

Milarski, K.L., Zhu, G., Pearl, C.G., McNamara, D.J., Dobrusin, E.M., MacLean, D., Thieme-Sefler, A., Zhang, Z.Y., Sawyer, T., Decker, S.J.*, et al.* (1993). Sequence specificity in recognition of the epidermal growth factor receptor by protein tyrosine phosphatase 1B. J Biol Chem *268*, 23634-23639.

Mukohara, T., Engelman, J.A., Hanna, N.H., Yeap, B.Y., Kobayashi, S., Lindeman, N., Halmos, B., Pearlberg, J., Tsuchihashi, Z., Cantley, L.C.*, et al.* (2005). Differential effects of gefitinib and cetuximab on non-small-cell lung cancers bearing epidermal growth factor receptor mutations. J Natl Cancer Inst *97*, 1185-1194.

Nahta, R., and Esteva, F.J. (2007). Trastuzumab: triumphs and tribulations. Oncogene *26*, 3637-3643.

Neel, B.G., Gu, H., and Pao, L. (2003). The 'Shp'ing news: SH2 domain-containing tyrosine phosphatases in cell signaling. Trends Biochem Sci *28*, 284-293.

Neelam, B., Richter, A., Chamberlin, S.G., Puddicombe, S.M., Wood, L., Murray, M.B., Nandagopal, K., Niyogi, S.K., and Davies, D.E. (1998). Structure-function studies of ligand-induced epidermal growth factor receptor dimerization. Biochemistry *37*, 4884-4891.

Neve, R.M., Chin, K., Fridlyand, J., Yeh, J., Baehner, F.L., Fevr, T., Clark, L., Bayani, N., Coppe, J.P., Tong, F.*, et al.* (2006). A collection of breast cancer cell lines for the study of functionally distinct cancer subtypes. Cancer Cell *10*, 515-527.

Nishimura, Y., Bereczky, B., and Ono, M. (2007). The EGFR inhibitor gefitinib suppresses ligand-stimulated endocytosis of EGFR via the early/late endocytic pathway in non-small cell lung cancer cell lines. Histochem Cell Biol *127*, 541-553.

Northrup, S., and Erickson, H. (1992). Kinetics of protein-protein association explained by Brownian dynamics computer simulation. Proceedings of the National Academy of Sciences *89*, 3338.

Offterdinger, M., Georget, V., Girod, A., and Bastiaens, P. (2004). Imaging phosphorylation dynamics of the epidermal growth factor receptor. Journal of Biological Chemistry *279*, 36972-36981.

Oka, T., Ouchida, M., Koyama, M., Ogama, Y., Takada, S., Nakatani, Y., Tanaka, T., Yoshino, T., Hayashi, K., Ohara, N.*, et al.* (2002). Gene silencing of the tyrosine phosphatase SHP1 gene by aberrant methylation in leukemias/lymphomas. Cancer Res *62*, 6390-6394.

Oksvold, M.P., Skarpen, E., Lindeman, B., Roos, N., and Huitfeldt, H.S. (2000). Immunocytochemical localization of Shc and activated EGF receptor in early endosomes after EGF stimulation of HeLa cells. J Histochem Cytochem *48*, 21-33.

Olsen, J.V., Blagoev, B., Gnad, F., Macek, B., Kumar, C., Mortensen, P., and Mann, M. (2006). Global, in vivo, and site-specific phosphorylation dynamics in signaling networks. Cell *127*, 635-648.

Omerovic, J., Clague, M.J., and Prior, I.A. (2010). Phosphatome profiling reveals PTPN2, PTPRJ and PTEN as potent negative regulators of PKB/Akt activation in Ras-mutated cancer cells. Biochem J *426*, 65-72.

Orton, R.J., Adriaens, M.E., Gormand, A., Sturm, O.E., Kolch, W., and Gilbert, D.R. (2009). Computational modelling of cancerous mutations in the EGFR/ERK signalling pathway. BMC Syst Biol *3*, 100.

Ostman, A., Hellberg, C., and Bohmer, F.D. (2006). Protein-tyrosine phosphatases and cancer. Nat Rev Cancer *6*, 307-320.

Paez, J., Janne, P., Lee, J., Tracy, S., Greulich, H., Gabriel, S., Herman, P., Kaye, F., Lindeman, N., and Boggon, T. (2004). EGFR mutations in lung cancer: correlation with clinical response to gefitinib therapy. Science *304*, 1497.

Palka, H.L., Park, M., and Tonks, N.K. (2003). Hepatocyte growth factor receptor tyrosine kinase met is a substrate of the receptor protein-tyrosine phosphatase DEP-1. J Biol Chem *278*, 5728-5735.

Parsons, R. (2004). Human cancer, PTEN and the PI-3 kinase pathway. Semin Cell Dev Biol *15*, 171-176.

Pedersen, M.W., Pedersen, N., Ottesen, L.H., and Poulsen, H.S. (2005). Differential response to gefitinib of cells expressing normal EGFR and the mutant EGFRvIII. Br J Cancer *93*, 915-923.

Pratilas, C.A., Hanrahan, A.J., Halilovic, E., Persaud, Y., Soh, J., Chitale, D., Shigematsu, H., Yamamoto, H., Sawai, A., Janakiraman, M.*, et al.* (2008). Genetic predictors of MEK dependence in non-small cell lung cancer. Cancer Res *68*, 9375-9383.

Reynolds, A., Tischer, C., Verveer, P., Rocks, O., and Bastiaens, P. (2003). EGFR activation coupled to inhibition of tyrosine phosphatases causes lateral signal propagation. Nature Cell Biology *5*, 447-453.

Robinson, D.R., Wu, Y.M., and Lin, S.F. (2000). The protein tyrosine kinase family of the human genome. Oncogene *19*, 5548-5557.

Roepstorff, K., Grandal, M.V., Henriksen, L., Knudsen, S.L., Lerdrup, M., Grovdal, L., Willumsen, B.M., and van Deurs, B. (2009). Differential effects of EGFR ligands on endocytic sorting of the receptor. Traffic *10*, 1115-1127.

Rotin, D., Margolis, B., Mohammadi, M., Daly, R., Daum, G., Li, N., Fischer, E., Burgess, W., Ullrich, A., and Schlessinger, J. (1992). SH2 domains prevent tyrosine dephosphorylation of the EGF receptor: identification of Tyr992 as the high-affinity binding site for SH2 domains of phospholipase C gamma. The EMBO Journal *11*, 559.

Ruivenkamp, C.A., van Wezel, T., Zanon, C., Stassen, A.P., Vlcek, C., Csikos, T., Klous, A.M., Tripodis, N., Perrakis, A., Boerrigter, L.*, et al.* (2002). Ptprj is a candidate for the mouse colon-cancer susceptibility locus Scc1 and is frequently deleted in human cancers. Nat Genet *31*, 295-300.

Saez-Rodriguez, J., Alexopoulos, L.G., Epperlein, J., Samaga, R., Lauffenburger, D.A., Klamt, S., and Sorger, P.K. (2009). Discrete logic modelling as a means to link protein signalling networks with functional analysis of mammalian signal transduction. Mol Syst Biol *5*, 331.

Schnell, S., and Turner, T.E. (2004). Reaction kinetics in intracellular environments with macromolecular crowding: simulations and rate laws. Prog Biophys Mol Biol *85*, 235-260.

Schoeberl, B., Pace, E.A., Fitzgerald, J.B., Harms, B.D., Xu, L., Nie, L., Linggi, B., Kalra, A., Paragas, V., Bukhalid, R.*, et al.* (2009). Therapeutically targeting ErbB3: a key node in ligand-induced activation of the ErbB receptor-PI3K axis. Sci Signal *2*, ra31.

Schulze, W.X., Deng, L., and Mann, M. (2005). Phosphotyrosine interactome of the ErbB-receptor kinase family. Mol Syst Biol *1*, 2005 0008.

Sebastian, S., Settleman, J., Reshkin, S.J., Azzariti, A., Bellizzi, A., and Paradiso, A. (2006). The complexity of targeting EGFR signalling in cancer: from expression to turnover. Biochim Biophys Acta *1766*, 120-139.

Sergina, N.V., Rausch, M., Wang, D., Blair, J., Hann, B., Shokat, K.M., and Moasser, M.M. (2007). Escape from HER-family tyrosine kinase inhibitor therapy by the kinase-inactive HER3. Nature *445*, 437-441.

Sevecka, M., and MacBeath, G. (2006). State-based discovery: a multidimensional screen for small-molecule modulators of EGF signaling. Nat Methods *3*, 825-831.

Sharma, S.V., and Settleman, J. (2009). ErbBs in lung cancer. Exp Cell Res *315*, 557-571.

Shtiegman, K., Kochupurakkal, B.S., Zwang, Y., Pines, G., Starr, A., Vexler, A., Citri, A., Katz, M., Lavi, S., Ben-Basat, Y.*, et al.* (2007). Defective ubiquitinylation of EGFR mutants of lung cancer confers prolonged signaling. Oncogene *26*, 6968-6978.

Sigismund, S., Woelk, T., Puri, C., Maspero, E., Tacchetti, C., Transidico, P., Di Fiore, P.P., and Polo, S. (2005). Clathrin-independent endocytosis of ubiquitinated cargos. Proc Natl Acad Sci U S A *102*, 2760-2765.

Sorkin, A., and Goh, L.K. (2009). Endocytosis and intracellular trafficking of ErbBs. Exp Cell Res *315*, 683-696.

Stamos, J., Sliwkowski, M.X., and Eigenbrot, C. (2002). Structure of the epidermal growth factor receptor kinase domain alone and in complex with a 4-anilinoquinazoline inhibitor. J Biol Chem *277*, 46265-46272.

Sturla, L.M., Amorino, G., Alexander, M.S., Mikkelsen, R.B., Valerie, K., and Schmidt-Ullrichr, R.K. (2005). Requirement of Tyr-992 and Tyr-1173 in phosphorylation of the epidermal growth factor receptor by ionizing radiation and modulation by SHP2. J Biol Chem *280*, 14597-14604.

Suarez Pestana, E., Tenev, T., Gross, S., Stoyanov, B., Ogata, M., and Bohmer, F.D. (1999). The transmembrane protein tyrosine phosphatase RPTPsigma modulates signaling of the epidermal growth factor receptor in A431 cells. Oncogene *18*, 4069-4079.

Suenaga, A., Hatakeyama, M., Kiyatkin, A.B., Radhakrishnan, R., Taiji, M., and Kholodenko, B.N. (2009). Molecular dynamics simulations reveal that Tyr-317 phosphorylation reduces Shc binding affinity for phosphotyrosyl residues of epidermal growth factor receptor. Biophys J *96*, 2278-2288.

Swarup, G., Speeg, K.V., Jr., Cohen, S., and Garbers, D.L. (1982). Phosphotyrosyl-protein phosphatase of TCRC-2 cells. J Biol Chem *257*, 7298-7301.

Tan, Y.H., Krishnaswamy, S., Nandi, S., Kanteti, R., Vora, S., Onel, K., Hasina, R., Lo, F.Y., El-Hashani, E., Cervantes, G.*, et al.* (2010). CBL is frequently altered in lung cancers: its relationship to mutations in MET and EGFR tyrosine kinases. PLoS One *5*, e8972.

Tao, R., and Maruyama, I. (2008). All EGF (ErbB) receptors have preformed homo-and heterodimeric structures in living cells. Journal of Cell Science *121*, 3207.

Tarcic, G., Boguslavsky, S.K., Wakim, J., Kiuchi, T., Liu, A., Reinitz, F., Nathanson, D., Takahashi, T., Mischel, P.S., Ng, T.*, et al.* (2009). An unbiased screen identifies DEP-1 tumor suppressor as a phosphatase controlling EGFR endocytosis. Curr Biol *19*, 1788-1798.

Tarrant, M.K., and Cole, P.A. (2009). The chemical biology of protein phosphorylation. Annu Rev Biochem *78*, 797-825.

Tartaglia, M., Mehler, E.L., Goldberg, R., Zampino, G., Brunner, H.G., Kremer, H., van der Burgt, I., Crosby, A.H., Ion, A., Jeffery, S.*, et al.* (2001). Mutations in PTPN11, encoding the protein tyrosine phosphatase SHP-2, cause Noonan syndrome. Nat Genet *29*, 465-468.

Tartaglia, M., Niemeyer, C.M., Fragale, A., Song, X., Buechner, J., Jung, A., Hahlen, K., Hasle, H., Licht, J.D., and Gelb, B.D. (2003). Somatic mutations in PTPN11 in juvenile myelomonocytic leukemia, myelodysplastic syndromes and acute myeloid leukemia. Nat Genet *34*, 148-150.

Tiganis, T. (2002). Protein tyrosine phosphatases: dephosphorylating the epidermal growth factor receptor. IUBMB Life *53*, 3-14.

Tiganis, T., Bennett, A.M., Ravichandran, K.S., and Tonks, N.K. (1998). Epidermal growth factor receptor and the adaptor protein p52Shc are specific substrates of T-cell protein tyrosine phosphatase. Mol Cell Biol *18*, 1622-1634.

Tiganis, T., Kemp, B.E., and Tonks, N.K. (1999). The protein-tyrosine phosphatase TCPTP regulates epidermal growth factor receptor-mediated and phosphatidylinositol 3-kinase-dependent signaling. J Biol Chem *274*, 27768-27775.

Tran, K.T., Griffith, L., and Wells, A. (2004). Extracellular matrix signaling through growth factor receptors during wound healing. Wound Repair Regen *12*, 262-268.

Tuveson, D.A., Weber, B.L., and Herlyn, M. (2003). BRAF as a potential therapeutic target in melanoma and other malignancies. Cancer cell *4*, 95-98.

Waterman, H., Katz, M., Rubin, C., Shtiegman, K., Lavi, S., Elson, A., Jovin, T., and Yarden, Y. (2002). A mutant EGF-receptor defective in ubiquitylation and endocytosis unveils a role for Grb2 in negative signaling. EMBO J *21*, 303-313.

Wiener, J.R., Kerns, B.J., Harvey, E.L., Conaway, M.R., Iglehart, J.D., Berchuck, A., and Bast, R.C., Jr. (1994). Overexpression of the protein tyrosine phosphatase PTP1B in human breast cancer: association with p185c-erbB-2 protein expression. J Natl Cancer Inst *86*, 372-378.

Wolf-Yadlin, A., Kumar, N., Zhang, Y., Hautaniemi, S., Zaman, M., Kim, H.D., Grantcharova, V., Lauffenburger, D.A., and White, F.M. (2006). Effects of HER2 overexpression on cell signaling networks governing proliferation and migration. Mol Syst Biol *2*, 54.

Wong, E.S., Lim, J., Low, B.C., Chen, Q., and Guy, G.R. (2001). Evidence for direct interaction between Sprouty and Cbl. J Biol Chem *276*, 5866-5875.

Wood, E.R., Truesdale, A.T., McDonald, O.B., Yuan, D., Hassell, A., Dickerson, S.H., Ellis, B., Pennisi, C., Horne, E., Lackey, K.*, et al.* (2004). A unique structure for epidermal growth factor receptor bound to GW572016 (Lapatinib): relationships among protein conformation, inhibitor off-rate, and receptor activity in tumor cells. Cancer Res *64*, 6652-6659.

Xu, Y., Tan, L.J., Grachtchouk, V., Voorhees, J.J., and Fisher, G.J. (2005). Receptor-type protein-tyrosine phosphatase-kappa regulates epidermal growth factor receptor function. J Biol Chem *280*, 42694-42700.

Yang, K.S., Ilagan, M.X., Piwnica-Worms, D., and Pike, L.J. (2009). Luciferase fragment complementation imaging of conformational changes in the epidermal growth factor receptor. J Biol Chem *284*, 7474-7482.

Yarden, Y., and Sliwkowski, M. (2001). Untangling the ErbB signalling network. Nat Rev Mol Cell Biol *2*, 127-137.

Yudushkin, I.A., Schleifenbaum, A., Kinkhabwala, A., Neel, B.G., Schultz, C., and Bastiaens, P.I. (2007). Live-cell imaging of enzyme-substrate interaction reveals spatial regulation of PTP1B. Science *315*, 115-119.

Yun, C.H., Boggon, T.J., Li, Y., Woo, M.S., Greulich, H., Meyerson, M., and Eck, M.J. (2007). Structures of lung cancer-derived EGFR mutants and inhibitor complexes: mechanism of activation and insights into differential inhibitor sensitivity. Cancer Cell *11*, 217-227.

Yun, C.H., Mengwasser, K.E., Toms, A.V., Woo, M.S., Greulich, H., Wong, K.K., Meyerson, M., and Eck, M.J. (2008). The T790M mutation in EGFR kinase causes drug resistance by increasing the affinity for ATP. Proc Natl Acad Sci U S A *105*, 2070-2075.

Yuvaniyama, J., Denu, J.M., Dixon, J.E., and Saper, M.A. (1996). Crystal structure of the dual specificity protein phosphatase VHR. Science *272*, 1328-1331.

Zhai, Y.F., Beittenmiller, H., Wang, B., Gould, M.N., Oakley, C., Esselman, W.J., and Welsch, C.W. (1993). Increased expression of specific protein tyrosine phosphatases in human breast epithelial cells neoplastically transformed by the neu oncogene. Cancer Res *53*, 2272-2278.

Zhang, J., Somani, A.K., and Siminovitch, K.A. (2000). Roles of the SHP-1 tyrosine phosphatase in the negative regulation of cell signalling. Semin Immunol *12*, 361-378.

Zhang, X., Pickin, K.A., Bose, R., Jura, N., Cole, P.A., and Kuriyan, J. (2007). Inhibition of the EGF receptor by binding of MIG6 to an activating kinase domain interface. Nature *450*, 741-744.

Zhang, Z., Shen, K., Lu, W., and Cole, P.A. (2003). The role of C-terminal tyrosine phosphorylation in the regulation of SHP-1 explored via expressed protein ligation. J Biol Chem *278*, 4668-4674.

Zhang, Z.Y. (2002). Protein tyrosine phosphatases: structure and function, substrate specificity, and inhibitor development. Annu Rev Pharmacol Toxicol *42*, 209-234.

Zhao, Z., Tan, Z., Diltz, C.D., You, M., and Fischer, E.H. (1996). Activation of mitogen-activated protein (MAP) kinase pathway by pervanadate, a potent inhibitor of tyrosine phosphatases. J Biol Chem *271*, 22251-22255.

Zhou, M.M., Harlan, J.E., Wade, W.S., Crosby, S., Ravichandran, K.S., Burakoff, S.J., and Fesik, S.W. (1995). Binding affinities of tyrosine-phosphorylated peptides to the COOH-terminal SH2 and NH2-terminal phosphotyrosine binding domains of Shc. J Biol Chem *270*, 31119-31123.